NTNU
Norwegian University of
Science and Technology

Design of Mooring Systems for Large Floating Wind Turbines in Shallow Water

Kjetil Blindheim Hole

Marine Technology
Submission date: June 2018
Supervisor: Kjell Larsen, IMT

Norwegian University of Science and Technology
Department of Marine Technology

NTNU Trondheim
Norges teknisk-naturvitenskapelige universitet
Institutt for marin teknikk

MASTER THESIS SPRING 2018

for

Stud. tech. Kjetil Blindheim Hole

Design of mooring systems for large floating wind turbines in shallow water

Design av forankringssystemer for store, flytende vindturbiner på grunt vann

Background

In the development of floating wind turbines (FWTs) for utilizing the offshore wind resource, various technologies from the offshore oil and gas (O&G) industry have been adopted, including mooring system solutions. The purpose of the mooring system is to keep the floating wind turbine safely at a required position. It normally consists of three mooring lines of chain. Compared to O&G installations, FWTs tend to be significantly smaller. The external loads are characterized with large mean loads (due to the rotor thrust) in moderate wave conditions and high wave motions in extreme wave conditions.

In order to bring FWTs closer to commercial feasibility, cost reductions are needed. The cost of the mooring system constitutes a considerable part of the total cost. Novel mooring system designs – using less or different materials, novel anchors, or new installation methods – offer therefore one possible area for cost reduction. Novel mooring systems may also allow FWTs to be applied in shallower water, such that they may become competitive in a wider range of locations. An interesting range of water depth is 50-100m.

The importance of the mooring system for a floating wind turbine is crucial. The moorings must be reliable enough to prevent any free drift where cable rupture and collisions are typical consequences and the cost of mooring must be as low as possible to make such developments profitable. Optimization of the mooring system is therefore an important task.
Mooring systems for shallow water, typically for water depth in the range 70-100m, is a challenging task. Feasibility of such systems will, however, open up large new areas where fixed turbines of the monopile type become too expensive.

The overall objective of this project is to learn about floating wind turbines and mooring system design. This includes mooring system concepts and building blocks as well as design methods and requirements stated in rules and regulations.

The main objective of the thesis work is to examine design requirements for the mooring system of the CSC 10MW floating wind turbine in 70 m water depth, and to establish feasible mooring systems. Development and use of a simplified model will be used to investigate the performance of different mooring systems, with a particular focus on ULS and ALS.

Scope of Work

1) Review relevant literature and give an overview of state-of-art of fixed and floating wind turbines. Describe possible mooring and station keeping systems for floating units in general and floating wind turbines in particular. Focus on station keeping principles and main hardware components.

2) Review relevant literature for mooring systems and time domain simulation of mooring systems and describe the theory related to coupled and un-coupled analysis methodology. Describe the relevant simulation tools available in SIMA and how SIMA can effectively be utilized is ULS and ALS design of mooring systems.

3) Describe the design limit states for mooring systems of floating wind turbines with corresponding acceptance criteria outlined in rules and regulations (use DNV-OS-J103).

4) Based on an existing SIMA model of a CSC 10MW FWT, further develop a simplified model in the SIMO/RIFLEX/SIMA with the objective of performing numerical time-domain simulations of wind turbine motions and mooring line tensions for typical ULS/ALS conditions.

5) Propose possible moorings system layouts for the FWT in 70m water depth. Both systems comprising chain and synthetic fiber shall be assessed. Use of clump weights or buoys to be applied if necessary. Concepts to be discussed with supervisor. Perform global numerical analysis and check with ULS and ALS requirements. Comparison of results for selected cases with the original, high-fidelity model established by other students to be agreed with supervisor.

6) Conclusions and recommendations for further work.

General information

The work scope may prove to be larger than initially anticipated. Subject to approval from the supervisor, topics may be reduced in extent.

In the project, the candidate shall present his personal contribution to the resolution of problems within the scope of work.

Theories and conclusions should be based on mathematical derivations and/or logic reasoning identifying the various steps in the deduction.

The candidate should utilise the existing possibilities for obtaining relevant literature.

Report/Delivery

The thesis report should be organised in a rational manner to give a clear exposition of results, assessments, and conclusions. The text should be brief and to the point, with a clear language. Telegraphic language should be avoided.

The report shall be written in English and shall contain the following elements: A text defining the scope, preface, list of contents, main body of the project report, conclusions with recommendations for further work, list of symbols and acronyms, reference and (optional) appendices. All figures, tables and equations shall be numerated.

The original contribution of the candidate and material taken from other sources shall be clearly defined. Work from other sources shall be properly referenced using an acknowledged referencing system.

The report shall be submitted in two copies:

- Signed by the candidate
- The text defining the scope included
- In bound volume(s)
- An electronic copy to be sent to the supervisor

Ownership

NTNU has according to the present rules the ownership of the project results. Any use of the project results has to be approved by NTNU (or external partner when this applies). The department has the right to use the results as if the work was carried out by a NTNU employee, if nothing else has been agreed in advance.

Thesis supervisor**:**

Prof. II Kjell Larsen, NTNU/Statoil

Deadline: June 11th, 2018

Trondheim, January 18th, 2018

Kjell Larsen (date and signature):
June 6th, 2018

Kjetil Blindheim Hole (date and signature):
June7th, 2018

Preface

This MSc thesis is the final part of my master's degree in Mrine Technology, specializing in Marine Hydrodynamics. This thesis has been completed at the Department of Marin Technology at the Norwegian University of Science and Technology (NTNU). The thesis is a specialization project for marine operations written and submitted during the spring semester of 2018 under the supervision of Professor Kjell Larsen.

The objective of this thesis was to continue the work done in my project thesis written during the fall of 2017 by further developing a simplified model of a 10MW wind turbine with the aim of conducting efficient mooring analysis for different mooring systems. During this semester i have had the opportunity to work with the SIMA workbench and learned much about mooring analysis and the different tools used by the industry.

I must sincerely thank my supervisor, Professor Kjell Larsen, for excellent guidance and encouragement during this semester. I am also grateful for the help and patience received from Yuna Zhao with respect to the SIMA software. I must also thank Tiril Stenlund for comparisons of our SIMA models, and useful discussions on all related topics. And finally i must thank my parents for supporting and encouraging me throughout my studies.

Trondheim, June 7th, 2018

Kjetil Blindheim Hole

Abstract

Hywind Scotland is the first operational floating wind turbine park in existence. It was developed by Equinor and is located off the coast of Scotland at a water depth of approximately 105m. In this thesis, a time domain model of a semi-submersible floating wind turbine is used to check the feasibility of floating wind turbines placed at 70m water depth. If this is proven feasible, new areas for floating wind turbine parks will become available for development.

This thesis describes relevant literature for mooring systems, and preexisting offshore wind turbine concepts. Rules and regulations for floating wind turbines are described with respect to ULS, ALS and line slack.

The environmental conditions for this thesis are empirical data from the cite of Hywind Scotland, given by a metocan design basis from Equinor. The design requirements for floating wind turbines states that it needs to be able to withstand a storm with a 50-year return period, and current with a 10-year return period.

The time domain model is created in SIMO-RIFLEX using SIMA, and is a simplification of a preexisting model crated by Qiang Wang. The aim of the simplification is to create a model with reduced simulation time which is able to efficiently and accurately perform mooring analyses for different systems. This was achieved by removing structures representing the wind turbine, and modeling the semi-submersible floater to behave as a full turbine. By comparing the simplified model with the original model, it is shown that the excited motions are similar, the simplified model uses 64% of the original simulation time.

To provide feasible mooring systems for a wind turbine in shallow water, chain mooring systems following the catenary equations and taut mooring systems compiled of polyester ropes are analyzed. It is found that for a water depth of 70m a full chain system is not feasible, and a significant reduction in axial stiffness is needed to meet the requirements for ULS. The simulations shows that a taut mooring system with 800m lines is feasible. Shorter lines can withstand ULS, but the dimensioning factor is slack, and longer lines are required.

Sammendrag

Hywind Scotland er den første flytende vindturbinparken i full størrelse. Denne parken er utviklet av Equinor og plassert utenfor Skotland på ca. 105m vanndyp. I denne oppgaven skal en tidsdomene modell brukes i et mulighetsstudie for å finne ut om man kan installere flytende vindturbiner på 70m vanndyp. Hvis dette viser seg å være mulig vil flere områder kunne vurderes som mulige steder for offshore vindproduksjon.

I denne oppgaven beskrives relevant litteratur for forankringssystemer og relevante turbinkonsepter presenteres. Retningslinjer og reglement for forankring av vindturbiner er beskrevet med vekt på ULS, ALS og lineslakk.

Værkondisjonene er hentet fra empirisk værdata gitt av Equinor for området Hywind Scotland er installert. Kravet for flytende vindturbiner er at de må tåle å bli truffet av en storm med en returperiode på 50 år. Strømmen som hører til denne kondisjonen er med 10 års returperiode.

Tidsdomene modellen er laget i SIMO-RIFLEX igjennom arbeidsbenken SIMA, og modellen er en forenkling av en allerede eksisterende modell laget av Qiang Wang. Målet er å lage en effektiv modell med redusert simuleringstid som kan foreta nøyaktige analyser av forankringssystemer. Dette ble oppnådd ved å fjerne elementer som representerte turbinestrukturen, for så å sitte igjen med en halvt nedsenkbar struktur som oppfører seg som en vindturbin. Gjennom sammenligninger med originalmodellen ble det vist at den forenklede modellen bruker 64% av simuleringstiden til original modellen, og kreftene på forankringslinene er like.

For å kunne foreslå mulige forankringssystemer for vindturbinen på grunt vann gjennomføres analyser av kjetting systemer som følger formen til en kjedeline og analyser av forankringssystemer med fibertau som henger i en rett linje. Det viste seg at et kjettingsystem på dette vanndypet ikke lar seg gjennomføre, og for å nå innenfor reglementet må aksialstivheten reduseres betraktelig. Et fungerende polyester line system er foreslått til å være av 800m lange liner med 3000kN i forspenning. Kortere liner er innenfor kravene for ULS, men det er lineslakk som er dimensjonere, og for å unngå dette må linene være lange.

Nomenclature

Acronyms

CoG	Centre of gravity
DEA	Drag embedded anchor
DTU	Technincal University of Denmark
FFT	Fast Fourier Transform
MBL	Maximum breaking load
ULS	Ultimeate limit state
VLA	Vertically loaded anchor

Variables

$F_y(y)$	Gumbel cumulative distribution
$f_y(y)$	Gumbel probability density function
$ULSU_{10}$	Wind speed at reference height=10m
α	Pewer-law exponent
$\bar{U}$	Mean wind velocity
$\bar{V}$	Current velocity
$\ddot{x}$	Acceleration for a given degree of freedom
$\dot{x}$	Velocity for a given degree of freedom
γ_{dyn}	Dynamic load factor
γ_{mean}	Mean load factor
λ	Wave length
ρ_a	Air density $[kg/m^2]$

ρ_{air} Air density

ρ_{water} Water density

A_{wl} Water line area

$A(\omega)$ Frequency-dependant added mass matrix

C_M Mass coefficient

$C(\omega)$ Frequency-dependant potential damping matrix

D_l Linear damping matrix

$D_l\dot{x}$ Linear damping matrix

D_q Quadric damping matrix

$D_q\dot{x}$ Quadratic damping matrix

GM_L Longditudinal metasentric height

GM_T Transverse metasentric height

H_s Significant wave height

k_E Elastic Stiffness

k_G Geometric stiffness

q_{CU} Current drag force

q_{cu} Current forces

q_{ext} Any other forces (wave drift damping, specified forces and forces from station-keeping and coupling elements,etc.)

q_{thr} Thruster forces

q_{wa} Wave forces

$q_{WA}^{(1)}$ First order wave excitation force

$q_{WA}^{(2)}$ Second order wave excitation force

q_{WI} Wind drag force

q_{wi} Wind forces

T_H Horizontal tension

T_p	Spectral peak period
T_z	Vertical tension
$T_{c,dyn}$	Characteristic dynamic tension
$T_{c,mean}$	Characteristic mean tension
T_d	Design tension in a mooring line
A	Area
A	Cross section area of tower sections [m^2]
a	particle acceleration
C	Drag coefficient
C	Vind coefficient
D	Diameter of cross section
EA	Young's modulus multiplied with a cross section
H	Reference height [m]
K	Stiffness matrix (non-linear)
M	Mass matrix
q	Exciting force vector
T	Thrust [kN]
u	horizontal particle velocity
U(H)	Wind velocity at reference height [m/s]
u(t)	Dynamic wind gust
U(z)	Wind velocity at position z [m/s]
V	Wind speed [m/s]
x	Position for a given degree of freedom
z	vertical position [m]

Contents

List of Tables

Chapter 1

Introduction

1.1 Background

Green energy production is a hot topic in the scientific society, and offshore wind energy is a promising field. Hywind Scotland is the first operational floating wind turbine park in existence, and a pilot project developed by Equinor. To make floating offshore wind energy competitive against other energy production methods, the cost of installation and production must be kept to a minimum.

For areas where the water depth is above 70m, the cost of a bottom fixed monopile solution starts to be too expensive, and the mooring of floating turbines below 100m is a challenging task. Feasibility of mooring systems at these depth will open up areas were the cost of installation traditionally has been to high.

Today, Hywind Scotland represents the newest installation of the sort, and the mooring system is a traditional chain system. This is an expensive system, and today, no operational floating wind turbines utilizes synthetic fibre ropes. If this proves feasible, the cost of development could be decrease and more potential areas for production becomes available.

1.2 Scope and objectives

The objective of this thesis is to review relevant literature for floating wind turbines with respect to mooring systems, and provide an overview of state-of-art of fixed and floating wind turbines. A description of the design limits of a floating wind turbine is to be presented with the corresponding acceptance criteria. The time-domain analysis for mooring systems is to be described, and a simplified model based on a pre-existing 10MW floating wind turbine concept is to be analysed and compared with the original model. Analysis of different mooring systems is to be conducted, and the results presented in a suitable and orderly fashion. Results and findings shall be discussed with respect to the theory provided in the thesis, and conclusions based on this knowledge is to be presented.

Recommendations for further work shall be proposed on the basis of the performed tests,

discussion and conclusions presented.

1.3 Structure of the report

- A presentation of relevant literature and description of components and state-of-art floating wind turbines.
- Rules and regulations determining the design limit.
- Description of relevant software and time domain analysis.
- Presentation of the initial model and the approach to simplify the model, with details of the performed calculations.
- Presentation of results from the time domain analysis, comparisons with the original model and discussions about the results.
- Conclusion and recommendations for further work.

Chapter 2

Mooring Systems

In this chapter, existing mooring systems and relevant structural components will be explained. This chapter is mainly based on the Handbook of Mooring [2].

2.1 Mooring lines

2.1.1 Chain

There are essentially two types of chain, studded and studless chain. The studded chain is stronger than the unstudded chain, and the stability of the links are better. This makes the chain easy to handle, also when laying down. For permanent mooring the use of studless chain has become more popular, because of less weight per unit. The handling on the other hand becomes more challenging. The chain size is defined by the diameter of the links, indicated D in figure 2.1. The properties of chains varies much, and has to be considered to optimize a mooring system. The properties of the chains used in this thesis are described in Ramnäs Bruk's product catalogue [16]. Chains are popular regarding permanent mooring because it is a durable option with a high breaking strength. The chain mooring lines can also be in contact with the seabed and are resistant towards bottom dragged objects coming in contact with the lines. Chain is an expensive solution, so this is an area where cost potentially can be reduced.

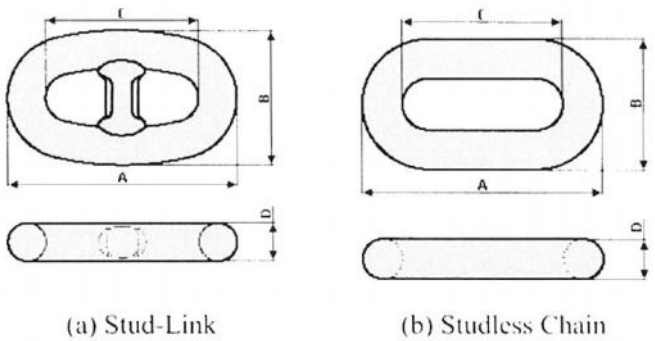

Figure 2.1: Studded and studless chain link [2]

2.1.2 Steel wire

A steel wire used in mooring system offshore is composed of several wires in a helical pattern called a strand, seen in figure 2.2. The configuration of the strands in the wire defines the characteristics, such as strength, fatigue life, etc. The pitch of the wires in a strand define the elasticity [2]. Steel wire is often used in a configuration with chain, with a chain segment at the sea bottom to avoid seabed wear and bending due to installation handling. The steel wire are lighter than the chain systems and steel wire will therefore increase the payload capacity of the system. This type of mooring is also cheaper than chain systems, and easier to handle with respect to installation.

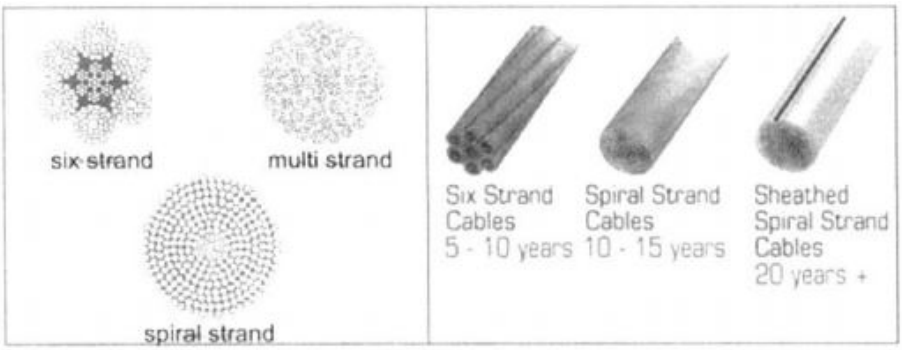

Figure 2.2: Steel wire build [2]

2.1.3 Synthetic fibre ropes

Synthetic fibre ropes are lighter and more elastic than chain and steel wires, this makes fibre ropes easier to handle. The light weight of the ropes combined with the buoyancy makes the weight in water negligible for many instances. This provides the moored structure with an enhanced payload capacity with respect to the traditional mooring systems. The synthetic fibre ropes are composed as illustrated in figure 2.3, with a braided jacket as the outer layer. This is to provide resistance against damage since the ropes are easier damaged than its steel counterparts. For this reason the synthetic ropes are not allowed to touch the seabed, and the lines must always be in tension because temporary slack may decrease the line strength.

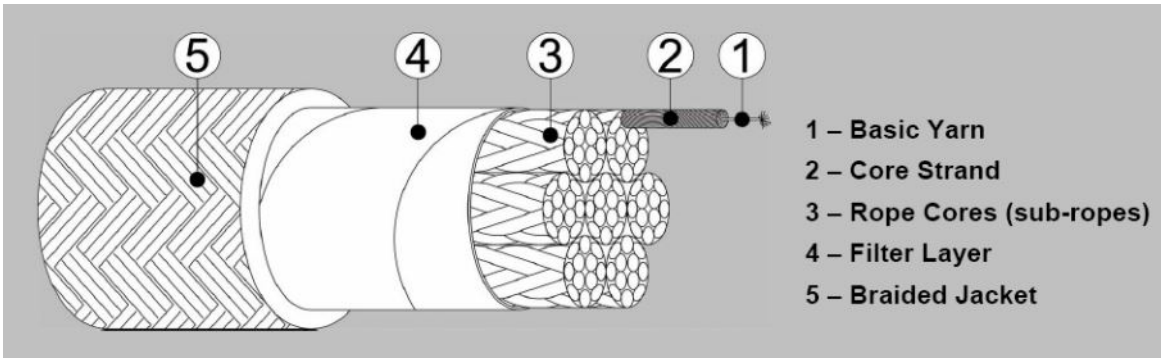

Figure 2.3: Typical build of a synthetic fibre rope [12]

Polyester ropes are not fully elastic, this means that the ropes undertakes plastic deformation and will have a permanent change in length. Figure 2.4 is a visualization of the different contributions to the elongation. Since the tension in a rope is dependent on the line length it will decrees when a line is stretched and plastic deformations makes the rope longer.

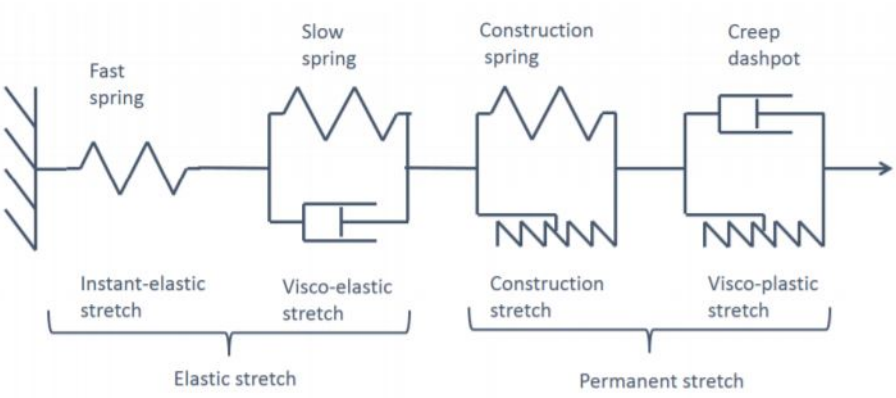

Figure 2.4: Sreatch properties of Syrope, polyester rope [5]

Figure 2.5 shows various tension curves associated with stretching of polyester ropes. The original curve shows the tension of rope under rapid elongation. When this happens the slower visco-elastic stretch don't have time to come into effect. The Original working curve is of a rope that is stretched and given time to elongate fully, this is the curve of interest because the line behaviour will never follow the original curve at offshore structures due to the installation time of the lines. The working curves are the tension in ropes that has been stretched along the original working curve, and will follow the curves below the orignial working curve. When the tension reaches the orignal working curve it will follow this curve until the elongation is reduced and an new working curve further to the right will apply. The Dynamic stiffness is plotted as linear along the points of the working curve. Here the change in tension happens to rapidly for full elongation due to visco-elastic stretch.

For modelling and installation purposes, we need to know the dynamic stiffness and be certain that the dynamic stiffness does not change due to elongation of the rope. To achieve this the ropes are usually stretch well beyond the the elongation expected for the system in working condition. This way the system will operate well below the original working curve, and a change in stiffness due to stretch will not occur.

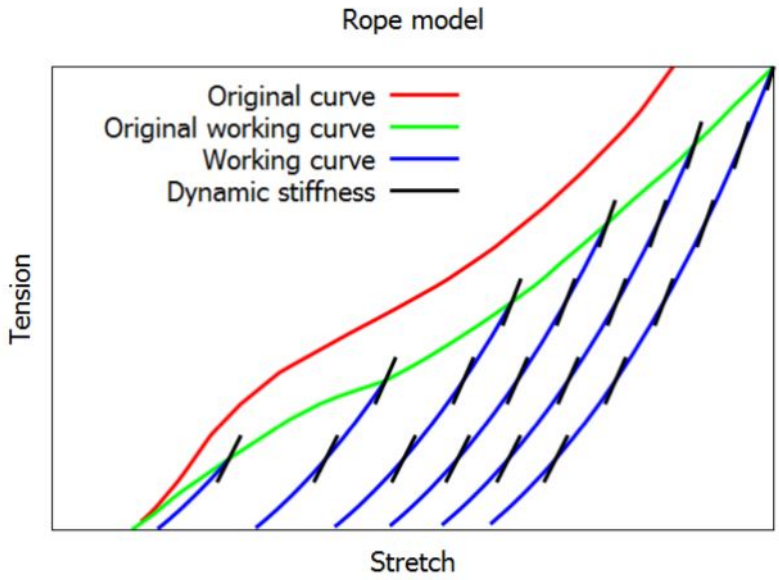

Figure 2.5: Syrope model [5]

The axial stiffness used in this thesis for modelling of mooring lines is given by equation 2.1 based on [5].

$$\frac{EA}{MBS} = 20 + 25\frac{T_m}{MBS} \tag{2.1}$$

2.2 Anchors

2.2.1 Drag embedment anchors

Drag enbedment anchors are one of the most popular anchor used for mooring installations [24]. Drag embedment anchors uses the the resistance in front of the anchor to stay in place. These anchors are usually embedded fully in the sea bottom by tilting the fluke area which is the area at the bottom of the anchor creating a downwards force when dragged against the soil. The depth of the embedment is governed by the type of soil and the pitch angle of the fluke. The drag embedded anchors are suited to large horizontal loads, but are not designed to withstand larger vertical force components. These anchors are designed for mooring lines where segments of the line lie on the sea bottom, typically chain and not fibre ropes.

2.2.2 Vertical loaded anchors

A verically loaded anchor (VLA) i shown in figure 2.7a. These anchors are installed by the same principle as the drag embedded anchors, but are designed to penetrate deeper into the sea bed. When installed the pitch of the anchor is changed to a more horizontal position by the fastening system as shown in figure 2.7b. This enables the anchor to withstand vertical as

Figure 2.6: Drag embedded anchor [25]

well as horizontal forces and can be used for systems where the entire mooring line is lifted from the sea bottom [24].

(a) VLA [25]

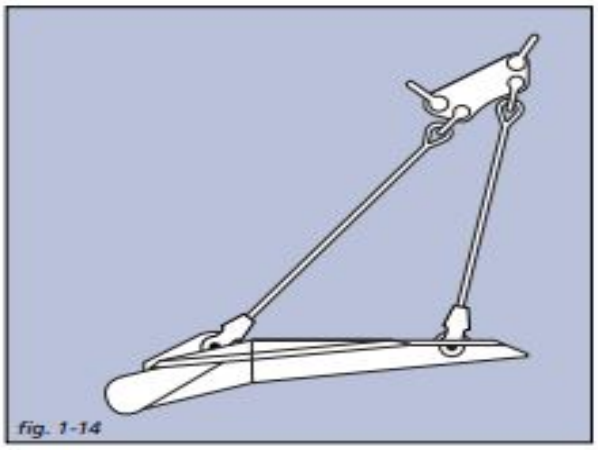

(b) VLA [24]

Figure 2.7: Vertical loaded anchor

These types of anchors are installed by dragging the anchor across the seabed until the predetermined position of the anchor i achieved as illutrated in figure 2.8.

2.2.3 Suction anchors

This anchor is formed like a cylinder with a closed top and a pump attached. When the anchor is lowered and put on the seabed, the water inside the cylinder is pumped ut creating low pressure inside the cylinder. This makes the anchor sink into the seabed utilizing the mass of the soil inside the anchor as weight providing a solid connection point for mooring lines. This type of anchor is well suited to withstand both horizontal and vertical load. The fastening point of the suction anchor is usually placed on the lower end of the anchor to prohibit large rotational forces on the anchor due to the mooring lines, illustrated in figure 2.9b. Suction anchors are expensive, and for a structure were the mooring system is a large part of the total cost other anchors may be considered.

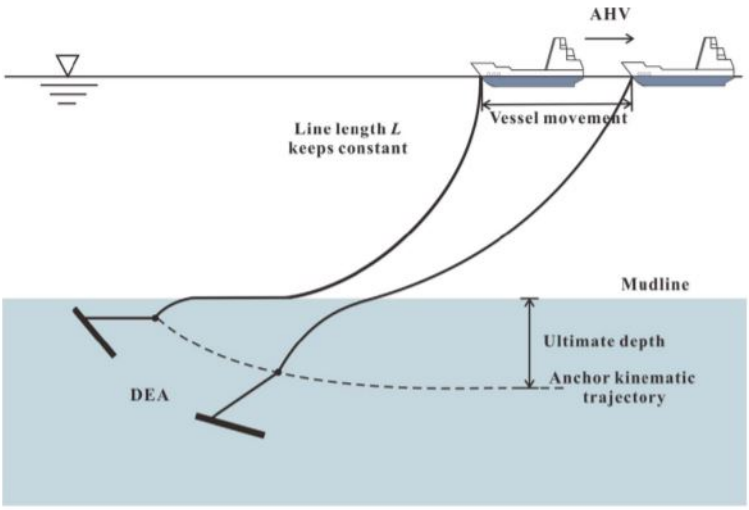

Figure 2.8: Installation of drag embedded anchors [26]

(a) [10] (b) [24]

Figure 2.9: Suction anchor

2.3 Mooring systems

2.3.1 Catenary lines

Catenary lines are considered the traditional mooring lines, and compiled of chain and steel wire. The mooring lines are installed in a hanging slope from the floating structure and down to the anchor, figure 2.10.

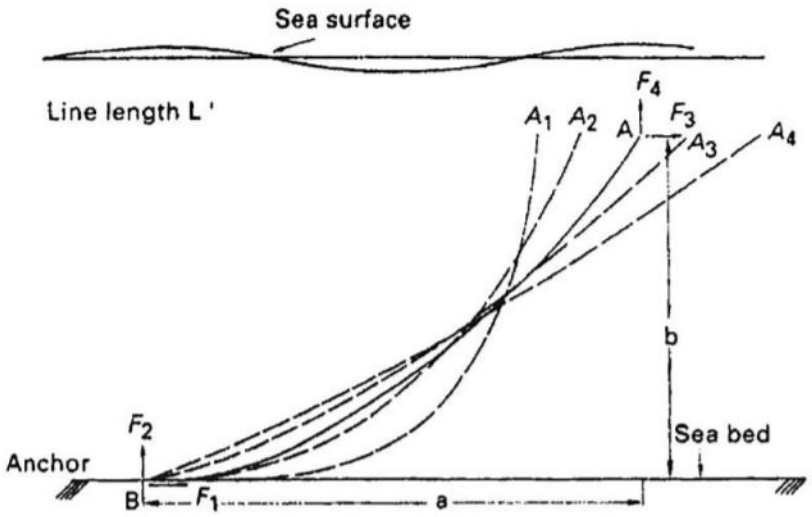

Figure 2.10: Catenary mooring lines [2]

Definition	**Symbol**
Horizontal dimension	a
Vertical dimension	b
Top point of the mooring line	A_n
Tension components	F_n
Line length	L
Possition of the anchor	B

Table 2.1: Symbols: Catenary mooring lines

A_n represents different variations of A, with corresponding line geometry. From a static point of view, the line tension at A corresponds to the weight of cable suspended in water. When A_1 moves to A_2, figure 2.10, the line lift-off due to the change position will increase the tension at point A. For a mooring system, the other side of the floating structure will have decreased cable weight due to a decrease in cable length suspended in water. The resulting tension at A_n is the restoring force for the floating structure.

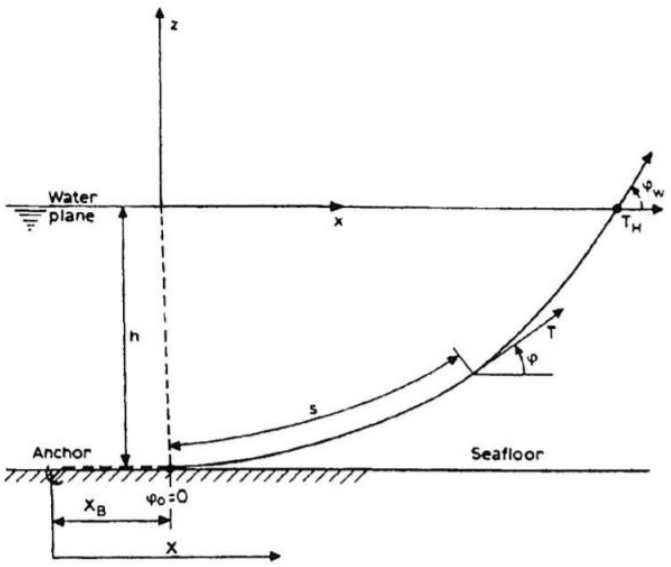

Figure 2.11: Cable line [2]

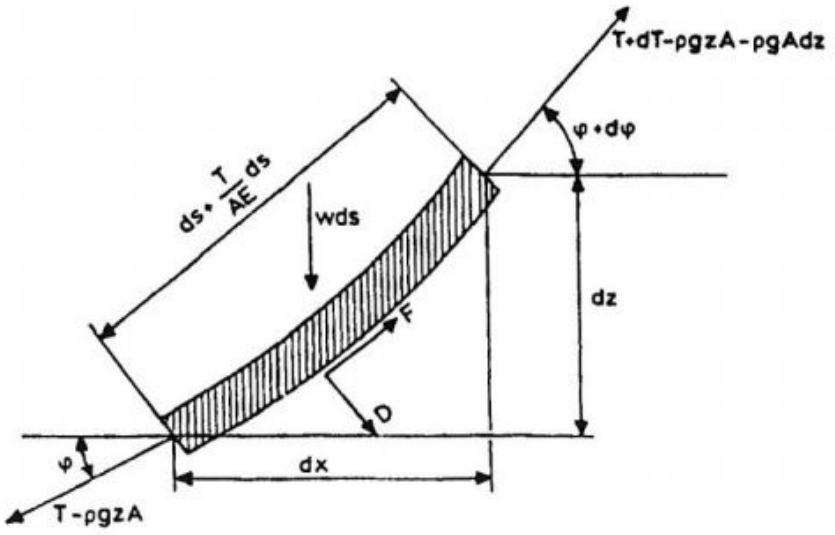

Figure 2.12: Forces acting on a cable [2]

Table 2.2: Symbols: Cable line forces

Definition	Symbol
Depth	h
Length from anchor	X
Cable length suspended in water to a given point	s
Cable tension	T
Horizontal tension	T_H
Tension angle	φ
Weight per unit length	w
Cross sectional area	A
Elastic modulus	E

Considering figure 2.11 the horizontal tension T_H is given by:

$$T_H = T \cdot cos(\phi_w) \tag{2.2}$$

The vertical tension is expressed by the total weight of the line in water:

$$T_H = w \cdot s \tag{2.3}$$

From the single line element shown in figure 2.12, the transverse forces are given by:

$$dT - \rho g A dz = \left[w sin(\phi) - F\left(\frac{T}{EA}\right)\right] ds \tag{2.4}$$

$$T d\phi = \rho g A z d\phi = \left[w cos(\phi) + D\left(1 + \frac{T}{EA}\right)\right] \tag{2.5}$$

2.3.2 Taut mooring

Taut mooring is when the mooring lines are fastened with a tension that keeps the line in a linear shape from the anchor to the floating structure as shown in figure 2.13. The taut mooring configuration depends only on the elasticity of the cable to provide elasticity to the system, i.e. the use of synthetic rope. Due to the light weight of the components, the payload of a structure moored with taut lines will be greater than for a systems with traditional mooring systems. Synthetic ropes are also cheaper than chain or steel cable, so the cost will reduce as well. Figure 2.13 shows a taut mooring line, and key parameters.

The drawbacks of using taut mooring lines in shallow water is that the cable length does not scale down as we move to shallow water. This is because the elasticity is provided by cable length, the cross section and it's elastic modulus, and the system stiffness needed does not change significantly from deep to shallow water. From [12].

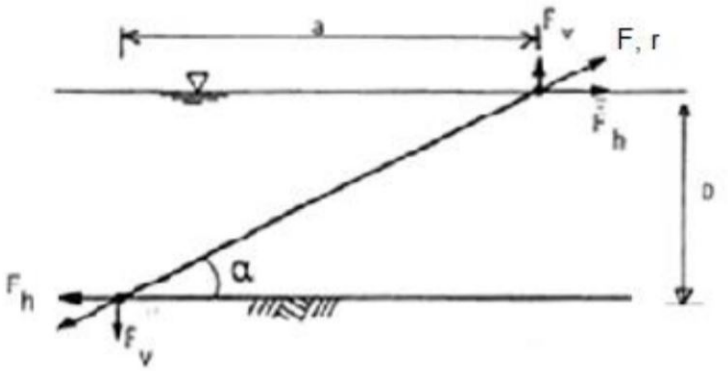

Figure 2.13: Taut mooring configuration [2]

2.3.3 Mooring stiffness

The stiffness of a mooring system can be categorized into two components, geometric stiffness (k_G) and elastic stiffness (k_E).

k_G is due to changes in the geometry of the mooring lines. Using moment equilibrium on the example in figure 2.14, the equilibrium is expressed as $F_h \cdot D = W_w \cdot a$, and F_h can be written:

$$F_h = W_w \cdot \frac{a}{D} \tag{2.6}$$

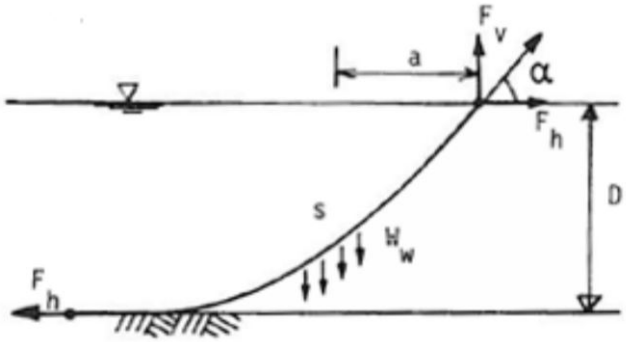

Figure 2.14: Example: Geometric stiffness [2]

The elastic stiffness (k_E) is dependent on the elongation of the mooring line and its elasticity. Considering figure 2.13, the moment equilibrium is $F_h \cdot D = F_v \cdot a$. The total stiffness is a combination of both k_G and k_E as indicated in figure 2.15, and can be written as:

$$\frac{1}{k_T} = \frac{1}{k_G} + \frac{1}{k_E} \tag{2.7}$$

For mooring systems consisting of chain and steel wire the geometric stiffness will be dominating. This means that the lines are inelastic and $k_E >> 1$, thus the only contribution is $\frac{1}{k_G}$. For a taut mooring line the opposite happens, and $k_G >> 1$

Figure 2.15: Representation of the stiffness components [12]

2.3.4 Line characteristics

The line characteristic is the relationship between the horizontal off-set and the horizontal tension. By changing the offset of the structure, the geometry of the mooring line will change or the elongation of the elastic rope will change, a combination of the two will occur for mooring lines with both a significant weight, and sufficiently elastic material. The line characteristic is thus a combination of geometric and elastic stiffness.

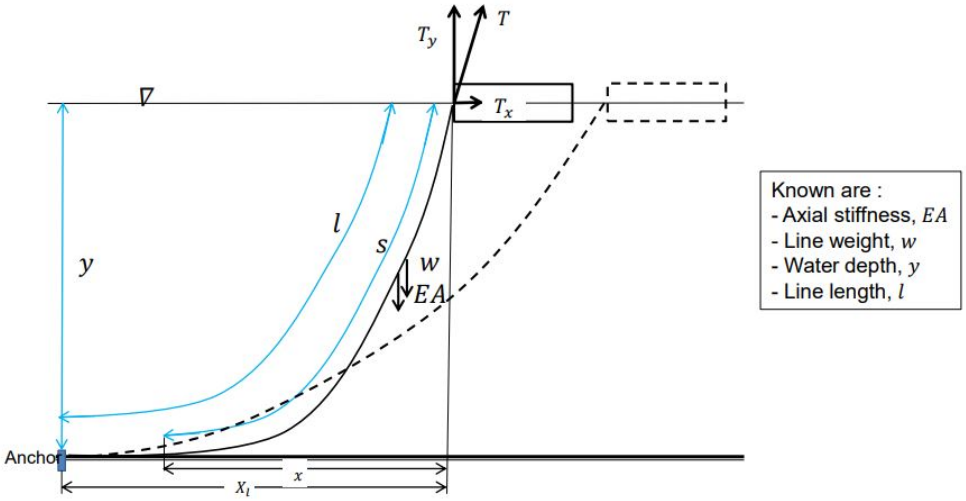

Figure 2.16: Visualization of the line characteristics variables [12]

The variables in the equations defining the line characteristics is defined in figure 2.16, which depicts a mooring line where the geometric stiffness is dominating, and the line has little elasticity by itself ($\frac{T}{EA} << 1$). For an inelastic line the distance from the anchor to the structure can than be expressed as:

$$X_l = l + \frac{T_x}{w} \cdot cosh^{-1}\left(1 + \frac{w \cdot y}{T_x}\right) - \sqrt{y \cdot \left(y + \frac{2T_x}{w}\right)} \tag{2.8}$$

For an elastic line where the weight is neglected the same information can be derived from moment equilibrium, $F_h \cdot D = W_w \cdot a$. In the line characteristic for a conventional chain mooring line, the tension will increase more rapidly when the offset becomes larger. For an elastic mooring line the increase in tension due to offset will follow a linear path, and for systems combining elastic and non-elastic materials the line characteristics will be a combination of the two.

Mooring systems can be compiled of many mooring lines positioned at different angles

with different characteristics. The total restoring forces acting on a system can be found by combining the horizontal tension (T_x) found from the line characteristics as a function of the offset, and the spread angle (ψ):

$$Surge: \qquad F_x = \sum_{i=1}^{n} T_{x_i} \cdot cos\psi_i \tag{2.9}$$

$$Sway: \qquad F_y = \sum_{i=1}^{n} T_{x_i} \cdot sin\psi_i \tag{2.10}$$

$$Yaw: \qquad M_r = \sum_{i=1}^{n} T_{x_i} \cdot [x_i \cdot sin\psi_i - y_i \cdot cos\psi_i] \tag{2.11}$$

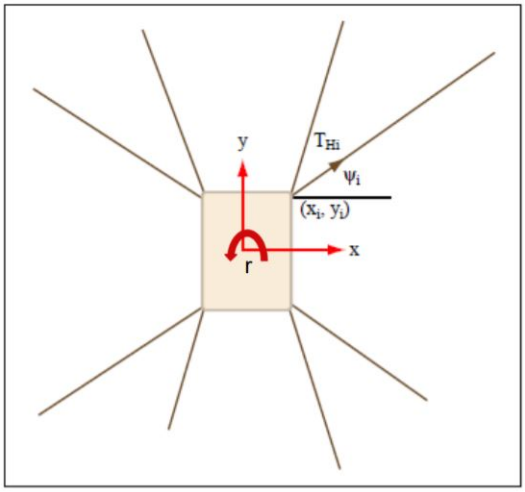

Figure 2.17: Restoring forces [12]

2.3.5 Combination of chain and synthetic fibre rope

Systems which combine the use of chain and synthetic fibre ropes are lighter than the full chain or steel wire systems, and less expensive due to the cost of fibre ropes. A problem with the use of only synthetic fibre ropes in mooring systems is that the line length has to be long independent of the depth. This is because the stiffness of a taut mooring rope system is only dependent on the axial stiffness, and to get the system to be able to absorb the environmental loads the lines need to be long enough to provide the required elasticity. By introducing chain sections to the system as shown in figure 2.18, the geometric stiffness will decrease as well as the total stiffness. As mentioned in section 2.3.2 a requirement for a synthetic line is that it will always be in tension. With at chain-polyester line as in figure 2.18 the pretension of the mooring line can be lower and due to the weight of the suspended chain the polyester section will always have tension. This can also be accomplished by clump weights and buoys.

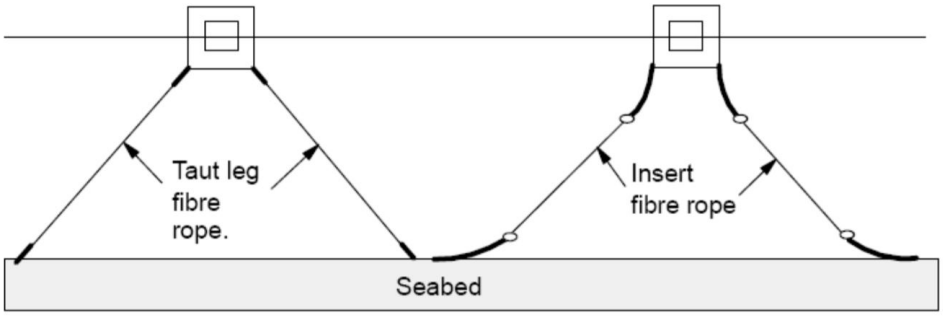

Figure 2.18: Combination of chain and synthetic fibre rope mooring [12]

2.3.6 Line weight and buoyancy

2.3.7 Clump weights and buoyancy elements

Clump weights and buoyancy elements are components added to the mooring lines to change the geometry or the weight of the lines. By using these components at one or several point of the line can be changed to get specific results. For example, taut mooring lines usually have a weight in water, and can therefore touch the ground if the tension gets low. By applying a buoyancy element, the line can be lifted from the seabed as seen in figure 2.19. This is also a way to provide a constant state of tension in polyester lines. The same principle applies for clump weights, were one can change the weight of a line to provide a larger geometric stiffness, and create an altogether stiffer mooring system.

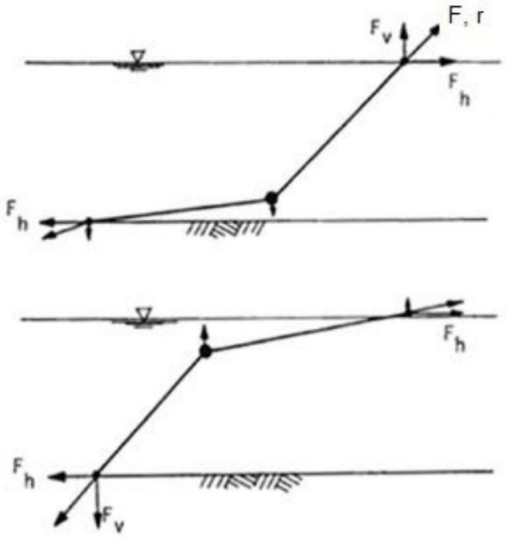

Figure 2.19: Weights and buoys on mooring lines [12]

For taut mooring lines, clump weights and buoyancy elements can also change the angle of tension acting on the structure, and the added or removed weight from a mooring system will affect the payload capacity of the system.

Chapter 3

The Gumbel distribution

The Gumbel distribution is used as an approximate distribution of the individual maximum value of a time series. For a sample $y_1, y_2, ..., y_n$ the cumulative distribution and the probability density function of the individual maxima $y = max\{x_1, x_2, ..., x_n\}$ will follow equations 3.1 and 3.2.

$$F_y(y) = exp{-e^{-\alpha(y-u)}} \quad -\infty \leq \infty \tag{3.1}$$

$$f_y(y) = \alpha \; exp{-\alpha(y-u) - e^{-\alpha(y-u)}} \tag{3.2}$$

The asymptotic behaviour of the Gumbel distribution gives the following Gumbel parameters estimated of a sample of extreme values:

$$c_1 = 1.28255$$
$$c_2 = 0.57722$$

$$\hat{\alpha} = \frac{c_1}{\hat{s}_y} \tag{3.3}$$

$$\hat{u} = \hat{\mu}_y - \frac{c_2}{c_1}\hat{s}_y \tag{3.4}$$

As seen in figure 3.1 the accuracy of this model increases with the number of samples used to calculate the Gumbel parameters. This model is regarded as a good model to determine extreme values and will be used to determine the maximum values of line tension in this thesis [13].

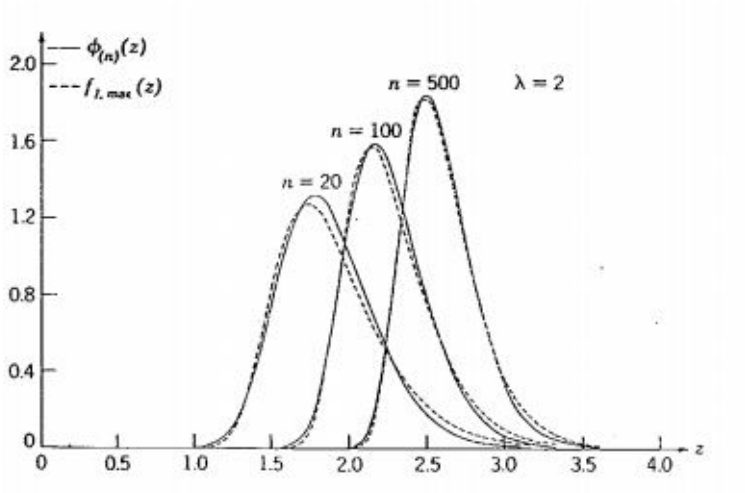

Figure 3.1: Excact and approximate extreme value densities for a weibull sample of σ=1 and λ=2 [13]

Chapter 4

Offshore turbine concepts

For structures installed in shallow water, 0-70m, bottom-fixed concepts are used. As indicated in figure 4.1, the mono-pile is used for water depth <30m, and the jacket structure for 30 to 70m. For larger water depths, floating wind turbines are installed. There are several concepts of offshore wind turbines available, some will be described in this chapter.

4.1 Bottom fixed turbines

Figure 4.1 shows bottom fixed turbines with the respective water depths for installation. At low water depths the cost of mooring systems out weights the cost of a bottom fixed structure, so bottom fixed structures are used. The mono-pile is a turbine tower that is placed into the seabed. The slender body of the mono-pile will cause minimal drag forces due to waves.

The other type shown in figure 4.1 is the jacket structure. These structures are wider than the mono-piles, and base forces of the tower will be reduced. When the water depths increases, the overturning moment will also increase, and jacket structures are favourable. The elements that compile the jacket structures are slender and drag will be minimal.

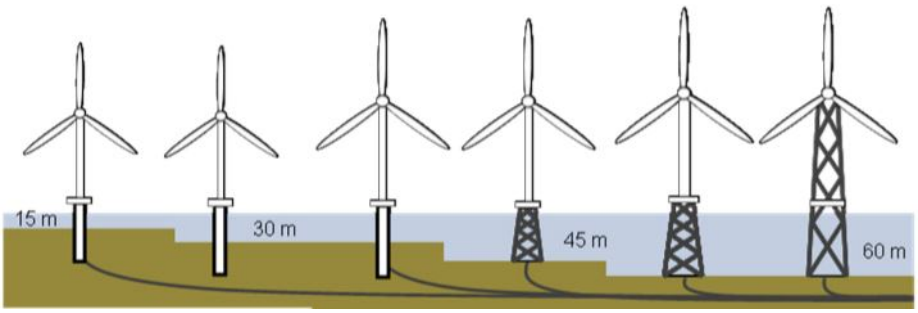

Figure 4.1: Bottom fixed offshore wind turbine concepts [8]

Bottom fixed turbines are rigid, and the turbine will not have large motions in any direction. This is favourable when designing a turbine, and a loss in mechanical output due to different attack angles are minimal.

4.2 Floating turbines

For larger water depths floating structures is used for wind turbines [8]. Figure 4.2 shows to concepts of floating turbines, the spar buoy and a semi submersible. The spare buoy is usually used for deep waters since the draft is relatively large, and the stability is due to weights in the buoy below the free surface. This concept provides a structure with a small free surface area, and good stability due to the long body. The second concept in figure 4.2 shows a semi-submersible structure below a wind turbine. Theoretically this will be favourable for shallow water, around 70m, since the draft is considerably lower than for the spar-buoy which can exceed 70m [9]. The stability for the semi-submersible structures are provided by the geometry in the water plane by utilizing hydrostatic and hydrodynamic forces. There are also concepts for floating wind turbines with dynamic ballasting which can reduce the draft by using the geometry and ballast to counter forces from different directions. For this thesis the CSC semi-submersible concept developed by Wang at NTNU is assessed [1].

Figure 4.2: Floating offshore wind turbine concepts [8]

4.2.1 Windfloat

Wind float is a floating foundation developed by Principle power for offshore wind turbines [14]. It is designed to operate at depths above 40m, and it is a semi-submersible structure compiled of 3 columns fastened together with trusses. In addition to the hydrodynamic stiffness provided by the geometry, stability is enhanced with active ballast through a hull-trim system in the columns and water entrapment plates at the base of each column as shown in figure 4.3.

The turbine is not placed at the centre of the structure and to compensate for the initial pitch due to an asymmetrical centre of gravity in x and y-direction the ballast tanks are filled

to correct the centre of gravity. The ballast tanks are shown in shown in figure 4.3. The water entrapment plates function as a heave compensator making it more stable in waves. The result is a structure that have less pitch and heave motion than a similar static semi-submersible.

This structure also makes it possible for a full assembly quay-side due to its low and adjustable draft. This will decrees the production cost and also make it possible to assemble at a larger range of sites. This concept has been tested in full-size by Principle Power off the coast of Portugal.

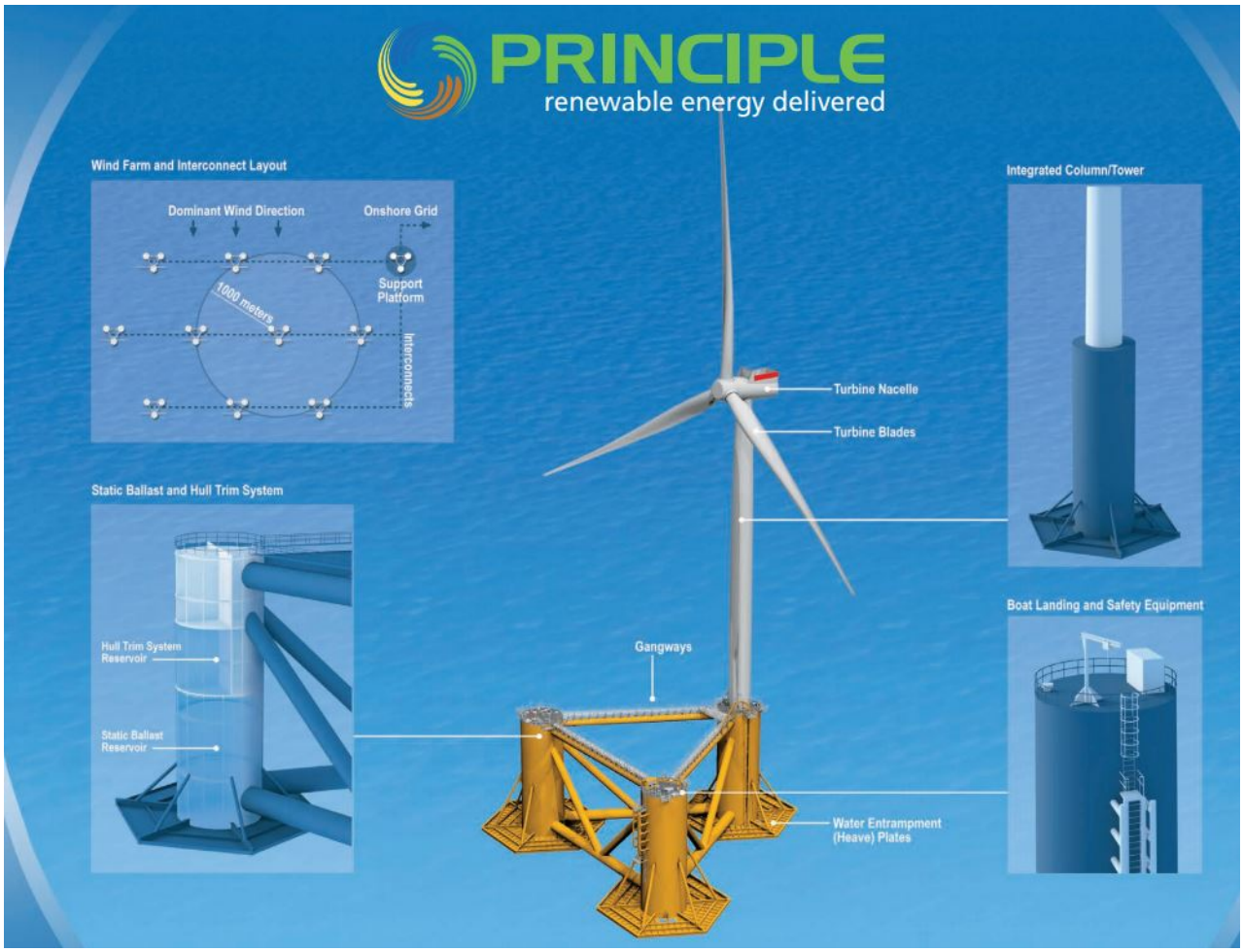

Figure 4.3: Principle power floating wind turbine [15]

4.2.2 CSC 10MW wind turbine

The design for the semi-submersible 10MW wind turbine was proposed by Qiang Wang [26], and is based on a earlier concept of a 5MW wind turbine. This is a semi-submersible structure with pontoons connecting three columns at the side of the turbine tower, as shown in figure 7.1. The stability of this model relies upon the buoyancy of at the columns rather than the dominating inertia forces from a low centre of gravity. It has ballast tanks located in the pontoons at the bottom of the structure which can be filled to lower the centre of gravity and

increase the total weight. This structure has no active ballast or hull-trim systems to provide stability, but a small surface area will make it less sensitive to wave motions.

The advantages of such structures as the 10MW CSC and Windfloat is that the draft is low, and they can be installed at small depths. When installing, it is not needed to tilt them into the right position as is needed for spar-buoy solutions.

This is the original model for this thesis and will be described in further detail in section 7.1.

4.3 Hywind Scotland

Hywind Scotland is the first full scale floating offshore wind turbine park in existence, shown in figure 4.4. It is Equinor's pilot project based on the Hywind Demo turbine off the coast of Norway. The geometry of the floater is a spare-buoy with a drought of 78m and sub structure diameter of 14.4m. Hywind Scotland is located off the coast of Peterhead Scotland, at a water depth of 105m and consists of 5 turbines with three mooring line each [9]. Due to its slender body and low centre of gravity this concept has little motion due to waves. Because of the large draft it cannot operate at water depths much lower than 100m due the risk of contact with the seabed.

Figure 4.4: Hywind Scotland pilot park [6]

The mooring line consists of two studless chain segments with different dimensions. The bridle is installed to add stiffness in yaw, and consists of a 132mm NVR4S, and the rest of the mooring line consists of a 147mm chain segment. This is a classical mooring system governed by the catenary equations found in section 2.3.1. Three suction anchors (5m ø x 15.5m) are used, with an anchor radius of 690m. The pretension at the triplate is 900 kN [20]. A bridle is not needed for the semi-submersible structures mentioned above because the

mooring lines are already fastened a sufficient distance from the centre of rotation, creating stiffness in yaw.

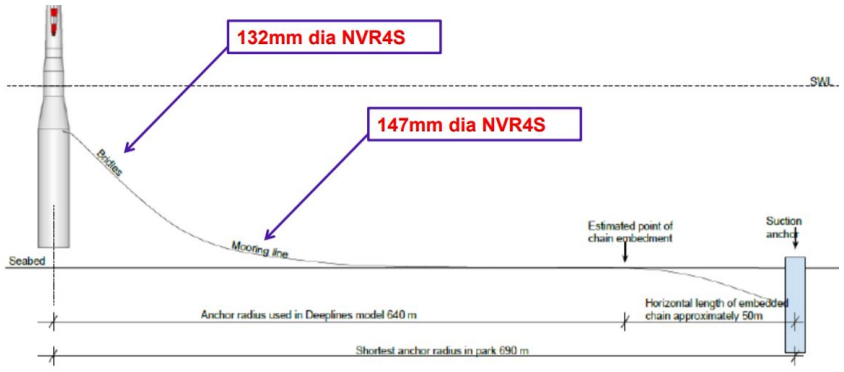

Figure 4.5: Hywind Scotland mooring line [20]

The mooring lines are fastened with a system that can rotate 180 deg horizontally and 70 deg vertically without crating additional tension at these points [20]. The advantages of this system is that large waves, for example during storms, will not affect the systems total braking strength. Also if one line is broken, the new angle for the mooring lines due to the structure drifting into a new position will not cause additional tensions.

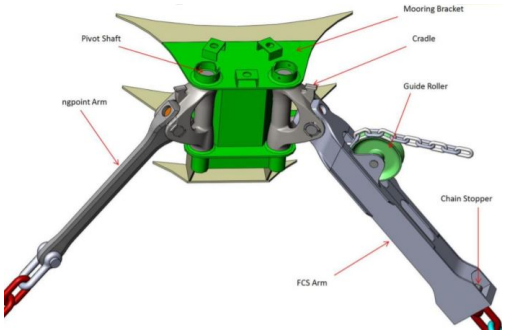

Figure 4.6: Hywind Scotland fastening system [20]

Chapter 5

Rules and regulations

5.1 Ultimate limit state

Ultimate limit state (ULS) for floating wind turbines is a storm with a 50-year return period, and current with a 10-year return period [23].

The design tension T_d in a mooring line is found the equation 5.1.

$$T_d = \gamma_{mean} \cdot T_{c,mean} + \gamma_{dyn} \cdot T_{c,dyn} \tag{5.1}$$

The characteristic mean tension $T_{c,mean}$ is defined as the mean part of the 50-year value of the line tension. $T_{c,mean}$ will be a combination of pretension and mean environmental loads from dynamic wind, current and wave drift. The characteristic dynamic tension $T_{c,dyn}$ is defined as the dynamic part of the 50-year value of the line tension and is caused by oscillatory low-frequency and wave-frequency effects. To estimate $T_{c,mean}$ and $T_{c,dyn}$ several trial sea states defined in terms of T_p,H_s and U_{10} along a 50-year contour plot. $T_{c,mean}$ and $T_{c,dyn}$ is selected from the particular sea state that gives the largest line tension response along the 50-year contour line from figure 9.1. The tension in the lines are dependent on the direction of the environmental loads, and the process of finding $T_{c,mean}$ and $T_{c,dyn}$ from the contour plot is done under the assumption that the environmental loads are coming from the least favourable direction.

Note that the 50-year value of the line tension may not occur during the sea state along the 50-year environmental contour. During wind speeds were the turbine is fully operational the thrust is often highest and this may cause the highest drift and largest loads in the mooring system, it is therefore important to evaluate these wind speeds. The load factors is given by table 8-1 in [23], shown in figure 5.1.

When dimensioning a wind turbine for ultimate limit state (ULS), equation 5.1 is considered with the 50-year value of the line tension for a system with intact mooring lines. The load factors are found from figure 5.1, and a system with a design tension below the maximum breaking load (MBL) of the mooring lines are within the requirements for ULS condition.

5.1.1 Accidental limit state

Accidental limit state (ALS) is a state were failure of one line has occurred, the design tension must be of a magnitude that ensures no further failure of mooring lines. The line that endures the highest loads is broken, and the characteristic mean tension and the characteristic dynamic tension, as well as the load factors, are found by the same procedure as for ULS. The condition which has the largest design tension, either ULS or ALS will be the dimensioning condition. This means the condition with the largest T_d

Table 8-1 Load factor requirements for design of mooring lines

Limit state	*Load factor*	*Safety class*	
		Normal	*High*
ULS	γ_{mean}	1.3	1.5
ULS	γ_{dyn}	1.75	2.2
ALS	γ_{mean}	1.00	1.00
ALS	γ_{dyn}	1.10	1.25

Figure 5.1: Load factor requirements for design of mooring lines [23]

In this thesis $T_{c,mean}$ is defined as the mean line tension taken from time series, and $T_{c,dyn}$ is the expected largest line tension found by the Gumbel distribution defined in chapter 3 with $T_{c,mean}$ subtracted.

5.2 Fibre ropes

For fibre ropes the same calculation of the design tension as for chain applies, for both ULS and ALS calculation. Another condition to be met for fibre ropes is that the ropes can not go slack, and slack in this thesis is defined as a most probable minimum tension below zero. This means that the allowed probability for slack can be well above 0, depending on the method used to calculate the minimum tension distribution.

Chapter 6

Time domain analysis

6.1 SIMA

The SIMA workbench offers a complete solution for the simulation and analysis of marine operations and floating systems. It supports the entire process from the definition of the simulation and its execution to the interpretation and documentation of the results. [17]

The workbench allows the user to work with different programs individually or coupled, for this thesis the programs of interest are SIMO and RIFLEX which respectively offer solutions for bodies and slender elements.

6.1.1 SIMO

SIMO (Simulation of marine operations) is a time domain simulation program for the study of motions and station keeping of multiple systems. Flexible modelling of station keeping forces are included, and the output from SIMO include time series of forces and motions, statistics and spectral analysis for all forces and motions [4].

The main features found in [4] makes SIMO a versatile tool for modelling marine structures and the forces action on them. Hydrodynamic coefficients can be directly importet from programs like WADAM and WAMIT. For this thesis the body of the wind turbine semi-submersible floater is modelled using SIMO and the forces are calculated from this software.

6.1.2 RIFLEX

RIFLEX (Riser system analysis program) is a program for analysis of flexible risers and other slender structures, such as mooring lines, fich cage systems, pipelines and also steel risers [3]. Riflex is based on finite element modelling, and performs dynamic time domain analysis based on all forces acting on the discretized finite element model.

6.2 Equation of motion

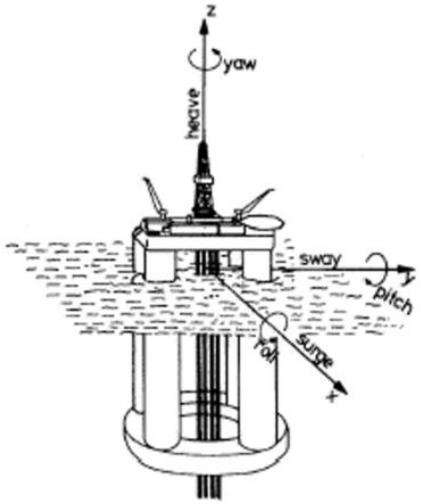

Figure 6.1: Degrees of freedom for a floating structure [11]

The equation of motion for 6 degrees of freedom as indicated in figure 6.1 is written:

$$\big(M + A(\omega)\big) \cdot \ddot{x} + C(\omega) \cdot \dot{x} + D_l \dot{x} + D_q \cdot \dot{x}|\dot{x}| + K \cdot x = q(t, x, \dot{x}) \tag{6.1}$$

This equation is solved by SIMO for every degree of freedom to get the total motion of the Wind turbine [4].

The first section ,$\big(M + A(\omega)\big) \cdot \ddot{x}$, is mass dependant, here the contribution of the mass and frequency-added mass are calculated. $C(\omega) \cdot \dot{x} + D_l + D_q \cdot \dot{x}|\dot{x}|$ are the damping terms. $C(\omega)$ is the linear damping matrix (D_l) is calculated by Wang using HydroD [1]. $D_q \cdot \dot{x}|\dot{x}|$ is the quadratic damping terms, with contribution from wind forces, calculated in section 7.3.5 and wave forces from HydroD.

The last term, $K \cdot x$, is the stiffness contribution. The stiffness in this model is defined by the mooring system as described in section 2.3.3 and by calculating the hydrostatic stiffness:

$$\bullet\ Heave = \rho g A_{wl} \tag{6.2}$$

$$\bullet\ Roll = \rho g \nabla G M_T \tag{6.3}$$

$$\bullet\ Pitch = \rho g \nabla G M_L \tag{6.4}$$

6.2.1 Excitation forces

The total excitation forces calculated by SIMA is given by the equation:

$$q(t, x, \dot{x}) = q_{wi} + q_{cu} + q_{wa} + q_{thr} \tag{6.5}$$

Characteristics of the components in equation 6.5:

• Wind forces, q_{wi}:

- Mean value due to mean velocity.
- Low frequency forces excited by wind gusts.

• Current forces, q_{cu}:

- Mean value due to mean current velocity.
- Current turbulence is neglected.

• Wave forces, q_{wa}:

- 1^{st} order forces proportional with wave amplitude is described by force transfer functions.
- Mean value due to 2^{nd} order wave loads.
- Low-frequency forces exited by 2^{nd} order wave loads.

• Thruster forces, q_{thr}:

- Mean forces and/or dynamic forces dependent on automatic or manual control. There are no thrusters in this model, so these forces are neglected.

This explanation is taken from the lecture notes given by Kjell Larsen [11].

6.2.2 Wind forces

For a given degree of freedom the wind forces can be calculated from equation 6.6.

$$q_{wi}(t) = \frac{1}{2} \cdot \rho_{air} \cdot C_D \cdot A \cdot (U(t) - \dot{x})^2 \tag{6.6}$$

Here $U(t) = \bar{U} + u(t)$ by this into equation 6.6 it can be separated into three different components:

$$q_{wi}(t) \approx \underbrace{\frac{1}{2} \cdot \rho_{air} \cdot C_D \cdot A \cdot \bar{U}^2}_{\text{Constant force}} + \underbrace{\rho_{air} \cdot C_D \cdot A \cdot \bar{U} \cdot u(t)}_{\text{LF excitation force}} - \underbrace{\rho_{air} \cdot C_D \cdot A \cdot \bar{U} \cdot \dot{x}}_{\text{LF damping force}} \tag{6.7}$$

The first component represents the constant forces acting on the structure due to wind loads, the second represents low-frequency excitation forces and the third component represents low-frequency damping forces.

6.2.3 Current forces

$$q_{cu} = \frac{1}{2} \cdot \rho_{water} \cdot C_D \cdot A \cdot |\bar{V} - \dot{x}| \cdot (\bar{V} - \dot{x}) \tag{6.8}$$

The current for this thesis is assumed constant and of equal velocity for every water depth. If $\bar{V}$ is larger than $\dot{x}$ equation 6.8 can be written as:

$$q_{cu}(t) \approx \underbrace{\frac{1}{2} \cdot \rho_{water} \cdot C_D \cdot A \cdot \bar{V}^2}_{\text{constant force}} + \underbrace{\rho_{water} \cdot C_D \cdot A \cdot \bar{V} \cdot \dot{x}}_{\text{LF domping force}} \tag{6.9}$$

The first term in equation 6.9 is the constant force acting on the model due to current, while the second represents low-frequency damping force.

6.2.4 Wave forces

The wave forces on the model is given by the Morrison equation [7] calculated by the RIFLEX software at predetermined slender elements to capture the structures shape:

$$q_{wa} = \int \rho_{water} \frac{\pi D^2}{4} \cdot C_M \cdot a \, dz + \frac{1}{2} \rho_{water} \cdot C_D \cdot A \cdot |u| \cdot u \tag{6.10}$$

6.3 Solving the equation of motion

There are two ways to solve the equation of motion for the time domain, separation of motions and the standard approach is by the convolution integral.

6.3.1 Convolution integral

Solving by the convolution integral is done by time integration where the aim is to get the entire equation of motion in to the time domain.

$$\underbrace{A(\omega) \cdot \ddot{x} + C(\omega) \cdot \dot{x}}_{f(t)} = q(t, x, \dot{x}) - D_l \dot{x} - D_q \cdot \dot{x}|\dot{x}| - K \cdot x - M\ddot{x} \tag{6.11}$$

When starting with the equation of motion 6.11, in the frequency domain the equation of motion can be expressed by:

$$F(\omega) = (-\omega^2 A(\omega) + i\omega C(\omega)) X(\omega) \tag{6.12}$$

$$X(\omega) = \frac{1}{2\pi} \int_{-\infty}^{\infty} x(t) e^{i\omega t} dt \tag{6.13}$$

Using the relations of equation 6.14 and 6.15 where $A_\infty = A(\omega = \infty)$ and $C_\infty = C(\omega = \infty) \equiv 0$ equation 6.12 is written as equation 6.16.

$$A(\omega) = A_\infty + a(\omega) \tag{6.14}$$

$$B(\omega) = C_\infty + c(\omega) \tag{6.15}$$

$$-\omega^2 A_\infty X(\omega) + (i\omega a(\omega) + c(\omega)) i\omega X(\omega) = F(\omega) \tag{6.16}$$

Using the inverse Fourier transform gives equation 6.17

$$A_\infty \ddot{x}(t) + \int_{-\infty}^{\infty} h(t-\tau)\dot{x}(\tau)d\tau = f(t) \tag{6.17}$$

The values for $h(t-\tau)$ for t<0 is the values before the simulation begins, and is equal to 0. This gives equation 6.18.

$$A_\infty \ddot{x}(t) + \int_{0}^{\infty} h(t-\tau)\dot{x}(\tau)d\tau = f(t) \tag{6.18}$$

To solve the equation of motion in the time domain equation 6.18 is put into equation 6.11:

$$A_\infty \ddot{x}(t) + D_l\dot{x} + D_q \cdot \dot{x}|\dot{x}| + K(x)\cdot x + M\ddot{x} + \int_{0}^{\infty} h(t-\tau)\dot{x}(\tau)d\tau = q(t,x,\dot{x}) \tag{6.19}$$

$h(\tau)$ is the retardation function and is found by a transform of the frequency-dependent added-mass and damping, and can be expressed as equation 6.20 for $\tau > 0$.

$$h(\tau) = \frac{2}{\pi}\int_0^\infty c(\omega)cos(\omega\tau)d\omega = -\frac{2}{\pi}\int_0^\infty \omega a(\omega)sin(\omega\tau)d\omega \tag{6.20}$$

This implies that the retardation function can be use to find the frequency-dependent added-mass and damping by equations 6.21 and 6.22

$$a(\omega) = -\frac{1}{\omega}\int_0^\infty h(\tau)sin(\omega\tau)d\tau \tag{6.21}$$

$$c(\omega) = -\int_0^\infty h(\tau)cos(\omega\tau)d\tau \tag{6.22}$$

From the SIMO theory manual [18].

The equation of motion given by equation 6.19 is solved by SIMO for each time step with respect to x. This means that the time sted chose for each simulation is importet with respect to the accuracy of the simulation.

6.3.2 Separation of motions

As an alternative to solving the equation of motion by the convolution integral, it can be solved separating the motions into a high frequency part $q^{(1)}$ and a low frequency part $q^{(2)}$. The high frequency motions are solved in the frequenzy domain, and the motions is needed to be linear responses to the waves.

$$\begin{aligned} q(t,x,\dot{x}) &= q^{(1)} + q^{(2)} \\ q^{(1)} &= q^{(1)}_{WA} \\ q^{(2)} &= q_{WI} + q^{(2)}_{WA} + q_{CU} + q_{ext} \end{aligned} \tag{6.23}$$

The position vector can then be separated to equation 6.24,

$$x = x_{LF} + x_{HF} \tag{6.24}$$

The high frequency motions to be solved in the frequency domain are expressed by equation 6.25

$$m + a(\omega)\ddot{x}_{HF} + D_l\dot{x} + C(\omega)\dot{x}_{HF} + Kx_{HF} = q^{(1)}_{WA}(\omega) \tag{6.25}$$

The low frequency motions are sloved in the the time domain, and the dynamic equilibrium equation is written as equation 6.26

$$m + A(\omega = 0)\ddot{x}_{LF} + D_l\dot{x}_{LF} + D_q\dot{x}|\dot{x}| + Kx_{LF} = q^{(2)} = q_{WI} + q^{(2)}_{WA} + q_{CU} + q_{ext} \tag{6.26}$$

From the SIMO theory manual [18]

6.4 Line tension

There are several ways of calculating the forces from the mooring system acting on the floating structure. In this thesis the quasi-static and dynamic solution will be described. The solution used in this thesis is the dynamic solution.

6.4.1 Quasistatic solution

A quasistatic solution of the equation of motion in this case means that the motions of the mooring lines are neglected. The tension from the mooring lines acting on the system can be considered as three springs with a magnitude given by the catenary equations for a system with internal equilibrium. This means that the drag an inertia forces acting on the mooring lines are not simulated but calculated with coefficients. The forces from the mooring lines is dictated by the system characteristics, and the equation of motion is solved for every position and is put into the line characteristic to extract the line tension.

6.4.2 Dynamic solution

There are two kinds of dynamic solutions proposed by SIMA, SIMO coupled with RIFLEX and an approach where the two solutions are separated.

RIFLEX is a program for modelling slender elements, so the moorig system is modelled in RIFLEX. The dynamic solution also takes the drag and inertia forces of the mooring lines into account, and this provides additional stiffness to the system.

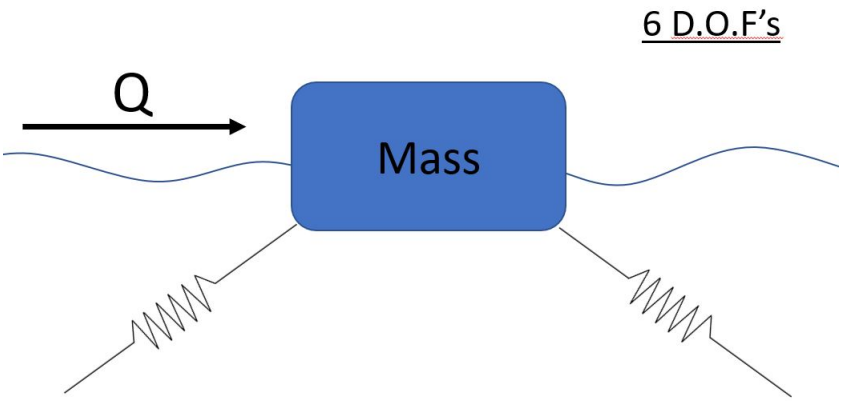

Figure 6.2: Illustration of forces considered in the quasistatic solution

Separated approach

The separated approach uses the motions of the model found by a simulation in SIMO with the same mooring system to be used in RIFLEX and transfers these motions directly to the RIFLEX model. By utilizing the motions of the SIMO model the forces along the cable can be estimated. The problem with this approach is that the motions introduced to the system is independent of the forces from the mooring system, and the contribution from the mooring system on the top-motions will be captured inaccurately. This approach is less time consuming than the coupled approach.

Coupled approach

The coupled approach accounts for the coupling effect between the motions of the floating structure, and the drag and inertia forces acting on the mooring lines. Using a SIMO-RIFLEX coupled model the motions and forces acting on the model will be calculated for all degrees of freedom at every time step. The accuracy of this simulation will be based on the discretization of the mooring lines, and the accuracy of the model imported into SIMO, and are generally regarded the most accurat of the simulation models used in SIMO-RIFLEX.

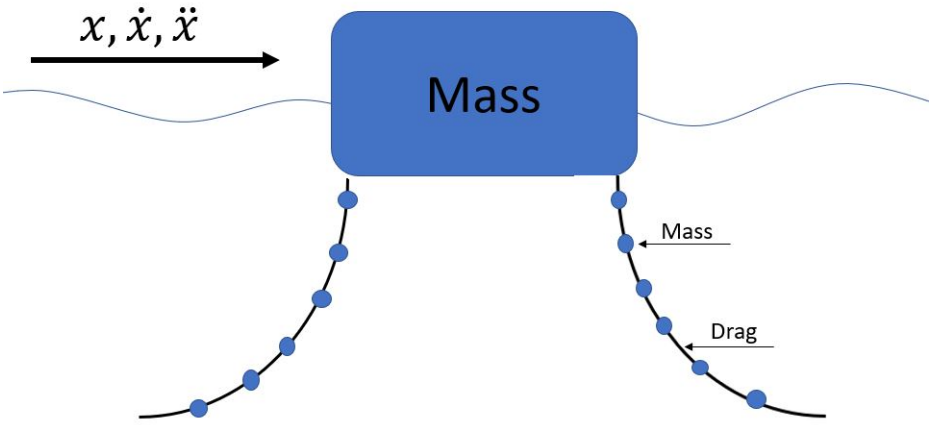

Figure 6.3: Illustration of the coupled approach

Chapter 7

Design

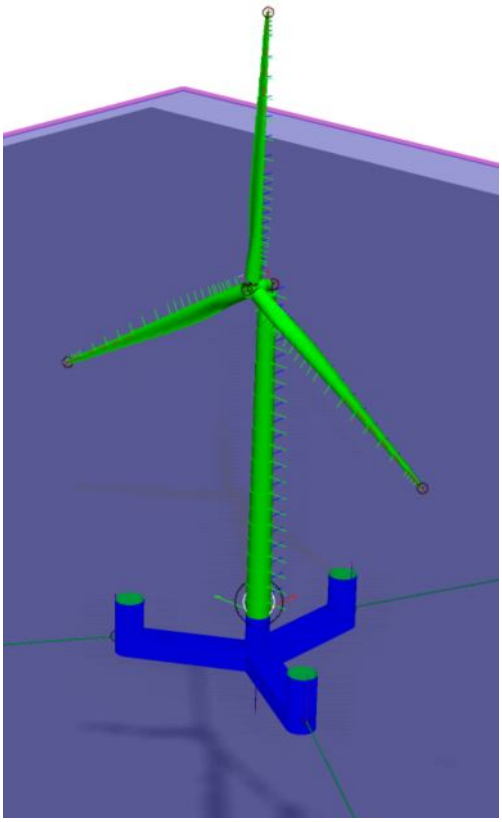

Figure 7.1: 3D view of given Sima task

7.1 Initial design

The basis of the model in this thesis is a pre existing semi submersible structure scaled by Wang [1] to support the DTU 10MW reference wind turbine developed by the department of Wind Energy at the Technical University of Denmark (DTU) [1]. The structure is shown in figure 7.1. The simplified model consists only of the semi-submersible structure, with the

additional weight of the wind turbine, and the tower. To account for the loss of thrust on the model from wind speed when the structure above the water surface is removed, a total wind coefficient is calculated based on the given data. This provides both thrust and a moment acting on the model.

Figure 7.2 shows the design of the semi-submersible structure of the wind turbine. Table 7.1 is the calculated mass and centre of gravity for each section and for the total simplified model.

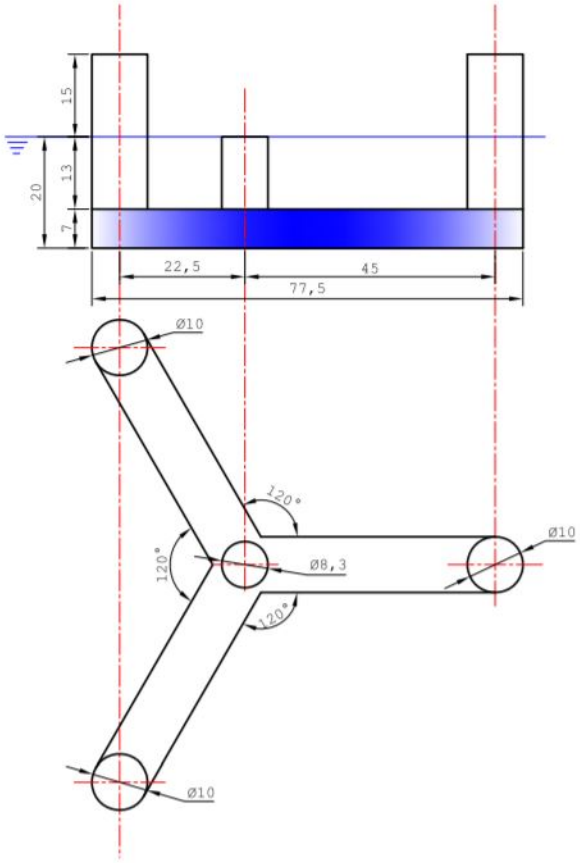

Figure 7.2: Main design of the sub structure of the floating wind turbine, [1]

Table 7.1: Mass of the turbine and Semi-submersible

Component	mass [t]	x [m]	y [m]	z [m]
Rotor	126.2	-7.073	0	119
Nacelle	446	2.687	0	119
Hubmass	105.5	-7.073	0	119
Tower	629.6	0	0	46.7
Overall	1307.3	-0.45	0	83.8
Semi	12642	0	0	-7.1442
Total	13949.3	-0.04	0	0.7934

7.2 Mass and inertia calculations

From the initial SIMA model, the mass and centre of gravity (CoG) for the Nacelle and Hub-mass could be directly extracted. The inertia forces and mass from the tower and wind turbine had to be calculated using the slender elements implemented in the orignal model, and the inertia forces from the semi had to be recalculated due to a change in ballast position relative to the orignal model. The results are found in table 7.2.

Table 7.2: Mass and inertia for the Turbine

	SEMI	NACELLE	HUBMASS	TOWER	TURBINE	TOTAL
Mass	1.2560E+07	4.46E+05	1.06E+05	6.30E+05	4.21E+04	1.3865E+07
Ixx	6.3667E+09	4.11E+05	3.26E+05	2.17E+09	-	1.7785E+10
Iyy	6.3667E+09	4.11E+06	3.26E+05	2.17E+09	-	1.7785E+10
Izz	1.1817e+10	4.11E+06	-	-	-	1.18E+10
CoG	-7.1442	119.00	119.00	47.6957951	119	0.7934

7.2.1 Semi-submersible

With the original model the natural period was calculated to just below 20s, and this may cause problems in extreme conditions when the wave period can get this high. To increase the natural period in pitch, the ballast was elevated to the centre of the three submerged columns. This places the centre of ballast mass to -6.5m below the sea surface, with the mass equally distributed within each column. The results are shown in table 7.3.

Table 7.3: Mass and inertia calculations for the SEMI

	COLUMNS	TOWER	PONTOON	BALLAST	TOTAL
CoG	1.2		-16.50	-6.5	-7.1442
Mass	1.0050E+06		1.583E+06	9.9722E+06	1.2560E+07
Ixx	1.0961E+09		8.32E+08	4.4389E+09	6.3667E+09
Iyy	1.0961E+09		8.32E+08	4.4389E+09	6.3667E+09

To calculate the inertia forces from the columns, tower and ballast equation 7.1 and 7.2 from table 9-1 in [21] was used. The inertia forces from the pontoons are assumed to be equal to $M \cdot r^2$. This simplification is due to the low weight of the pontoons in comparison with the ballast.

$$I = \frac{1}{2}MR^2 + \frac{1}{12}ML^2 \tag{7.1}$$

$$I = \frac{1}{4}MR^2 + \frac{1}{12}ML^2 \tag{7.2}$$

7.2.2 Turbine tower

The tower and the turbine blades are cut into sections with different shapes and mass. The mass coefficient for every tower section captures the weight due to different geometry and was extracted from SIMA. The length of each section was also extracted and the total mass is calculated by:

$$mass = \sum_{i=1}^{n} C_{M_i} \cdot L_i \tag{7.3}$$

C_{M_i} is the mass coefficient and L_i is the length of each section. The corresponding centre of gravity is calculated in a similar fashion:

$$CoG = \frac{\sum_{i=1}^{n} C_{M_i} \cdot L_i \cdot L_{C_i}}{\sum_{i=1}^{n} C_{M_i} \cdot L_i} \tag{7.4}$$

L_{C_i} is the distance from the reference height to the centre of gravity for section. The results are found in table 7.1. When importing the results into SIMA it is assumed that the turbine will always be positioned in head wind. To account for this it is assumed that the centre of mass for every section is located at x=0 and y=0. This is a minor change to the centre of gravity since the actual centre of gravity is placed 4 cm in negative x direction. In this thesis the surge and pitch motions are of interest, and the total moment of inertia is calculated from the initial model. The moment of inertia is known for the Nacelle and Hubmass at each centre of gravity. These inertia forces was added to the inertia moment of the semi by utilizing the parallel axis theorem [21]. The same procedure is used to calculate the moment of inertia for the tower, by assuming a hollow cylinder and equation 7.5 from [21]. Here R_1 is the inner radius and R_2 is the outer radius.

$$I = \frac{1}{4} M(R_1^2 + R_2^2) + \frac{1}{12} ML^2 \tag{7.5}$$

For the turbine blades, the moment of inertia for each section was not calculated, and the total inertia force is calculated using the parallel axis theorem neglecting the inertia moment of the blade itself. The moment of inertia about the z-axis is found be adding the known inertia forces from the Semi, Hubmass and nacelle, thus neglecting the contribution from the tower and turbine.

7.3 Thrust coefficient

The aim of this model is to efficiently evaluate different mooring systems, and a complicated top structure to capture all wind forces acting on the turbine is not needed, so a combined thrust coefficient is calculated. It is assumed that the thrust curve given in Wang's master thesis, shown in figure 7.3, represents the thrust curve of the turbine with a wind reference height at 119. Note that figure 7.3 does not take the tower into account. It is assumed that the thrust curve follows the function $T = C * V^2$.

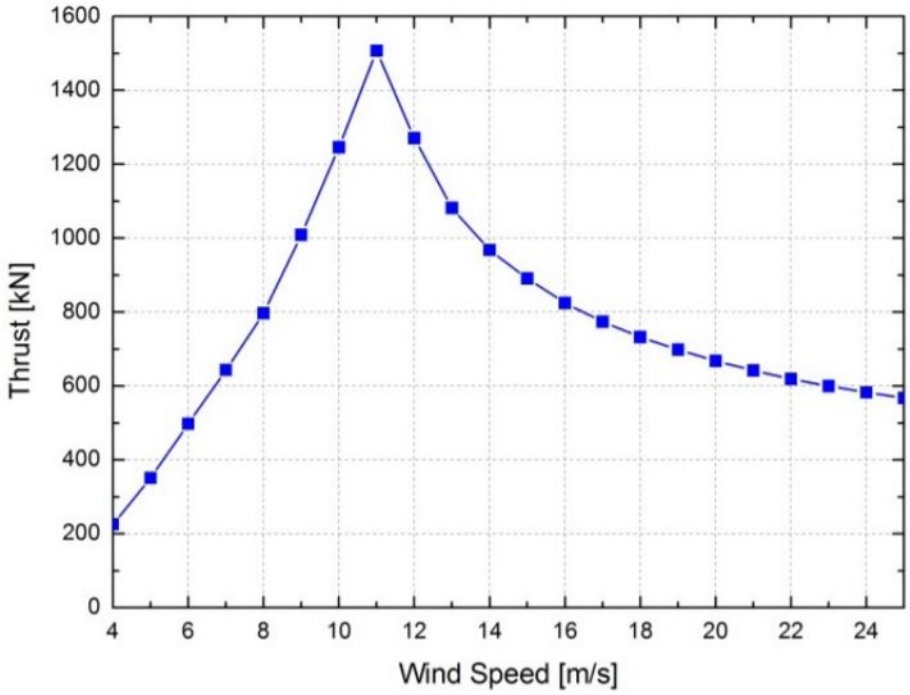

Figure 7.3: Thrust curve for the DTU 10MW wind turbine, [1]

Since the tower is not part of the initial thrust curve, the thrust coefficient is calculated using an experimental drag coefficient for a cylinder from figure 7.4, and the wind velocity at each section along the tower. The drag coefficient used is for a smooth cylinder and it is assumed to be converging towards 0.7 for high Reynold's numbers.

The wind velocity profile is calculated by assuming a power law profile [22], and equation 7.6 is used to obtain the profile.

$$U(z) = U(H)\left(\frac{z}{H}\right)^{0.12} \tag{7.6}$$

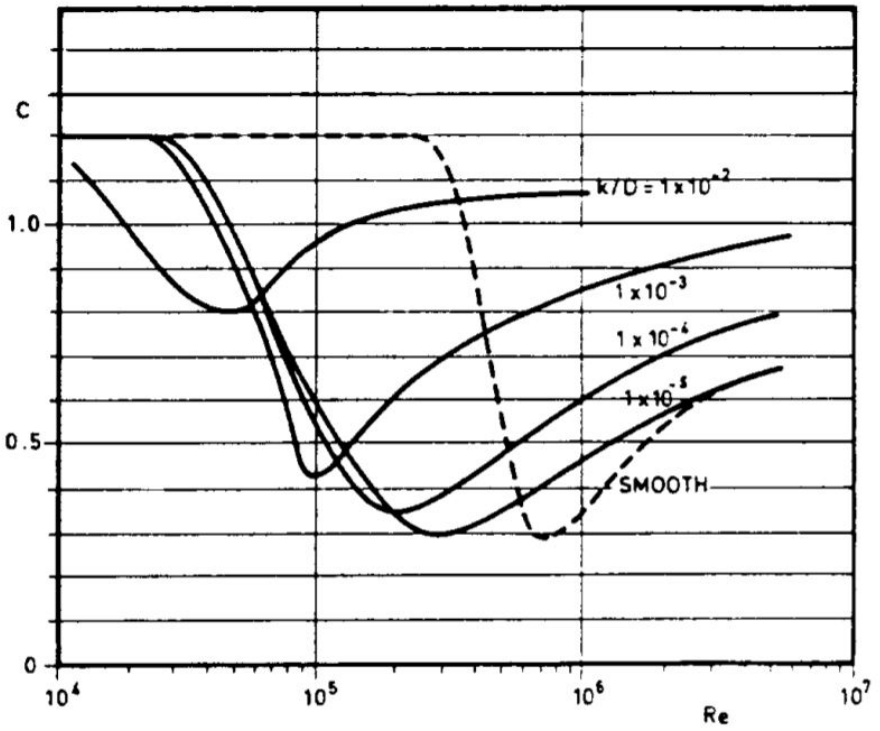

Figure 7.4: Drag coefficient for fixed circular cylinder for steady flow in critical flow regime, for various roughness. Figure 6-6 [22]

The thrust for each section of the tower and the turbine is calculated using equation 7.7, then summarized to get the total thrust coefficient. The same procedure is done for the total moment acting on the structure by multiplying the drag force with the distance between each section and origo.

$$T = \frac{1}{2}\rho_{air} A C_d \cdot U(z)^2 \tag{7.7}$$

The 10MW DTU reference turbine has a control system which ensures that the mechanical power output won't get above approximately 10700kW. This means that the blade pitch changes as a with respect to the wind speed, and therefore has to be taken into account when calculating the thrust coefficient on the structure. To account for this the model is designed with three different thrust coefficients, depending on which wind speeds are present at a reference height of 10m.

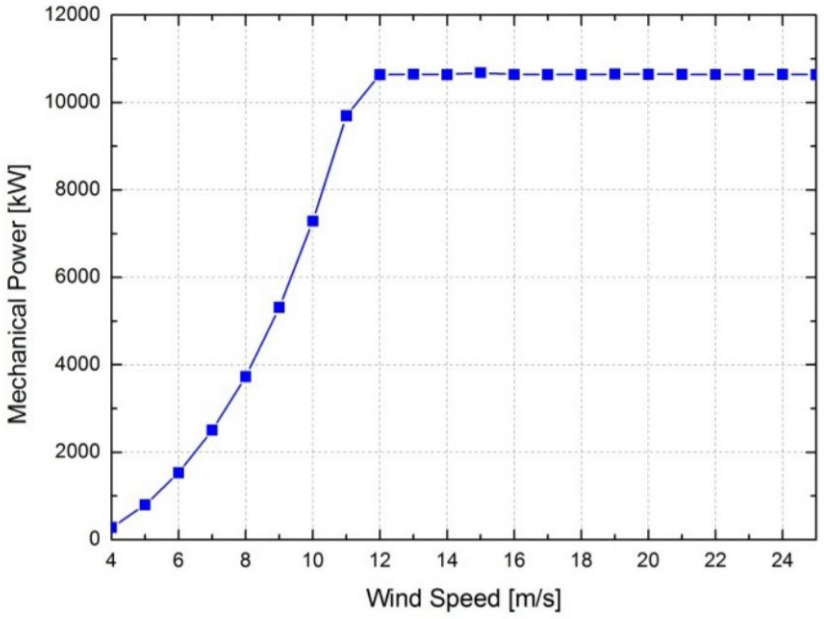

Figure 7.5: Mechanical power output 10MW DTU Reference Turbine [1]

7.3.1 Low wind speeds (0-11m/s)

For wind speeds in the interval 0-11m/s the thrust coefficient for the turbine is calculating by assuming the turbine thrust to be equal the thrust at 11m/s (hub height). The tower thrust is calculated by the wind speeds at each tower section and a drag coefficiant of 0.65 for each section. The moment coefficients are found by multiplying the height between the section centre and origo to the thrust coefficients. The moment contribution from the turbine is calculated as the total turbine force at hub height (119m).

Table 7.4: Thrust coefficients for low wind speeds (0-8.17m/s) at 10m reference height

Dir [deg]	C1	C2	C3	C4	C5	C6
0	22916.2026	0	0	0	2700316.37	0
30	19846.0136	11458.1013	0	-1350158.18	2338542.57	0
60	11458.1013	19846.0136	0	-2338542.57	1350158.18	0
90	1.40E-12	22916.2026	0	-2700316.37	1.65E-10	0
120	-11458.1013	19846.0136	0	-2338542.57	-1350158.18	0
150	-19846.0136	11458.1013	0	-1350158.18	-2338542.57	0
180	-22916.2026	2.81E-12	0	-3.31E-10	-2700316.37	0
210	-19846.0136	-11458.1013	0	1350158.18	-2338542.57	0
240	-11458.1013	-19846.0136	0	2338542.57	-1350158.18	0
270	-4.21E-12	-22916.2026	0	2700316.37	-4.96E-10	0
300	11458.1013	-19846.0136	0	2338542.57	1350158.18	0
330	19846.0136	-11458.1013	0	1350158.18	2338542.57	0
360	22916.2026	-5.61E-12	0	6.61E-10	2700316.37	0

7.3.2 Medium wind speeds (11-25m/s)

The thrust coefficient on the turbine for this interval is calculated to be correct at 25 m/s and also assumed to follow $T = C \cdot V^2$. This means that the thrust curve for the turbine will see a reduction when the wind speed is lower, in contrast to the actual thrust curve for the turbine which is increasing as seen in figure 7.3. Table 7.5 contains the thrust coefficients for a operating turbine in 25m/s wind, and to use this model for lower wind speeds the thrust coefficients has to be recalculated for every step by reading figure 7.3 to get accurate results. This should make the model sufficiently accurate for wind speeds close to 25m/s. Since the interval of interest with respect to T_d is close to 25m/s, this should be a tolerable assumption.

Table 7.5: Thrust coefficients for 8.17-18.57m/s at 10m reference height

Dir [deg]	C1	C2	C3	C4	C5	C6
0	2171.20035	0	0	0	229606.356	0
30	1880.31466	1085.60018	0	-114803.178	198844.937	0
60	1085.60018	1880.31466	0	-198844.937	114803.178	0
90	1.33E-13	2171.20035	0	-229606.356	1.41E-11	0
120	-1085.60018	1880.31466	0	-198844.937	-114803.178	0
150	-1880.31466	1085.60018	0	-114803.178	-198844.937	0
180	-2171.20035	2.66E-13	0	-2.81E-11	-229606.356	0
210	-1880.31466	-1085.60018	0	114803.178	-198844.937	0
240	-1085.60018	-1880.31466	0	198844.937	-114803.178	0
270	-3.99E-13	-2171.20035	0	229606.356	-4.22E-11	0
300	1085.60018	-1880.31466	0	198844.937	114803.178	0
330	1880.31466	-1085.60018	0	114803.178	198844.937	0
360	2171.20035	-5.32E-13	0	5.62E-11	229606.356	0

7.3.3 Extreme conditions (above 25m/s)

By assessing the thrust acting on the wind turbine without the tower it is seen that the thrust curve is steeper than $T = C \cdot V^2$. The thrust for the 50 year return period was therefore chosen as a reference point because this is the most likely condition to be defining for the mooring system. This means that for lower wind speeds, the thrust will be slightly higher than the actual thrust. The thrust coefficients for extreme conditions are shown in table 7.6.

Table 7.6: Thrust coefficients for extreme conditions (18.57m/s<) for 10m reference height

Dir [deg]	C1	C2	C3	C4	C5	C6
0	1297.68521	0	0	0	125658.054	0
30	1123.82836	648.842605	0	-62829.0271	108823.067	0
60	648.842605	1123.82836	0	-108823.067	62829.0271	0
90	7.95E-14	1297.68521	0	-125658.054	7.69E-12	0
120	-648.842605	1123.82836	0	-108823.067	-62829.0271	0
150	-1123.82836	648.842605	0	-62829.0271	-108823.067	0
180	-1297.68521	1.59E-13	0	-1.54E-11	-125658.054	0
210	-1123.82836	-648.842605	0	62829.0271	-108823.067	0
240	-648.842605	-1123.82836	0	108823.067	-62829.0271	0
270	-2.38E-13	-1297.68521	0	125658.054	-2.31E-11	0
300	648.842605	-1123.82836	0	108823.067	62829.0271	0
330	1123.82836	-648.842605	0	62829.0271	108823.067	0
360	1297.68521	-3.18E-13	0	3.08E-11	125658.054	0

7.3.4 Slender elements

The semi-submersible has several slender elements incorporated in the structure where the wave and drag forces are calculated. There is one element in each of the pontoons, one in each of the cylinders including the tower going up to the water surface. To capture the wave and wind forces above the sea level, slender elements with correct diameter are placed on top of each column reaching 10m above sea level. These slender elements define the structure to the calculation program, and all effects of the equation of motion is solved here. With a SIMO-RIFLEX coupled model, the mooring system would also be compiled by slender elements, and drag and inertia forces will be considered.

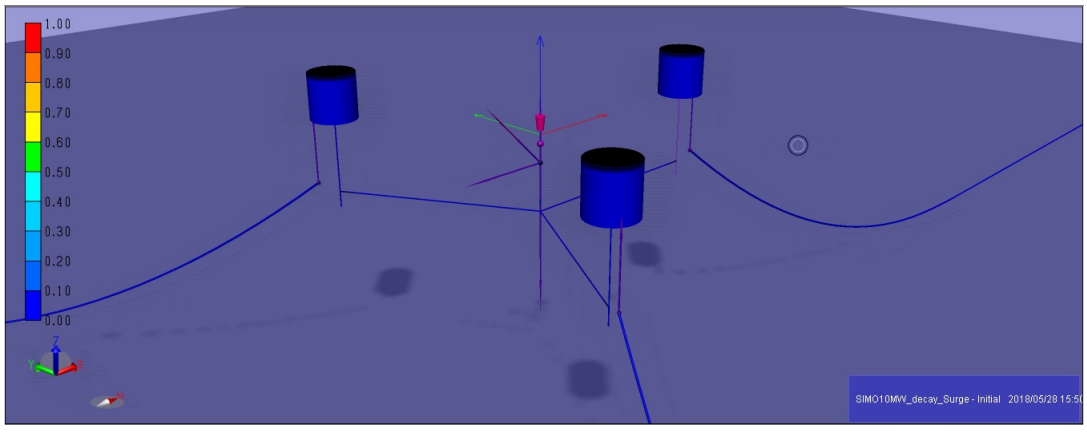

Figure 7.6: Slender elements for the simplified model

7.3.5 Damping

Linear damping

The linear damping matrix is given, and calculated by Wang [1] using HydroD. When scaling down the turbine structure it was noticed by comparisons with the original model that the damping in pitch on the simplified model was to low. To account for this the critical damping was added to the linear damping matrix in pitch and roll. The critical damping is given by equation 7.8 where m is mass and ω_n is the natural frequency of the system.

$$C_{crit} = 2m\omega_n \tag{7.8}$$

Quadratic damping

Since the structure above water is removed from the model, the quadratic damping coefficients needs to be calculated. By utilizing the drag forces acting on the tower due to pitch motion, shown in figure 7.7. By integrating equation 7.9 and 7.10 we get equations 7.11 and 7.12. When these are solved for $\dot{\theta}$ the cuadratic damping coefficients are obtained.

$$dF = C_d \cdot dz\,(\dot{\theta}\cdot z)^2 = \underbrace{C_d \cdot z^2}_{C}\cdot \dot{\theta}^2 \cdot dz \tag{7.9}$$

$$dM = dF \cdot z = C_d \cdot z \cdot dz\,(\dot{\theta}\cdot z)^2 = \underbrace{C_d \cdot z^3}_{C_m}\cdot \dot{\theta}^2 \cdot dz \tag{7.10}$$

$$F = C_d \cdot \dot{\theta}^2 \int_0^L z^2 dz \tag{7.11}$$

$$M = \int_0^L C_m \cdot \dot{\theta}^2 dz = C_d \cdot \dot{\theta}^2 \int_0^L z^3 dz \tag{7.12}$$

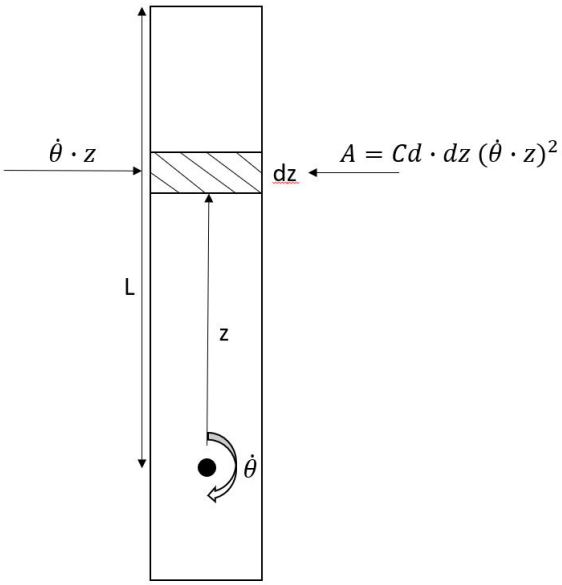

Figure 7.7: Damping forces due to pitch motion

Chapter 8

Quality analysis

8.1 Comparison with original model

These comparisons were executed with a model of the Hywind Scotland mooring system for both the simplefid and original model. The structral model studied in this thesis is a model consisting of a semi-submersible that has been modified to operate as a full wind turbine. To assess the accuracy of the model, several cases for comparison with the original model used as a starting point for this thesis was proposed and executed with the help of Tiril Stenlund, listed in table 8.1. Wind speeds for in this chapter is given for a reference height of 119m, at the hub height.

Table 8.1: Cases for comparison between simplified and original model

Case nr.	Description
1	Static equilibrium
2	Constant wind with no waves or current present
3	Turbulent wind, 50 year condition with no waves or current present
4	50 year condition waves with no wind or current present

8.1.1 Case 1

For case 1 a static simulation of the system was conducted by both candidates. As seen in table 8.2 there is a difference in pretension. This is due to different ways of calculating the anchor positions. For the simplified model, a SIMO model was constructed and used to calculate the anchor positions, and for the original model the catenary equations was utilized. For the horizontal tension it is seen that the original model has a higher tension. This could be due to differences in element length for the RIFLEX calculations of the mooring lines. The original model has longer segments along the line suspended in water than the simplified model. The simplified model is created with symmetry around the z-axis, thus has no initial pitch or displacement along the x and y axis. This is not the case for the original model

which has a centre of gravity that does not coincide with origo, thus creating an initial pitch.

Table 8.2: Static equilibrium

	Pretension T, [kN]	Pretension Th, [kN]	x [m]	y [m]	z [m]	Pitch [deg]
Simplified	992.6	794.4	0	0	0	0
Original	978	798.1	-0.0049	0	-0.00021	0.2353

The differences in natural periods of the original and simplified model is sufficiently small to compare results from the two models as seen in table 8.3. The ballast of the simplified model is elevated to get similar natural periods for this purpose.

Table 8.3: Natural periods for original and simplified model

	Surge [s]	Heave [s]	Pitch [s]	Yaw [s]
Simplified	68.3	20.5	24.5	81.9
Original	68	19.2	26	85

The response amplitude operators generated from the two models are as expected similar. For the surge motion as shown in figure 8.1, the RAO is rising linearly with the increased wave period with a some cancellation around the natural period in pitch. This is due to resonance pitch motions that will have a contribution to surge motion. The RAO in heave are also similar, with a peak at the natural period in heave. They are also converging at 1 for long wave periods, which is expected. The RAO in heave for the orignal model is converging against a value lower than 0, this is due to a initial draft that is lower than 0 most probably due to a smaller specified force countering the weight of the mooring system. It is still very small, and should do little to affect the RAO's.

The RAO in pitch also have a peak at the natural period for pitch motion. At around a wave period of 10 there is also a peak as seen in figure 8.3, this is due to the wave length $\lambda = \frac{2\pi}{k}$ and for 10 seconds the wave length becomes 156m [7]. The distance between the wave top and bottom is $\frac{\lambda}{2}$ and yields 78m. The largest force contribution from the waves on the turbine is when a wave top and bottom hits the ends of the structure at the same time, and since the structure is 75m long in x direction this is a good explanation for this effect. For the original model the RAO goes towards 0 at around 16s. This effect would probably happen for the simplified model also if the natural period was the same. Since the natural period for the simplified model is slightly less, the resonance effect happens at lower wave periods and this effect is cancelled. By assessing the first order wave transfer function in pitch shown in figure 8.4 it is reasonable to have a peak around $T_p = 10s$ and a cancelling effect for larger periods. For very large periods the RAO in pitch is expected to go towards 0.

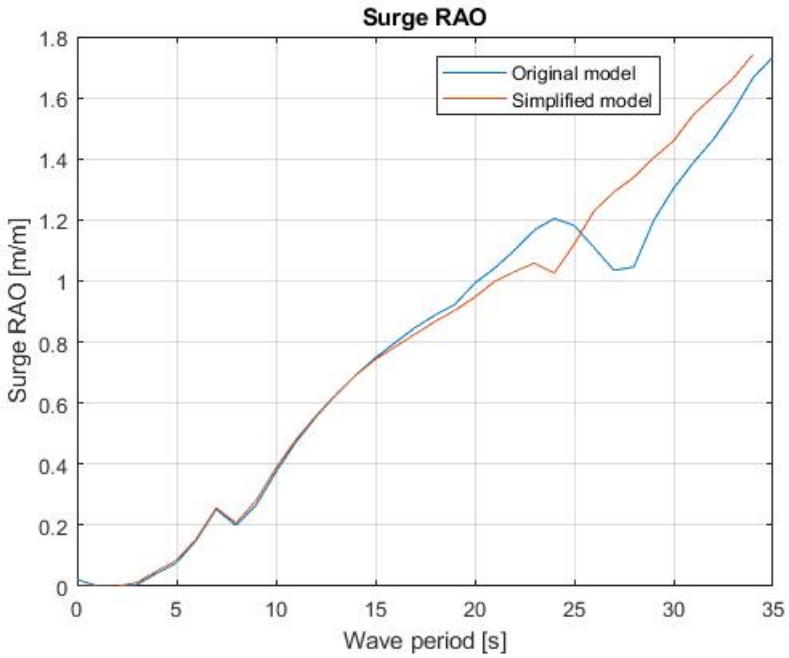

Figure 8.1: RAO in surge

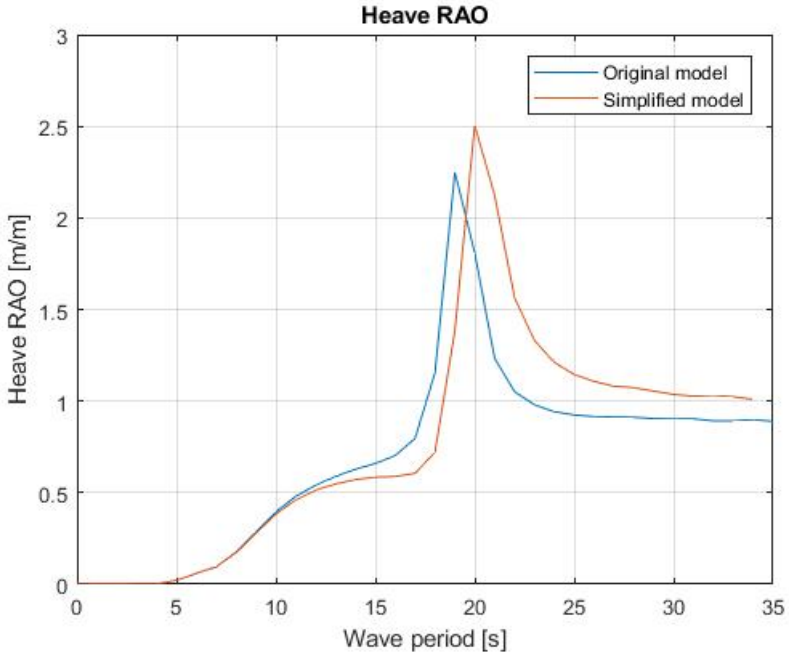

Figure 8.2: RAO in heave

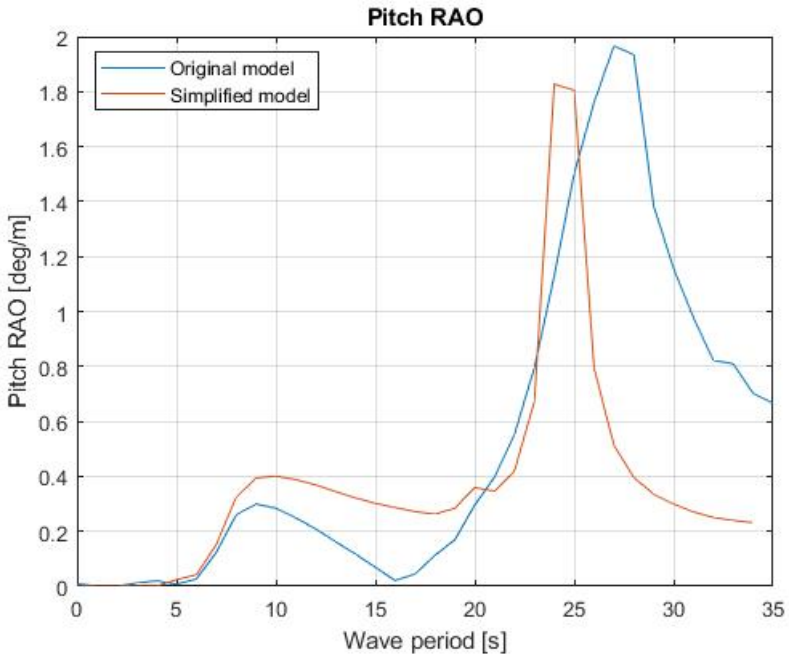

Figure 8.3: RAO in pitch

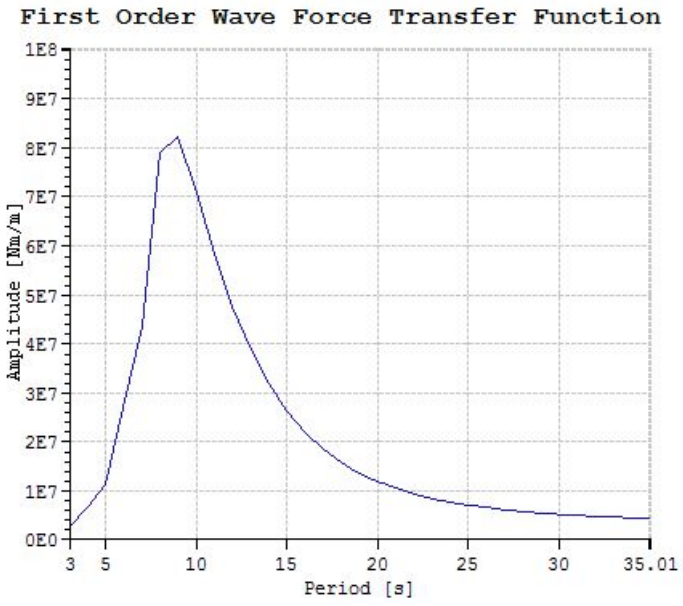

Figure 8.4: First order wave trensfer function for pitch

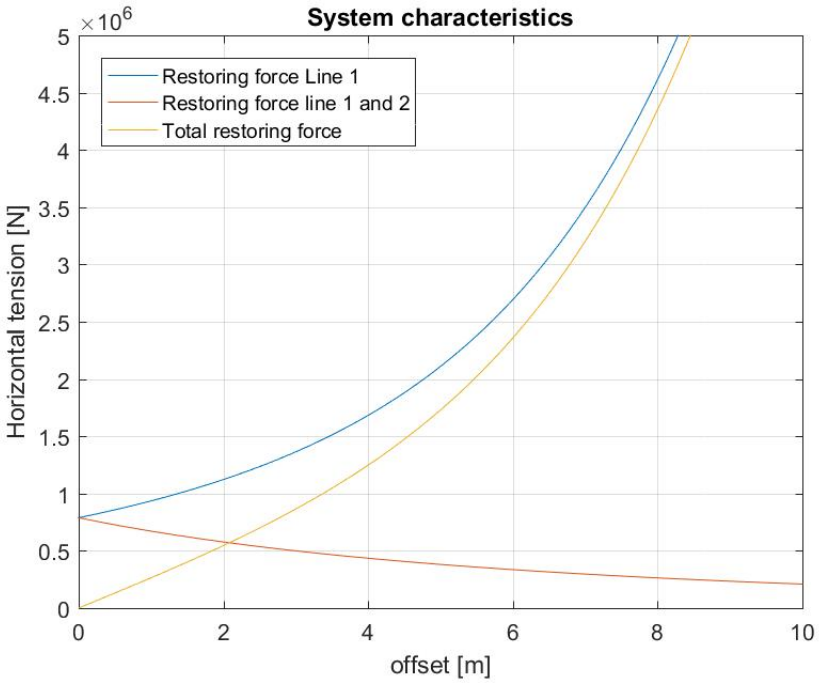

Figure 8.5: System characteristic (horizontal tension) for Hywind Scotland mooring system, simplified model.

8.1.2 Case 2

Case 2 is a comparison of offset and line tension for constant wind speeds with no waves or current present. The aim of this case is to verify that the models behave similarly in static conditions, and can be used for further simulations with regard to mooring analysis.

Figure 8.6 shows the surge motions for the different models. It is observed that the motions are similar with the exception of the ULS condition (46.4 m/s). Since the thrust coefficients are calculated with certain simplifications presented in section 7.1, some differences will occur. However, the differences are quite small and assumed to be sufficient for further calculations.

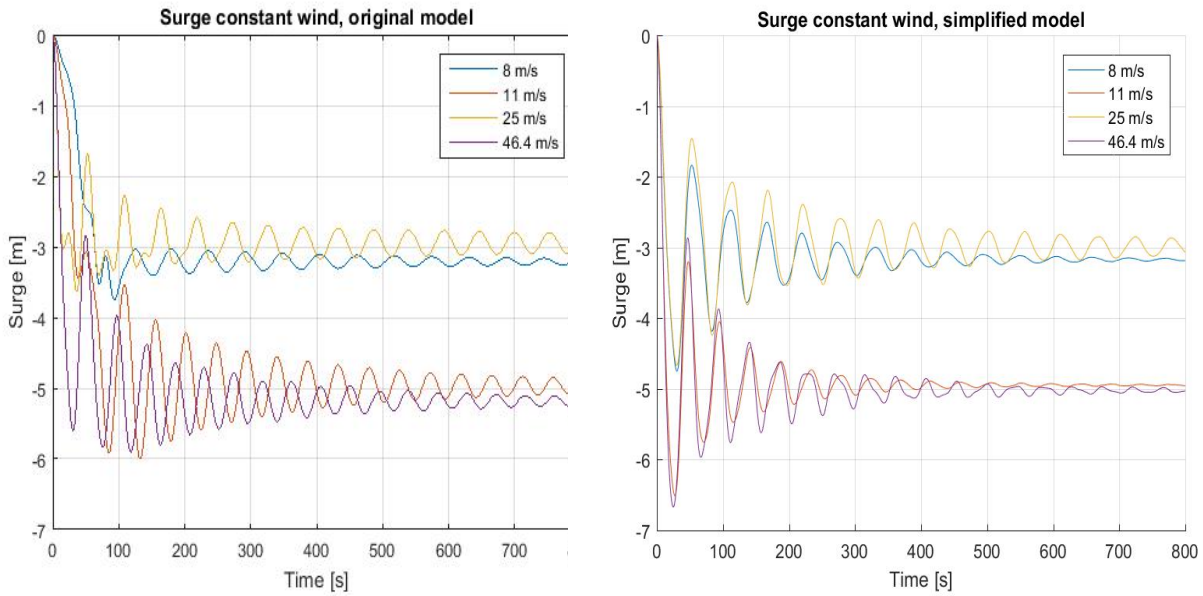

(a) Constant wind, original model (b) Constant wind, simplified model

Figure 8.6: Comparison of surge motion in constant wind

The comparison for heave motions found in figure 8.7 shows very small heave motions. Both models has been compensated with specific forces to get the draught equal to 20 m, and this will give some difference in initial draught. Since the differences is so small and the scale which it operates is also very small it is concluded that the heave motions are similar, and fit for further calculations.

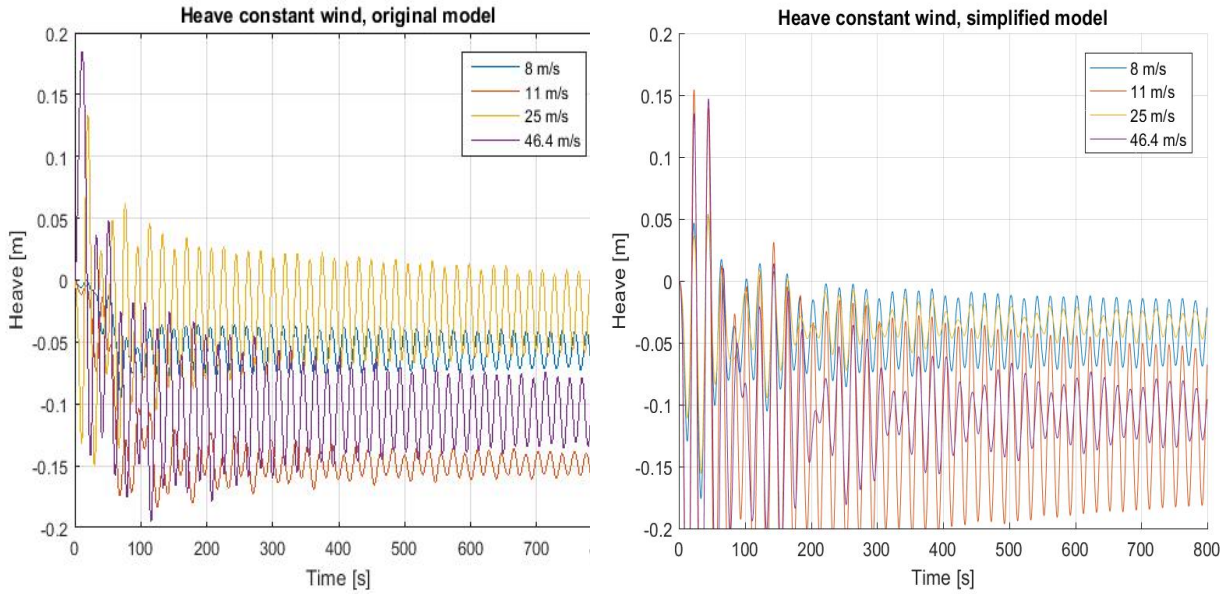

(a) Constant wind, original model (b) Constant wind, simplified model

Figure 8.7: Comparison of heave motion in constant wind

The overall results from the pitch comparison shown in figure 8.8 shows that the pitch motion of the simplified model is lower than for the original model. This implies that the

calculation of the thrust coefficients for moment are to small. The difference in pretension shows that the stiffness of the simplified mooring system is higher, and therefore the pitch motion will be smaller. This is a very little difference, and should not give significant differences.

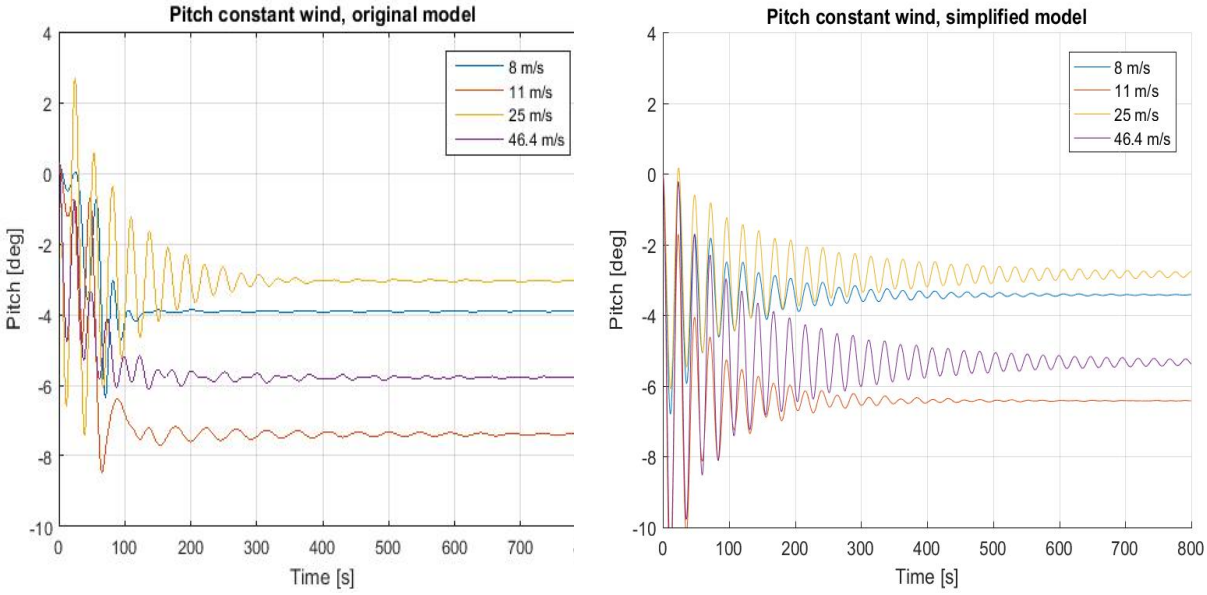

(a) Constant wind, original model

(b) Constant wind, simplified model

Figure 8.8: Comparison of pitch motion in constant wind

Line tension in line one is equal for every line except for the ULS condition. From figure 8.9 it is seen that the tension is approximately 100kN more for the simplified model than for the original model. Initially the difference in pretension is contributing with a 14.5 kN increase in line tension for the simplified model. From figure 8.5 the restoring force follows an exponential curve, thus the difference from an initial difference will increase with larger forces. The larger line tension for the simplified model will render it conservative, and proposed feasible mooring systems will not be to weak.

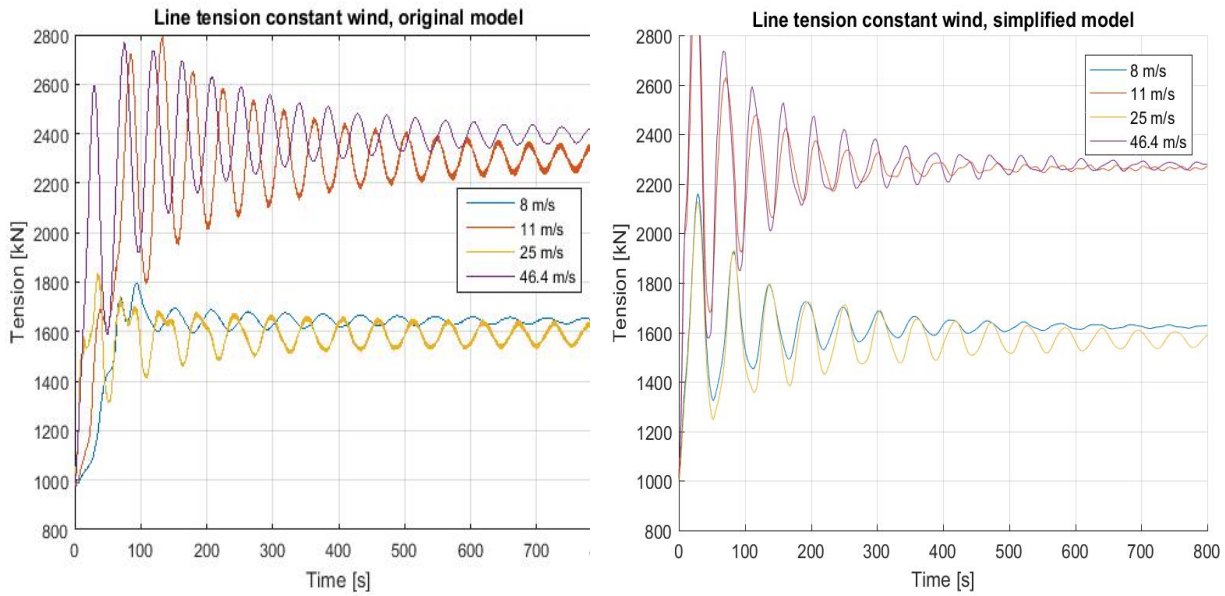

(a) Constant wind, original model

(b) Constant wind, simplified model

Figure 8.9: Comparison of line tension constant wind

8.1.3 Case 3

In this case the simplified and original model is tested for turbulent wind with no waves or current present. The turbulent wind used for both models are NPD wind, as described in the SIMO theory manual [4]. For the original model, turbulent wind generated with TurbSim is also simulated , and the results are shown in table 8.4.

The line tension for the simplified model in constant and NPD wind is similar. This also appears to be accurate with respect to the original model with the exception of NPD wind for the original model. Here it is seen that the line tension is lower, with respect to constant wind and wind generated with TurbSim. Since all the other line tensions are similar it is reasonable to conclude that the simulations of the original model with NPD wind is flawed. This effect is probably due to the wind speed of the simulations. By calculations, the wind speed at hub height should be 46.4 m/s, but the actual wind speed for the original model in NPD wind at hub height is 44.46 m/s. This will give smaller forces acting on the turbine. Another note is that the standard deviation for the NPD wind for both models is higher than for the generated turbulent wind. This does not seem to effect the mean line tension, but for calculation of the design tension, it will probably lower the dynamic contribution. This will effect the dimensions of the mooring system, making the systems for generated turbulent wind lighter and less durable. The variation should not be significant, but the mooring systems designed for NPD wind will be more conservative.

The offsets are quite similar, and it is noted that the offset for the original model in NPD wind is lower than for constant and turbulent wind. This further explains the effect of smaller wind speed for this condition. For Pitch, the offset follows the same trend as for the degrees of freedom mentioned above. Here it is also found that the pitch of the simplified model

is lower than for the original model with respect to constant and generated turbulent wind. This could be due to a difference in the calculations of thrust on the tower and turbine for the simplified model as well as the difference in ballast which gives a slightly different inertia and hydrostatic stiffness. The deviation is found to be very small, and it is concluded that it will not effect the line tension, thus the mooring system analysis in a significant way.

Table 8.4: Turbulent wind results, no waves or current present

	Simplified model (constant wind)	Origianl model (constant wind)	Simplified model (NPD wind)	Original model (NPD wind)	Original model (TurbSim)
Line tension, mean [kN]	2275.4	2396	2294.4	2137	2302
Line tension, std [kN]	-	-	472.03	443.4	355.3
x, mean [m]	-5.025	-5.1	-4.86	-4.42	-4.88
x, std [m]	-	-	1.096	1.08	0.81
y, mean [m]	0	-0.098	-0.002	-0.14	-0.55
y, std [m]	-	-	0.343	0.33	0.67
z, mean [m]	-0.107	-0.11	-0.117	0.085	-0.1
z, std [m]	-	-	0.164	0.071	0.088
pitch, mean [deg]	-5.508	-5.78	-5.382	-4.99	-5.83
pitch, std [deg]	-	-	2.914	2.16	1.76

8.1.4 Case 4

For waves of a 50 year condition the motions and line tension for the two models are almost exactly similar. The standard deviation for line tension is larger for the original model, which implies that the dynamic motions are larger. The pitch is also seen to be different, and this is due to the geometrical differences of the two models. The original model has a static pitch of around 0.25 degrees due to the centre of mass of the turbine, and the simplified model symmetric about the z-axis. The standard deviation in pitch is higher for the simplified model, which implies larger dynamic motions. This pitch motion is not found to affect the line tension significantly as seen by te lower standard deviation for line tension for the simplified model.

Table 8.5: 50 year condition waves, no wind or current present

	Simplified Model	Original Model
Line tension, mean [kN]	1001	1000
Line tesnion, std [kN]	370.3	456
x, mean [m]	0.032	-0.07
x, std [m]	1.64	1.66
y, mean [m]	0	0
y, std [m]	0	0
z, mean [m]	0.017	0.12
z, std [m]	1.514	1.68
pitch, mean [deg]	-0.007	0.25
pitch, std [deg]	0.934	0.59

8.1.5 ULS comparison

When comparing the results from the simplified and original model for ULS it is seen that the line tension is very similar. The simplified model has a mean tension of 5490kN and the original model has a mean tension of 5328kN in line 1. The dynamic tension is almost identical and it is observed a few more tension peaks above 20000kN for the simplified model, but the maximum tension in both models are approximately the same. The standard deviation varies with 0.64% wich is very small, and further suggest that the motions are similar. The most significant difference is how the models captures the negative line tensions. For the simplified model, the minimum line tension is quite close to 0, and for the original model the minimum line tension seems to go further below 0. The reason for this effect is not known, and may cause problems with respect to slack of polyester lines, and should be investigated further.

Time series and FFT plots from this comparison is found in appendix A.1.

The simulation time used for the simplified and original is respectively 375.4s and 579.6s, this shows that simulations with the simplified model uses 64.8% of time needed with the original model. With the reduced simulation time, and similar force and displacement output the simplified model is a good tool for conducting extensive mooring line analysis. It is concluded that the model is sufficiently accurate with respect to the original model that it can be used for further mooring analysis.

It is important to note that for the comparisons with the original model, few simulations were conducted, and the statistical foundation for the results are uncertain. A more extensive analysis comparing the models is needed for a firmer conclusion.

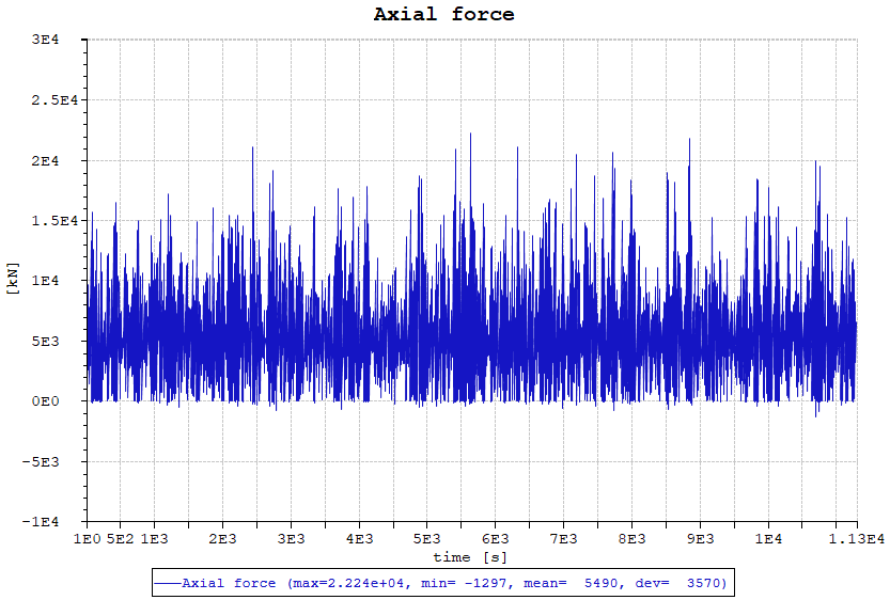

(a) Simplified model

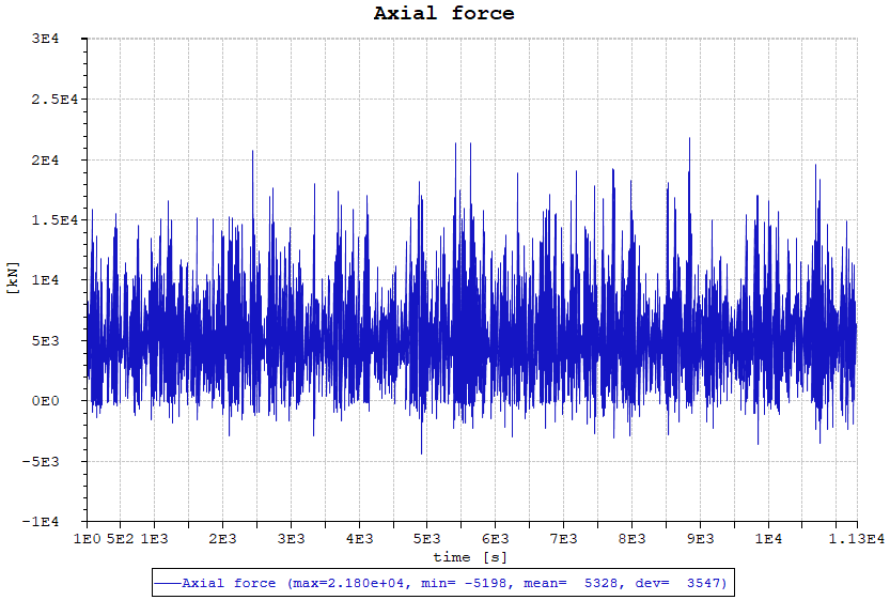

(b) Original model

Figure 8.10: Time series of tension in Line 1 for the simplified and original model with the Hywind Scotland mooring system.

8.1.6 Sensitivity analysis

To accurately predict T_d in the mooring lines several simulations has to be conducted to get a sufficient statistical accuracy. Depending on the combination of wave and wind seeds used in the simulations the results can change significantly. To find a reasonable number of simulations conducted to get accurate results a series of 50 simulations in 50 year return period were assessed.

In figure 8.11 the mean value of the maximum tension and standard deviations for all simulations up to each point are plotted. The number of different wind and wave seeds

used for further calculations are found by isolating which number is needed to keep the converging mean values within 10% of the initial value. From figure 8.11 it is seen that at 20 simulations the mean values won't diviate with more than 10 %, and 20 different seed value combinations will be used.

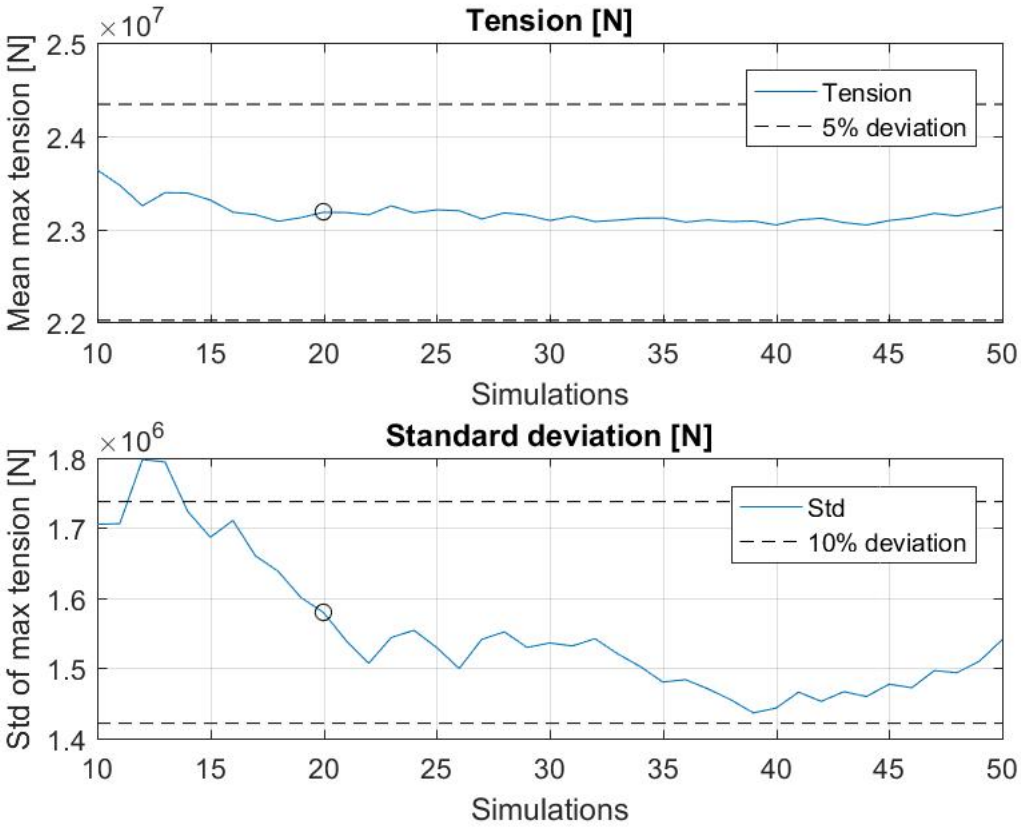

Figure 8.11: Mean max tension and standard deviation for different number of simulations

To calculate the T_d by utilizing equation 5.1 the most likely maximum dynamic tension is used. The maximum line tension for line 1 is assumed to follow the Gumbel distribution which is shown in figure 8.12. In this figure the 10% interval around the distribution for 20 simulations is plotted, and the most probable maximum value stays within this range for simulations with up to 50 different seed values. It is concluded that this is true for infinite number of different seed values, and 20 simulations is sufficient to get accurate results.

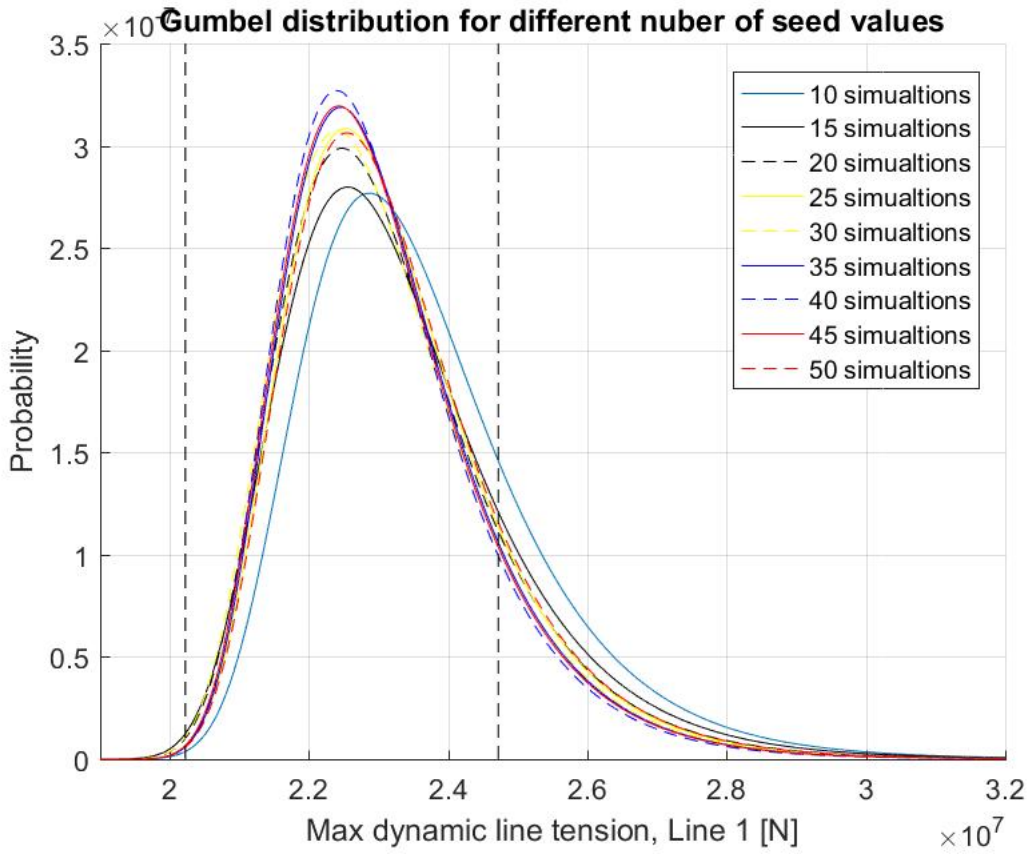

Figure 8.12: Gumbel distribution of maximum line tension for line 1 for different number of simulations

Chapter 9

Results

9.1 Metocean design basis

The meatocean design basis is provided for the area were the Hywind Scotland pilot park is installed and will be used for this thesis [19]. The H_s and T_p values used are extracted directly from the contour plot of a 50-year storm shown in figure 9.1. The most critical direction for environmental loads are set to be directly towards line 1, as shown in figure 9.2. With the environmental loads directly against one line the largest possible tensions for this system will occur, and no additional safety factor is needed for ULS calculations. Several different H_s and T_p combinations are compared to evaluate which combination yields the highest line tensions. For this thesis the majority of the simulations are conducted with $H_s = 10.4$ and $T_p = 14$.

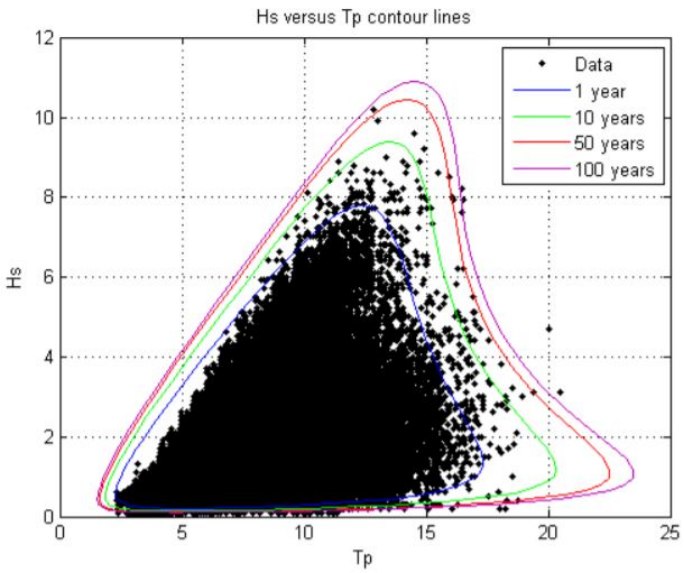

Figure 9.1: Contour plot of 1, 10, 50 and 100-year condition of Bushan deep [19]

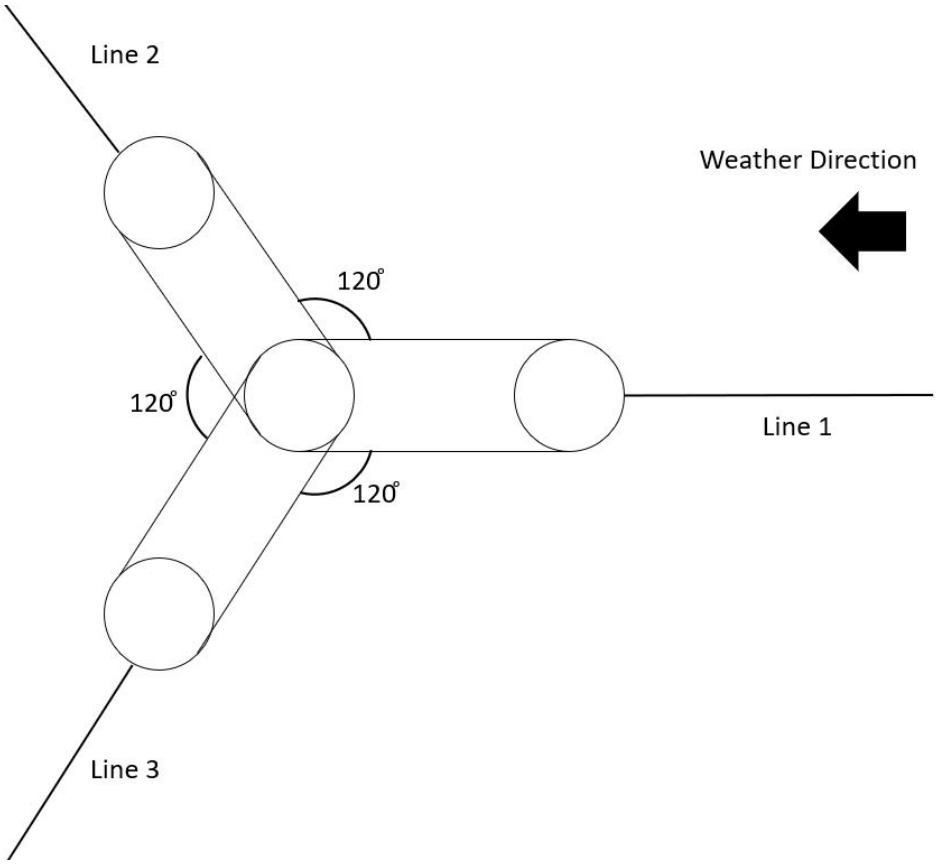

Figure 9.2: Line configuration of the model in question

The extreme wind conditions for Bushan deep is listed in table 9.3 and 34.5m/s at a reference height of 10m, and is used for these simulations.

	Return period					Return period		
Direction	**1 year**	**10 yrs**	**50 yrs**		**Month**	**1 year**	**10 yrs**	**50 yrs**
	m/s	**m/s**	**m/s**			**m/s**	**m/s**	**m/s**
0°	24.0	28.0	30.5		**Jan**	27.5	31.5	33.5
30°	21.0	25.5	28.5		**Feb**	26.0	29.5	32.0
60°	19.5	23.5	26.0		**Mar**	24.5	27.5	29.5
90°	21.0	25.0	27.0		**Apr**	22.5	26.0	28.0
120°	24.0	28.0	30.5		**May**	19.0	21.5	23.0
150°	25.0	29.0	31.0		**Jun**	18.5	21.0	22.5
180°	26.0	30.0	32.0		**Jul**	19.0	22.0	24.0
210°	26.5	29.5	31.5		**Aug**	19.0	21.5	23.5
240°	24.0	27.0	29.0		**Sept**	23.0	26.0	28.0
270°	25.0	29.0	31.0		**Oct**	25.5	29.0	31.0
300°	26.0	30.0	32.5		**Nov**	26.0	29.5	31.5
330°	26.5	30.0	32.0		**Dec**	25.5	29.0	30.5
0° - 360°	**29.0**	**32.5**	**34.5**		**Year**	**29.0**	**32.5**	**34.5**

Figure 9.3: Extreme wind speeds at Bushan deep [19]

The dimensioning current for this system is for a 10 year return period, and are extracted from the metocean design basis [19]. The velocities for different depths are combined into a current profile, shown in figure 9.4 that is put into the model. The current at the seabed is probably to high because it is the current measured at a depth of 70m at a location with 90m water depth. This neglects the friction of the seabed, but the model has a small draft and

effects of the current below the draft of 20m is small.

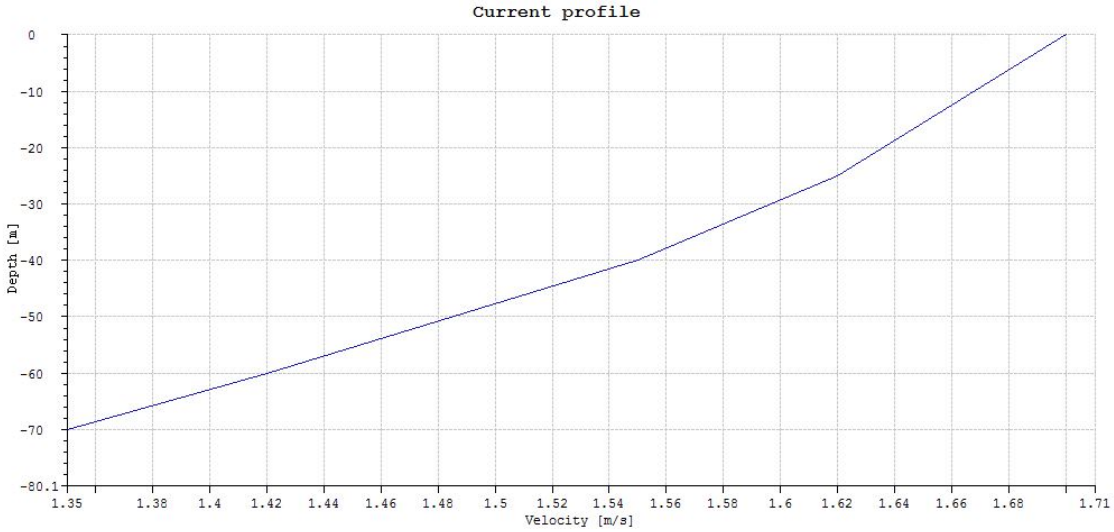

Figure 9.4: Current profile

9.2 Hywind Scotland mooring system

The natural periods of the Hywind Scotland mooring system is found in table 8.3 for the simplified model. The natural periods, with the exception of heave motion are above the maximum wave period seen in the contour plot of the 50 year condition given in figure 9.1. This ensures no resonance from the waves in most degrees of freedom, but conditions with a wave period of 20.5s should be assessed.

The response amplitude operators have been found by running the model in regular waves with an amplitude of 1m and different periods, and are of the same system modelled in chapter 8.

The results from the sensitivity analysis found in figure 8.12 is for the Hywind Scotland mooring system, which has a 147mm R4S studless chain from [16] with 1000kN pretension. By solving equation 5.1 for 20 runs the T_d is 36862kN and the max braking load is 21179kN. Thus the system don't met the requirements provided by the DNV standard [23], and further analysis of different H_s and T_p combinations are not needed.

9.3 Chain mooring system

To provide a feasible mooring system of chain several systems with varying length, dimensions and pretensions were assessed. The different design tensions are listed in table 9.1 and non are within the requirements for T_d [23]. Note tat the seed values for the simulations does not vary from case to case.

For the two systems with 660m line length the design tension rises with a larger chain diameter. This is expected because a line that weights more will add stiffness to the system.

This is also the case for the systems with 1250m line length.

With the same line weight a longer line should give a lower maximum expected line tension and a lower T_d. This is because a longer line will be more elastic and the line characteristic will become less exponential. This is the case for a chain diameter of 147mm. For the chain with a diameter of 172mm, the opposite is observed. This implies that when the system consists of a chain of a certain weight, the stiffness provided to the system puts the end of the chain resting at the seabed, and the only contribution from the extended line is the added elasticity. The differences are also quite low, so T_d can be evaluated to have the same value for these cases. Even if the reduced stiffness is low, T_d should be reducing, and the difference can also come from different calculations in SIMA.

For the system with 600kN pretension a notable reduction in T_d is observed as shown in table 9.1. When the system is not especially sensitive to line length, the other parameter to change are weight and pretension. As expected the reduced pretension lowers T_d for this system. This is because the mean tensions is lowered, and the geometric stiffness of the system i reduced. This effect can be described by the system characteristics shown in figure 8.5 for the Hywind Scotland mooring system were a reduction in pretension will cause a larger offset and a lower line tension in line 1 with same restoring forces.

Table 9.1: Characteristic line tension for studless chain systems

Pretension [kN]	Line length [m]	Diameter [mm]	Weight [kg/m]	MBL R4S [kN]	MBL R5 [kN]	Td[kN]
1000	659.6	147	432	21179	22294	36862
1000	659.6	172	648	27196	28628	37913
1000	1250	147	432	21179	22294	34599
1000	1250	172	648	27196	28628	38468
1000	1500	172	648	27196	28628	38651
600	1500	177	686	28420	29915	36614

Table 9.2: Natural periods for chain system 172mm, lenght= 1500m

Natural period	[s]
Surge	136.5
Heave	20.5
Pitch	24.8
Yaw	102.4

Figure 9.5 shows the Gumbel distributions for the largest line tension of line 1 for a several systems with varying dimensions with the condition $H_s = 10.4m$ and $T_p = 14s$. The lowest maximum expected line tension is found for the system with 147mm chain links and 1250m

line length. This is the system with the lowest stiffness, thus should have the lowest tensions. The system with a lowered pretension also shows a smaller expected maximum line tension.

The three lines with a diameter of 172mm is seen to have similar expected maximum values, this further implies that for dimensions of this size, the length of the cable has little impact on the tension due to the small difference in elasticity.

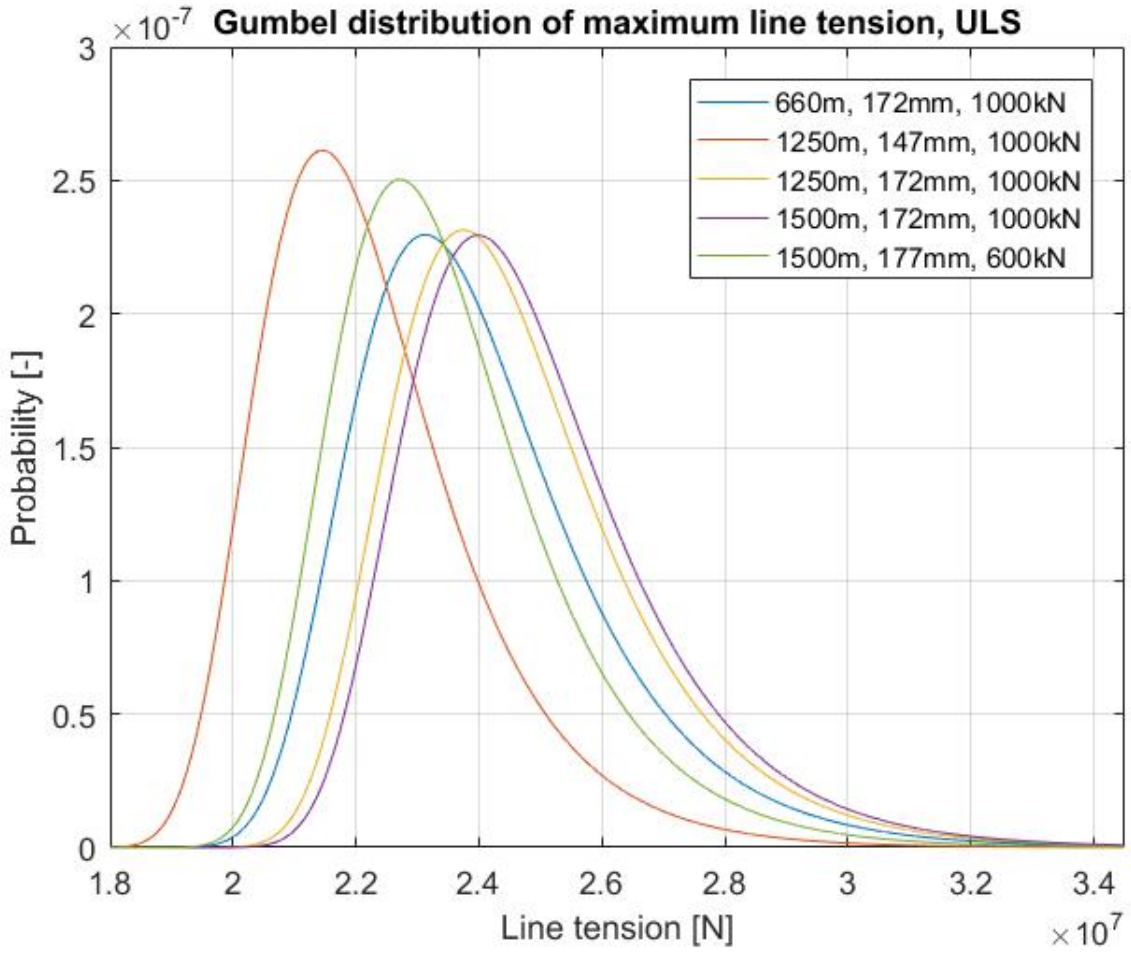

Figure 9.5: Gumbel distribution of the largest line tension for a system with 172mm studless chain, 1000kN pretension and 1250m line length

As mentioned in section 8.1.6, the wave condition with the same period as the natural period in heave should be assessed. The results are shown in figure 9.6, and it is seen that the expected tension is well below the expected tension for conditions with higher H_s. T_d for this condition is 14632kN. The low desig tension is a result of the low significant wave height which is to small to excite large forces on the mooring lines despite a wave period which coincide with the natural period in heave.

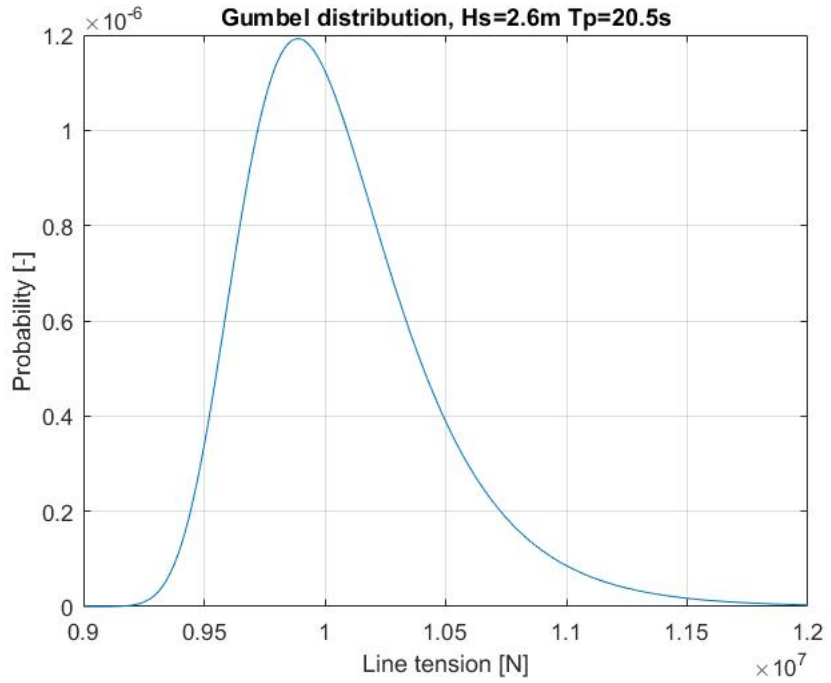

Figure 9.6: Gumbel distribution of line tension, L=1500m d=172mm $T_{pretension}$=600kN

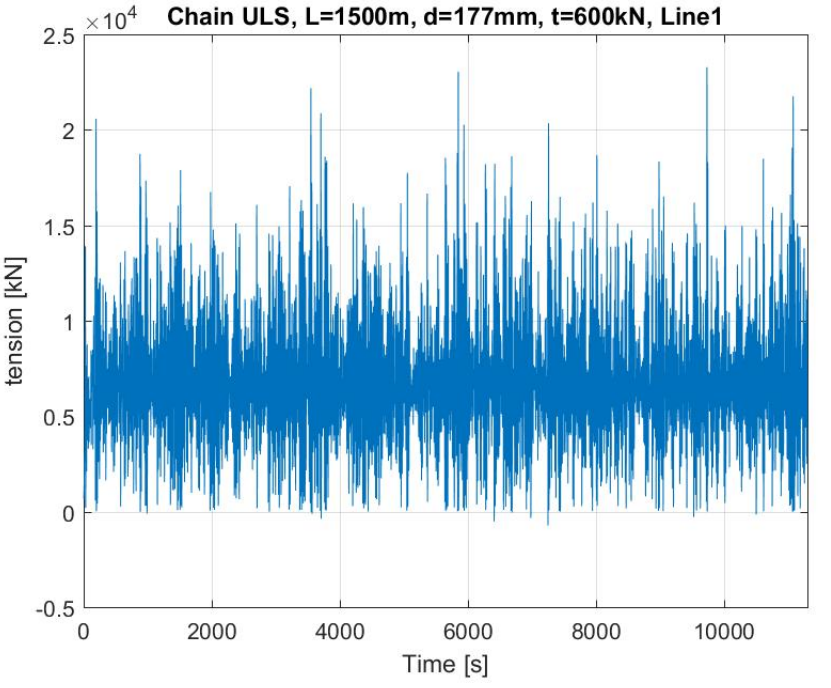

Figure 9.7: Line tension for Line 1 in ULS, Hs=10.4m Tp=14s

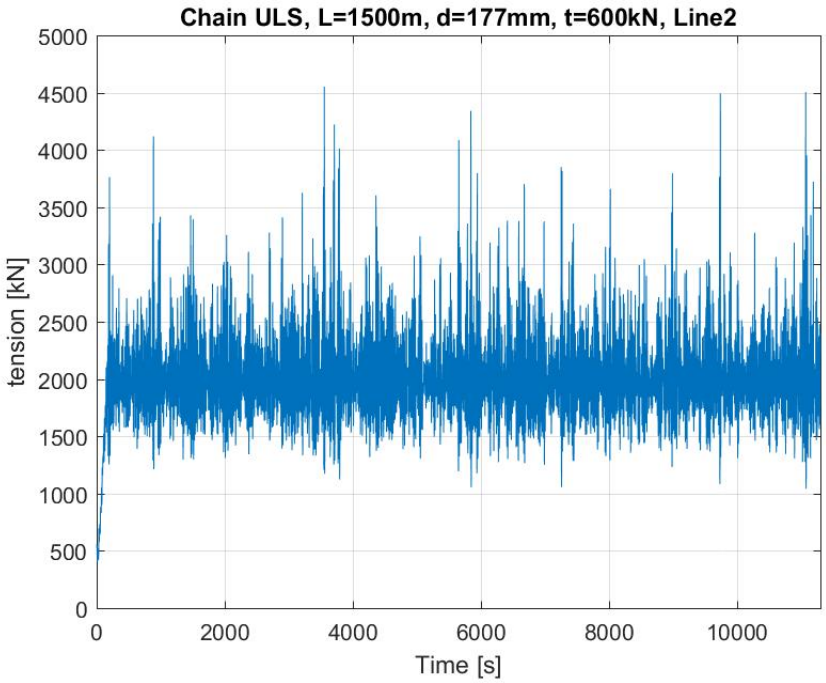

Figure 9.8: Line tension for Line 2 in ULS, Hs=10.4m Tp=14s

The time series of the line tension in line 1 and 2 for a system of length=1500m, d=177mm and a pretension of 600kN is shown in figures 9.7 and 9.8. The mean tension in line 1 is much higher than for line 2, this is expected due to the direction of the environmental loads.

The reason for the lower dynamic tension in line 2 is due to angle of the line. The system oscillates in x direction, so the same movement at fair 1 will give a grater offset than for a motion in fair 2 in x-direction. By looking at the shape of the system characteristic in figure 8.5 the same offset for a higher mean tension will excite higher tensions, so these findings are in accordance with the calculations done for the system.

When assessing the FFT plots given in appendix A.2 it is seen that most of the forces contributing to the line tension are excited by the waves. The lack of spikes at the structure's natural periods prove that no resonance is occurring.

The mean offset in surge is found to be increasing with longer lines, which is expected due to an increase in elasticity. Figure A.15a shows the offset in surge for the 1250m line with a diameter of 147mm. By comparison with the 172mm chain of the same length it is seen that the offset offset of the lighter chain is smaller. A possible reason for this is that the line tension is the same for both cases, but the horizontal tension will be different. The lighter line will have a larger horizontal tension due to a reduction in vertical tension, and thus have ha smaller offset horizontally. From appendix A.2 it is seen that the mooring system does not influence the mean or dynamic pitch motion in any significant way, and it stays with a mean value of approximately -4 degrees for every system.

Since no system has a sufficiently low design tension, the required elasticity is found by an iterative process of simulations for a system with 1500m line length, a chain diameter of

177m and 600kN pretension. Figure 9.9 shows the Gumbel distribution for the most probable maximum line tension for the systems with reduced EA. T_d for EA=3E+09 is 27788kN and for EA=4E+09 T_d=31782kN. To get a sufficiently low T_d, EA needs to be reduced with approximately 50%.

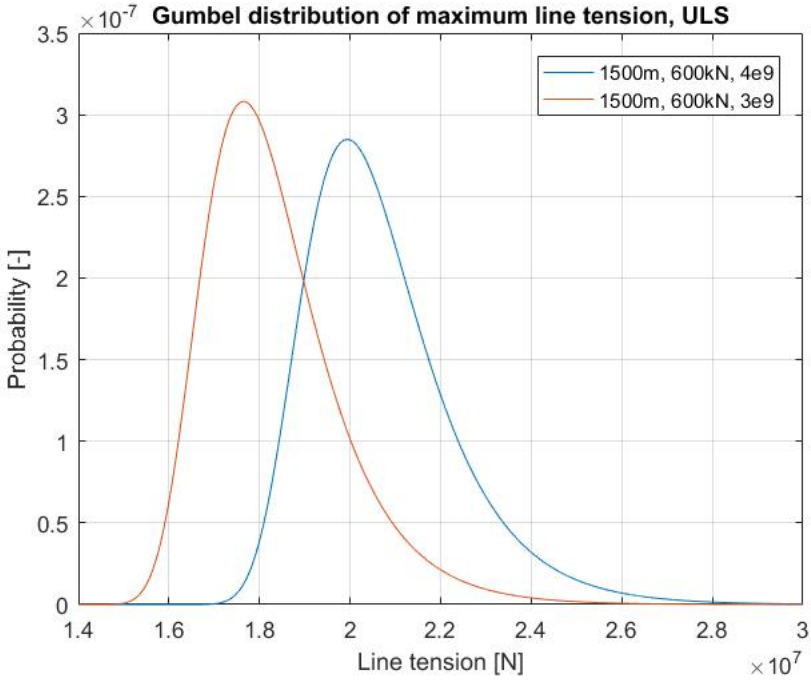

Figure 9.9: Gumbel distribution of most probable maximum line tension, line 1 L=1500m d=177mm T=600kN

9.3.1 Accidental limit state

It is seen in figure 9.10 that the expected maximum line tension is much lower for the ALS condition, for this system $T_d = 25682kN$ and it can be concluded that the ultimate limit state is the dimensioning state. The difference in T_d is so large that a comprehensive study is not needed.

The difference is due to the geometry of the mooring system. The forces of each line in ALS condition should have the same tension as line 1 in ULS, but when line 1 is broken, the configuration changes from 9.11a to 9.11b shown in figure 9.11 and the tension contribution from line 2 and 3 in the weather direction is removed. This reduces the combined mean tension in the lines acting against the weather and the over all maximum line tension is reduced.

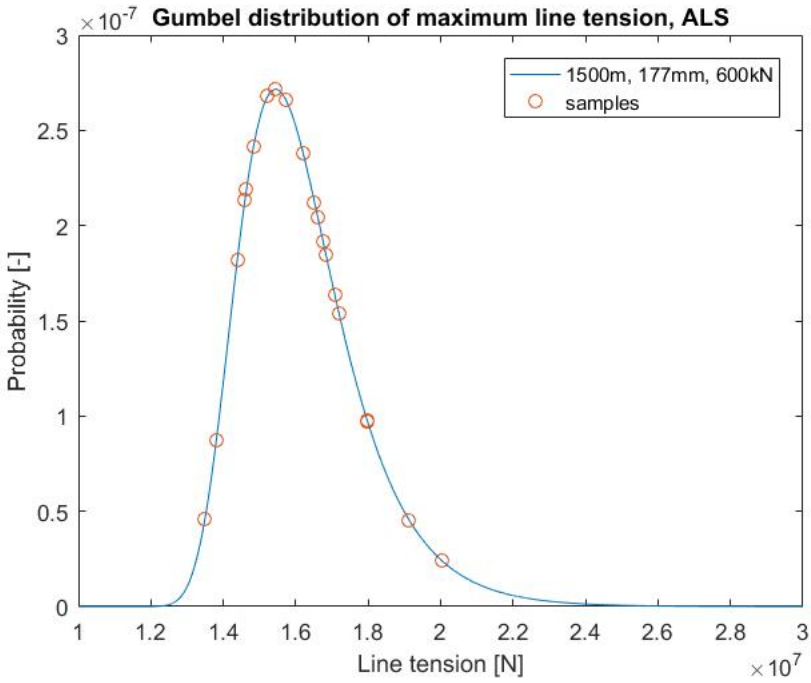

Figure 9.10: Gumbel distribution of most probable maximum line tension, line 1 L=1500m d=177mm T=600kN

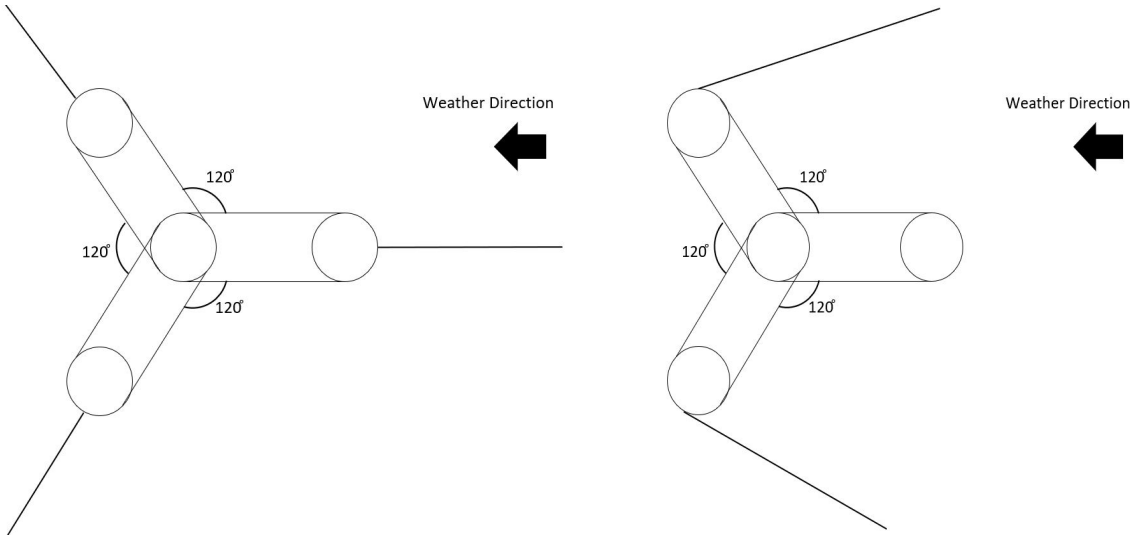

(a) ULS (b) ALS

Figure 9.11: Line configuration for ULS and ALS conditions

By assuring that the fastening system for the mooring lines are similar to the system used for Hywind Scotland shown in figure 4.6 no additional safety factors needs to be applied for ALS calculation. These systems make it possible for large changes in fastening angles without reducing the total breakingstrength of the mooring system.

9.3.2 50-year conditions

To check if the largest H_s from the contour plot shown in figure 9.1 gives the largest tensions in the system several combinations along the contour of the 50-year condition was tested for a chain system of L=1500m, d=172mm and a pretension of 600kN. As seen in figure 9.12 the condition with $H_s = 10m$ and $T_p = 15.6s$ gives the most probable largest tension in line 1. This condition also gives the largest design tension of 34957kN for this system.

To explain this it is necessary to loo at the RAO's of the chain system. Wind turbines are usually associated with large wave forces, so that the larges H_s values generates the largest tensions is to be expected. When looking at the RAO in surge shown in figure 8.1 it is steadily rising with a small contribution around the pitch natural period, and the increased motions from a rise in T_p is larger than the reduction due to a lower H_s. This effect will not continue with increased T_d due to the shape of the contour plot. Around $T_p = 15.6s$ the significant wave height is rapidly decreasing, and will give much lower line tensions as seen in figure 9.12.

Figure 9.13 shows the two most probable maximum line tension in line 1 with the sample values used to generate the Gumbel distributions. An interesting observation is the two largest samples from the condition with $T_p = 15.6s$ which indicates that there are two combinations of seed values used for this condition that is especially unfavourable. This makes the Gumbel distribution to shift to the right, thus a larger T_d. It can be argued that the distribution is artificially high, and that the actual most probable maximum would be closer to the condition with the largest H_s. This would imply that the difference in the conditions is small, and a comprehensive analysis of $T_p = 15.6s$ would yield little difference in T_d. Due to the sensitivity analysis, 20 simulations is sufficient to get consistent results, and analysis of this condition should be conducted.

Since the chain system does not meet the requirements for a condition which yields a smaller line tension, it is not conducted.

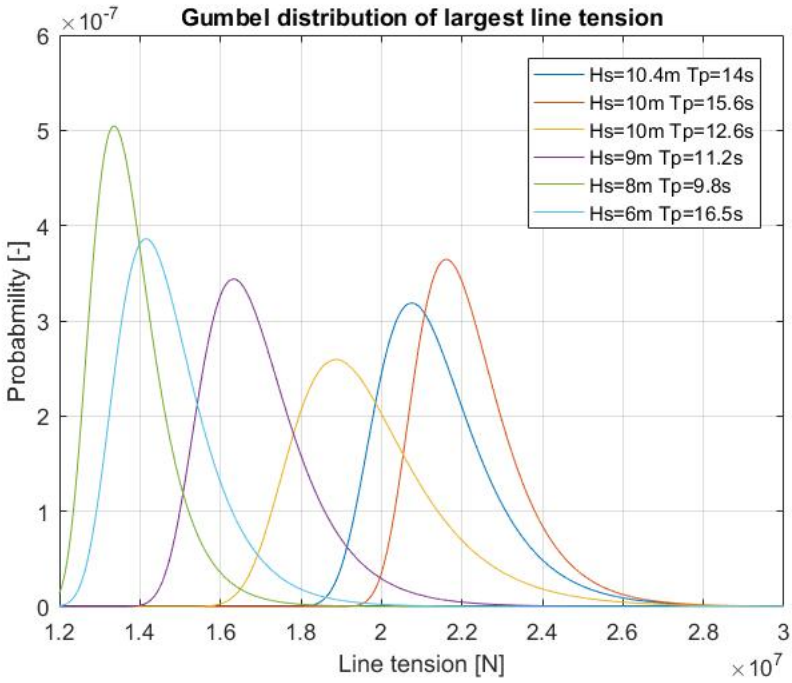

Figure 9.12: Most probable max line tension, Line1, L=1500m d=172mm T=600kN

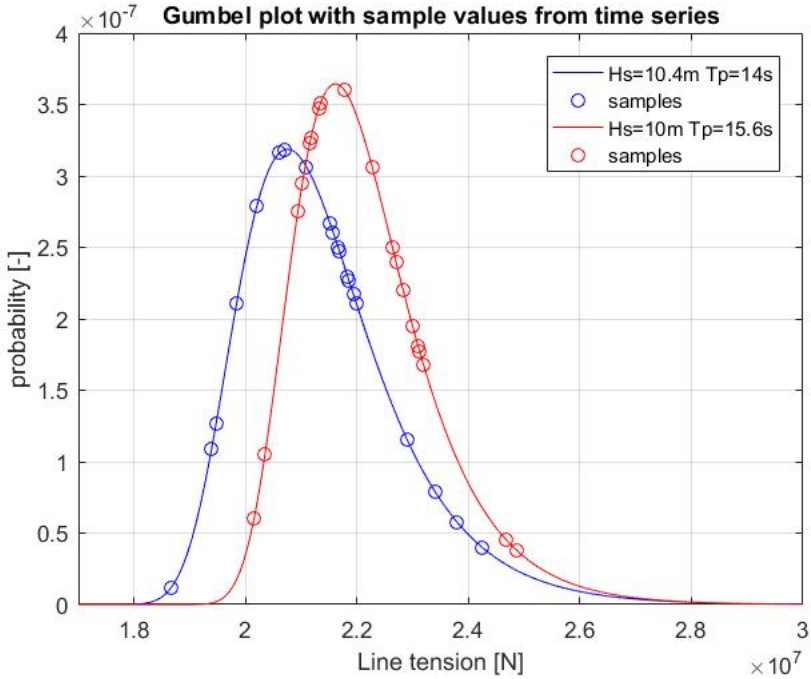

Figure 9.13: Most probable max line tension with sample values, Line1, L=1500m d=172mm T=600kN

9.3.3 Conclusion points

- UlS is the dimensioning condition, meaning that T_d will be largest in this state.

- For this wind turbine a chain mooring system is not a feasible options, and it is found that a significant reduction in axial stiffness is needed to meet the requirements.
- The chain system will be able to withstand ALS, and since T_d for ALS is much lower than MBL, it is concluded that the normal safety factor for T_d calculations is sufficient.
- The condition generating the higest design tension is with a wind speed of 34.5m/s, $H_s = 10m$ and $T_p = 15.6s$.

9.4 Polyester mooring system

Table 9.3 shows the results from the polyester mooring analysis for different line length with varying pretension for line 1. It is seen that the only systems that does not meet the requirements for the T_d is for 500m line length with a pretension of 1000kN and 1500kN. The trend with increased pretension is that the mean forces is elevated and the dynamic forces is reduced with the exception of pretension 1500kN where the dynamic tension seems to be slightly increasing for 500m and 600m line length. With respect to mooring analysis, the design tension is observed to be more or less constant for each line length and varying pretension between 1000 and 2000kN. The dynamic tension is slightly lowered, and mean tensions are rised, due to the different safety factors applied in equation 5.1, T_d remains unchanged.

Table 9.3: Design tension for polyester mooring systems

Diameter [mm]	Length [m]	Pretension [kN]	MBL [kN]	Mean [kN]	Dynamic [kN]	Td [kN]
281	500	1000	21582	57366	89853	23182
281	500	1500	21582	58697	89983	23378
281	600	1000	21582	58487	75583	20830
281	600	1500	21582	59794	75536	20992
281	600	2000	21582	61476	75384	21184
281	800	1000	21582	61231	59209	18322
281	800	1500	21582	62542	58908	18439
281	800	2000	21582	64201	58499	18583
281	800	3000	21582	69007	57232	18986
281	1200	4000	21582	80382	43298	18027

The Gumbel distributions of probable maximum line tension for line 1 is plotted in figure 9.14 for the systems listed in table 9.3. For increased pretension the most probable max is increased for all systems. This development coincide with T_d, and it is still observed that significant changes with the pretension is not occurring.

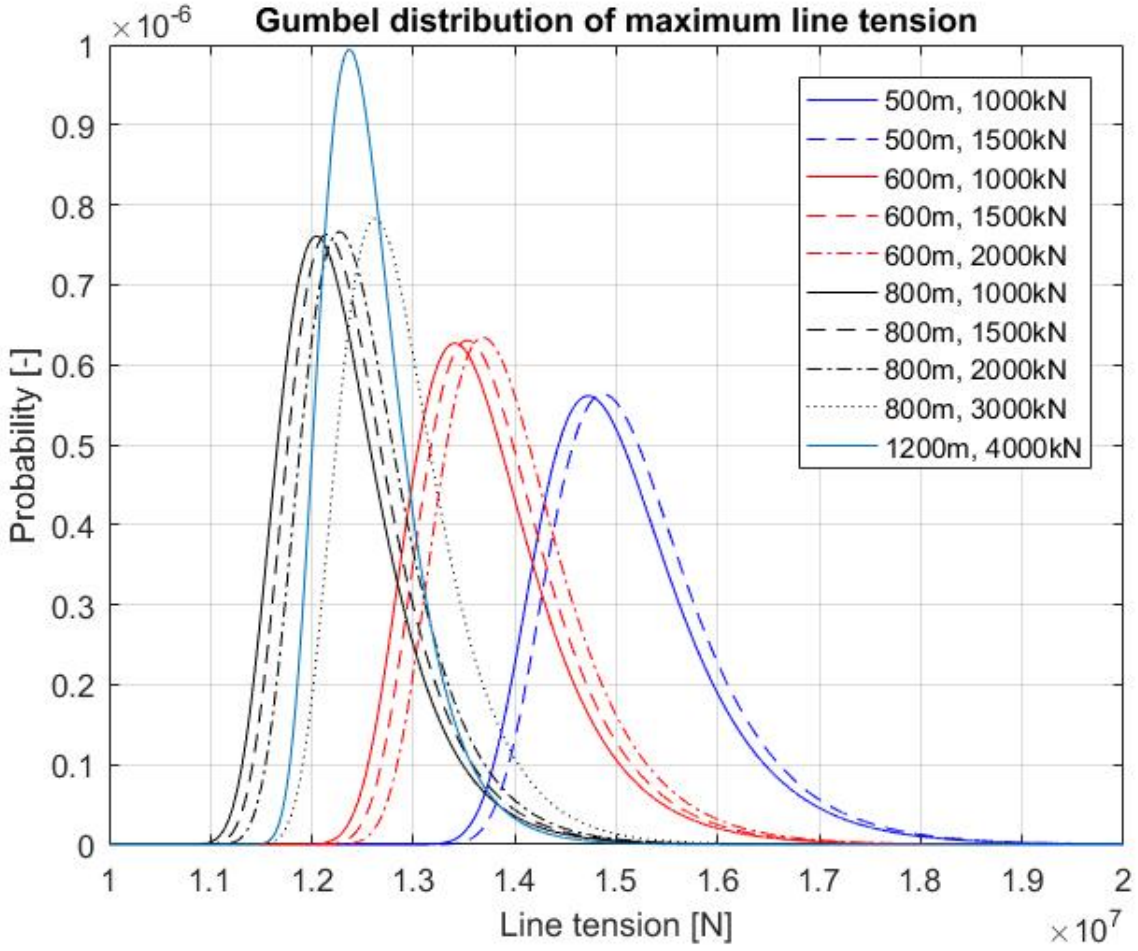

Figure 9.14: Gumbel distribution of expected maximum line tension for polyester lines with different length

Figure 9.15 shows the Gumbel distribution for the system with 800m line length and 3000kN pretension. The sample values used to determine the Gumbel distribution is plotted as a verification of the statistical model used to determine the most probable maximum values.

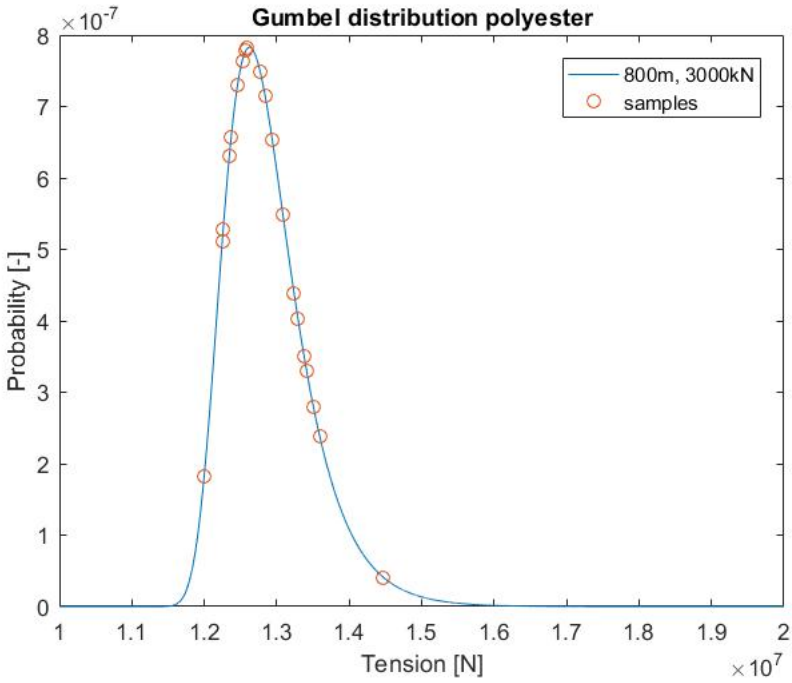

Figure 9.15: Gumbel distribution of expected maximum line tension with sample values for line 1

Since the polyester lines must be prohibited from going slack, and as mentioned in section 5.2 it is necessary to evaluate the most probable minimum line tension. Figure 9.16 shows the Gumbel distribution for the most probable minimum line tension in line 2. Line 2 is evaluated because it is in line 2 and line 3 that the lowest tensions will occur due to the weather direction. It is seen that all systems with the exception of the 800m line with 3000kN in pretension and the 1200m line has a most probable minimum line tension below zero. The most probable minimum value goes towards positive tension with increasing pretension and line length. This is due to an increased mean tension in the system.

This finding shows that for polyester mooring system, the dimensioning factor is slack. Another factor that has to be evaluated is the natural periods, shown in table 9.4. As discussed previous, the natural period in heave is within the wave range of the 50-year condition, shown in figure 9.1, but the significant wave height is to small to excite considerable forces on the system as discussed previous. For pitch, the natural periods of the polyester rope systems are just outside the range of the 50-year condition and resonance should be avoided. Resonance in surge will excite the largest forces on the mooring system due to the direction of the motion, so the natural period should be well outside the limit. For 500m systems the natural period is evaluated to be too close to the limit, and a natural period above 30s and favourably closer to 40s and higher are recommended. The 600m systems are quite close to 30 and should be avoided, so a polyester system for this turbine should have a minimum of 800m mooring lines.

Table 9.4: Natural periods for polyester mooring systems

Length [m]	diameter [mm]	Surge [s]	Heave [s]	Pitch [s]
500	281	28.5	19.7	23.3
500	281	28.5	19.7	23.3
500	281	28.5	19.7	23.3
600	281	32	19.7	23.3
600	281	32	19.7	23.3
800	281	36.6	19.7	23.3
1200	281	36.6	19.7	21.3

One of the reasons for the occurrence of slack in short taut mooring lines is that the elongation due to tension follows $\epsilon = T\frac{L}{EA}$, so for a short rope, the tension needs to be very high to get a large elongation. This means that the system can not absorb large horizontal motions, and goes slack. By installing a clump weight or a buoyancy element, this can be change by changing the geometry of the lines shown in figure2.19. In this configuration, a larger offset can theoretically be absorbed, and slack may be avoided.

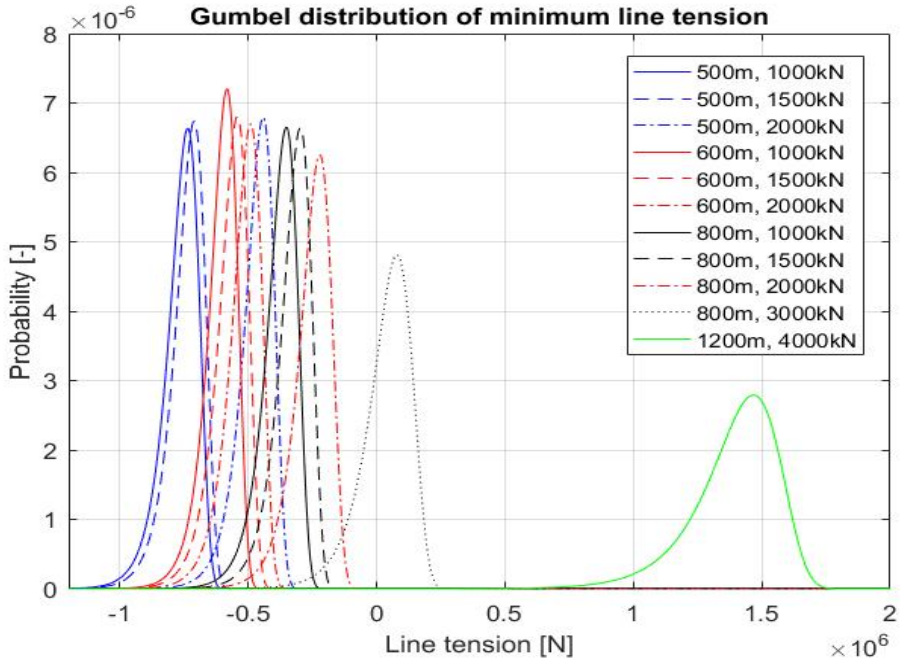

(a)

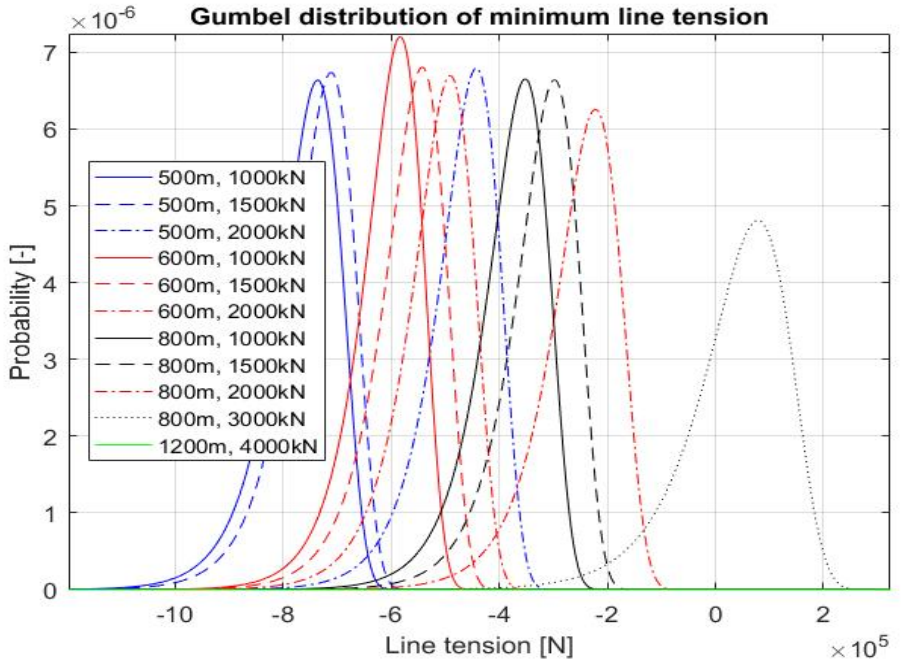

(b)

Figure 9.16: Gumbel distribution of expected minimum line tension for line 2

As seen by figure 9.17 8 of 20 values used to determine the Gumbel distribution for the expected minimum line tension of line 2 in ULS condition is below 0. By integration of the Gumbel distribution for minimum values in line 2 there is a 30% chance that line 2 or 3 goes slack in a 50-year weather conditions. By looking at the sample values this chance is 50%. The large difference in these prediction is due to the two largest values for the distribution which shifts it to the right. A 30% chance of slack would seem like a large chance, but by

definition a storm this strong would only appear once in 50 years. Also, by ensuring inspections of the mooring lines after the passing of a 50-year storm there should be little chance of failure.

As discussed in section 9.3.2 the condition that gives the largest motions is for $H_s = 10m$ and $T_p = 15.6s$. Figure 9.18 shows the expected minimum value for line 2 of this condition, and the minimum tension is also positive for this condition. It can be seen that this condition gives larger motions, and the distribution is shifted to the left. The practical result of this shift is that the chance of slack for a 50-year condition is increased, but the requirement for slack is met.

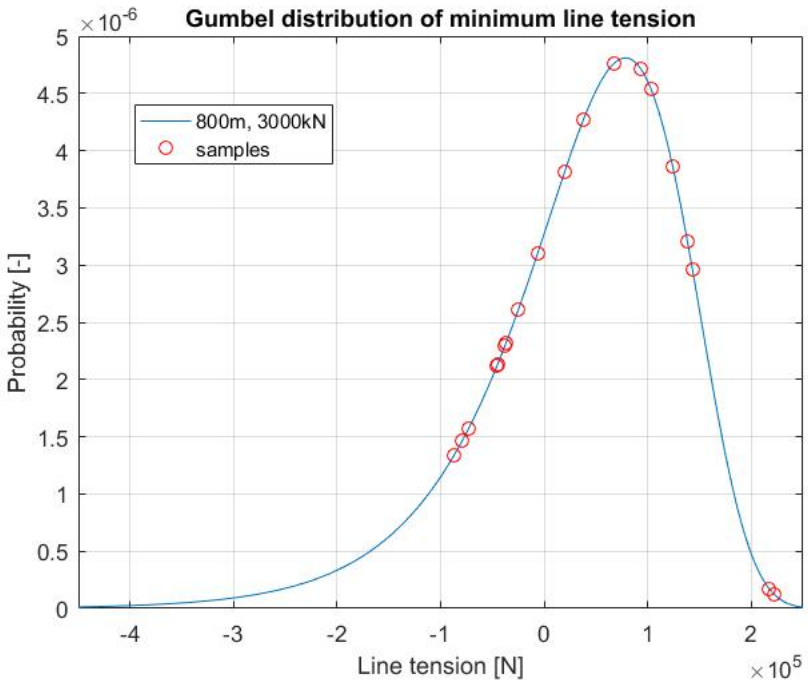

Figure 9.17: Gumbel distribution of expected minimum line tension with sample values for line 2

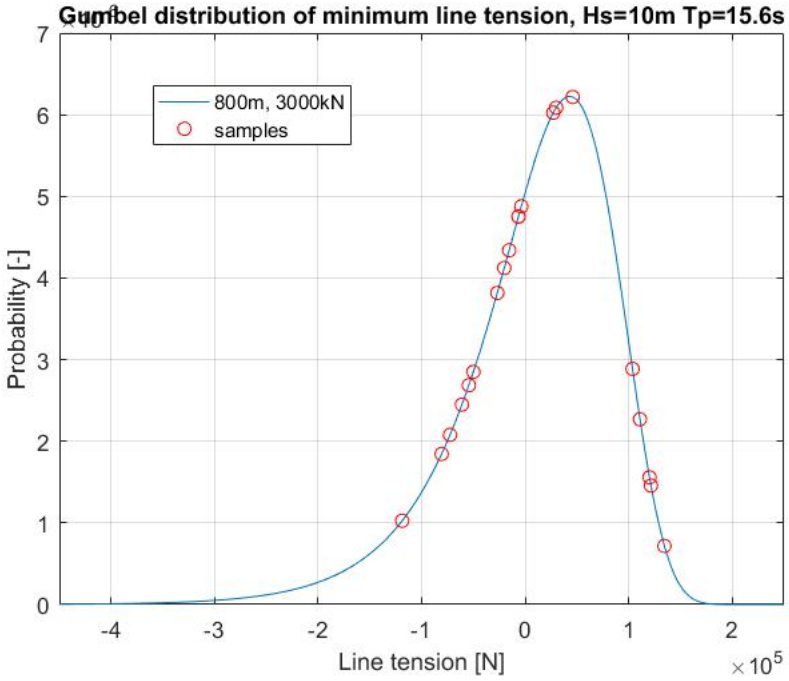

Figure 9.18: Gumbel distribution of expected minimum line tension with sample values for line 2, $H_s = 10m$ and $T_p = 15.6s$

The time series for line 1 and 2 for the polyester systems in table 9.3 are plotted in appendix A.3 with corresponding FFT plots. As seen from most of the plots, the minimum peaks of the line tension in line 2 are negative, including the 800m system with 3000kN pretension. It is only by increasing the pre tension that the mean tension will rise, and the minimum peaks stays positive.

It is difficult to see the change in tension and dynamic tension for line 1 because the differences are small. This is seen in table 9.3, and it is only for high pretensions that a significant shift in tension occurs. The spectre shows that the waves excite the most motions on the structure. This is expected due to the natural periods shown in table 9.4. Non of the natural periods are within the interval of wave periods that is used for these simulations. The natural period in surge are low for short mooring lines, but it does not have any influence on these simulations.

9.4.1 Polyester ALS

The polyester system with 800m line length and a pretension of 3000kN is within the accepted T_d for the ULS condition. To check if the accidental limit state is within the requirements [23] line 1 is unfastened and a set of 20 simulations in a 50-year condition is conducted.

Figure 9.19 shows the extreme value distribution for line 2 in ALS condition, and it is observed that the expected line tension is significantly lower than for the ULS condition. To calculate T_d lower safety factors are also applied 5.1. This provides a T_d of 7311.4kN and it is

concluded that the ULS condition is the dimensioning condition. The reason for the lower line tension in ALS is discussed in subsection 9.3.1

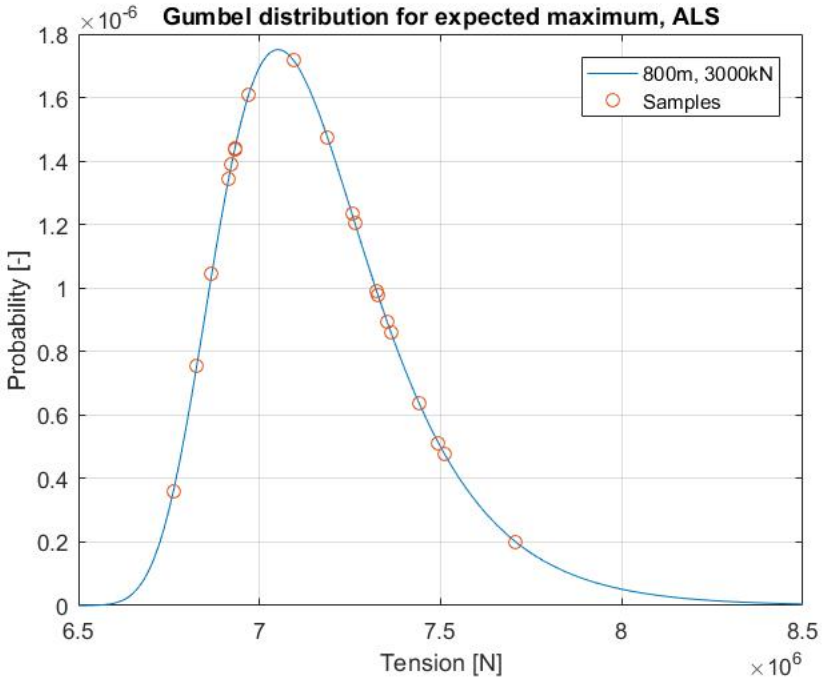

Figure 9.19: Gumbel distribution of expected maximum line tension for line 2 in ALS condition

Since the design tension of the system in ALS is much lower than the braking strength of the lines the consequences of a broken line is not large, and would make a successful rescue operation possible with no damage to other structures as long as they are spaced far enough from each other. The low risk of free floating structures due to storms confirms that the normal safety class factors for dynamic tension is sufficient for design tension calculations.

9.4.2 Conclusion points

- The dimensioning factor for a polyester system for this wind turbine i slack, and the requirements for ULS and ALS are met before this criterion.
- Most of the mooring systems goes slack, and to avoid this a mooring system of 800m with 3000kN pretension is needed. Systems with longer lines and higher pretension will also work, but there is a limit to how much tension in lines it is possible to install.

Chapter 10

Recommendations for further work

10.1 Model verification

It is concluded that the simplified model is accurate with respect to the simplified model. For static winds, the results is assumed to be accurate because of the static nature of the loads. All comparisons between the models was conducted with a minimal number of simulations. Note that the simulations was done with the same seed numbers. For cases were the model experienced a lot of motions, several more simulations should have been conducted to assure the accuracy of the simplified model.

The dynamic response of the simplified model is also only compared with the original model for extreme conditions, so if the model is accurat for all conditions are not known.

A more extensive comparison with the original model should be conducted to assure the accuracy for extreme environmental conditions.

10.2 Sensitivity analysis

A sensitivity analysis is conducted in this thesis to establish the required number of different seed values combinations to get accurate results. This analysis was conducted with 50 different seed values, and as a result 20 different combinations is required to satisfy a 10% deviation for maximum tension and standard deviation. If 50 simulations is sufficient to get convergence are not known and a more extensive analysis should be conducted.

The aim of the simplified model is to reduce calculation time and time step and number of elements simulated for the mooring lines will have a significant impact. To estimate how large the time step can be and how few elements the mooring lines can be assessed to further reduce the simulation time. Much of the mooring lines for the chain systems is resting on the seabed for most of the simulations, and by modelling the mooring lines with smaller elements where large motions will occur should reduce the required amount of elements.

10.3 Clump weights and buoyancy elements

Mooring analyses with clump weights or buoyancy elements should be executed to find out if the line length and can be reduced. Interesting observations for these analyses would be change in natural periods due to reduced stiffness, how the elements will affect the distribution of minimum line tension and how short or long lines are needed. If this should prove feasible, optimization of rope dimensions and length could be done to find a system where both requirements for slack and ULS are met with a small margin, this will reduce cost.

10.4 SIMO model

To further develop the simplified model, a comparison between mooring systems modeled with RIFLEX and SIMO should be done for the simplified model. Mooring lines modelled in SIMO have a much lower simulation time than Mooring lines in RIFLEX. If the forces on the model is similar for the two modelling approaches, a quicker model can be established. If the difference between the models are of consequence, it is still useful to know how much, and if the SIMO model can be used for large scale preliminary analysis of mooring systems with the intent of further analysis with the RIFLEX model.

References

[1] Qiang Wang. Design of a Steel Pontoon-type Semi-submersible Floater Supporting the DTU 10MW Reference Turbine. Master's thesis, Norwegian university of science and technology, Norway, 2014.

[2] Chakrabarti, Subrata K. *HANDBOOK OF OFFSHORE ENGINEERING*, volume 2. Elsevier, 2005.

[3] DNV GL. RIFLEX, Riser System Analysis Program, -.

[4] DNV GL. SIMO, Simulation of Marine Operations, -.

[5] Eirik Falkenberg. Best practice for analysis of mooring systems with polyester ropes, 2015.

[6] Equinor, oktober 2017.

[7] Faltinsen, O. *Sea Loads on Ships and Offshore Structures.* Cambridge Ocean Technology Series. Cambridge University Press, 1993.

[8] Gao, Zhen and Bachynski, Erin. Design and analysis of offshore wind turbines. University Lecture, 2017.

[9] Ghazali, Amir Mohd. Hywind scotland floating wind pilot park. Company presentation, 2016.

[10] Global Energy Group. gegroup, 2018.

[11] Larsen, Kjell. Station keeping and mooring systems. University Lecture, 2015.

[12] Larsen, Kjell. Station keeping and mooring systems. University Lecture, 2017.

[13] Leira, Bernt J. Stochastic theory of sealoads. Kompendium, 2010.

[14] Principle Power. www.principlepowerinc.com, 2018.

[15] Principle power inc. WindFloat Brochure, -.

[16] Ramnas Bruk. Top quality mooring products for harsh offshore conditions, 2015.

[17] SINTEF. Sima - sintef software, *https://www.sintef.no/en/software/sima/*, 2017.

[18] SINTEF Ocean. Simo4.10.1 theory manual. Theory manual, 2017.

[19] Statoil. Hywind, Bushan Deep, Metocean Design Basis, RE2014-002, 2014.

[20] Statoil. Mooring: Detail design. Company presentation, 2014.

[21] Tipler, Paul A and Mosca, Gene. *Physics for scientists and engineers*. W. H. Freeman and Company, 2008.

[22] Veritas, Det Norske. Dnv-os-e301: Position mooring. *Nor-way: DNV*, 39, 2010.

[23] Veritas, Det Norske. DNV-OS-J103: Design of Floating Wind Turbine Structures, 2013.

[24] Vryhof. Anchor manual 2010, 2010.

[25] Vryhof, may 2018.

[26] L. zhong Wang, K. min Shen, L. ling Li, and Z. Guo. Integrated analysis of drag embedment anchor installation. *Ocean Engineering*, 88:149 – 163, 2014.

Appendix A

Appendix

A.1 Comparison with original model

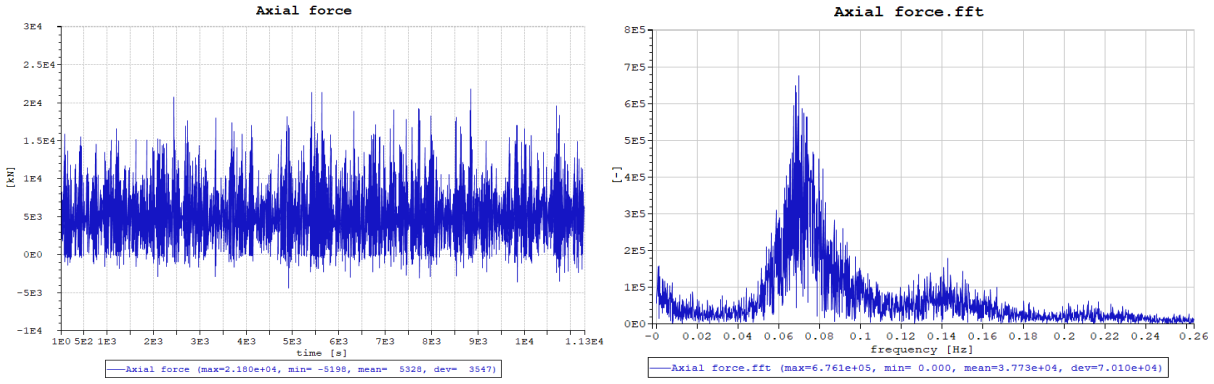

(a) Original

(b) Original FFT

(c) Simplified

(d) Simplified FFT

Figure A.1: Time series and FFT plot of the original and simplified model for tension in line 1, L=660m d=147mm $T_{pretension}$=1000kN

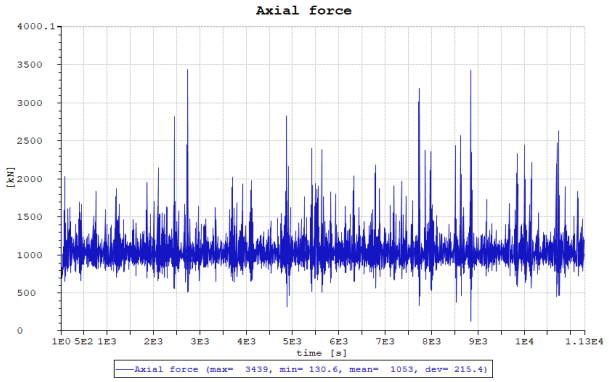

(a) Original

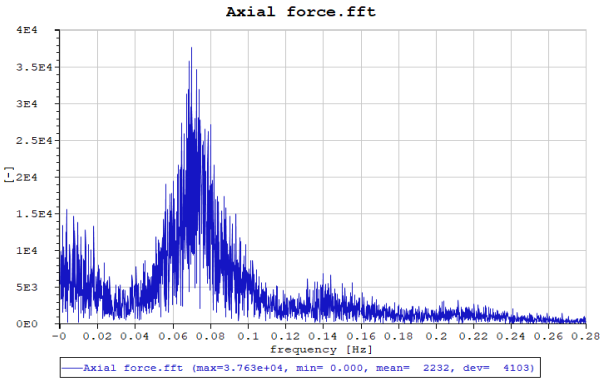

(b) Original FFT

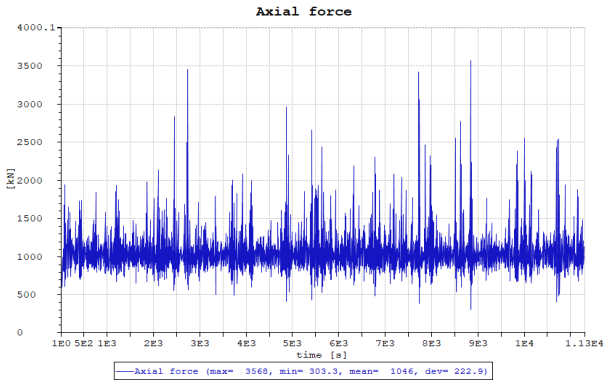

(c) Simplified

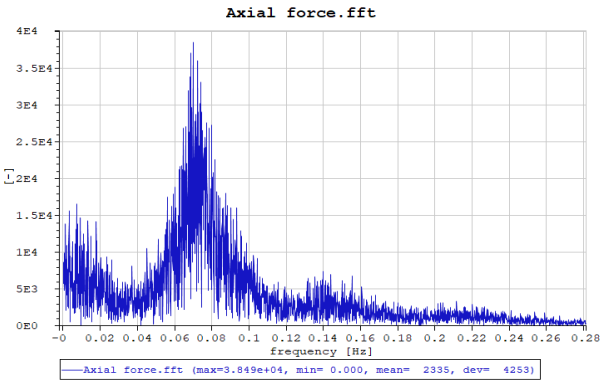

(d) Simplified FFT

Figure A.2: Time series and FFT plot of the original and simplified model for tension in line 2, L=660m d=147mm $T_{pretension}$=1000kN

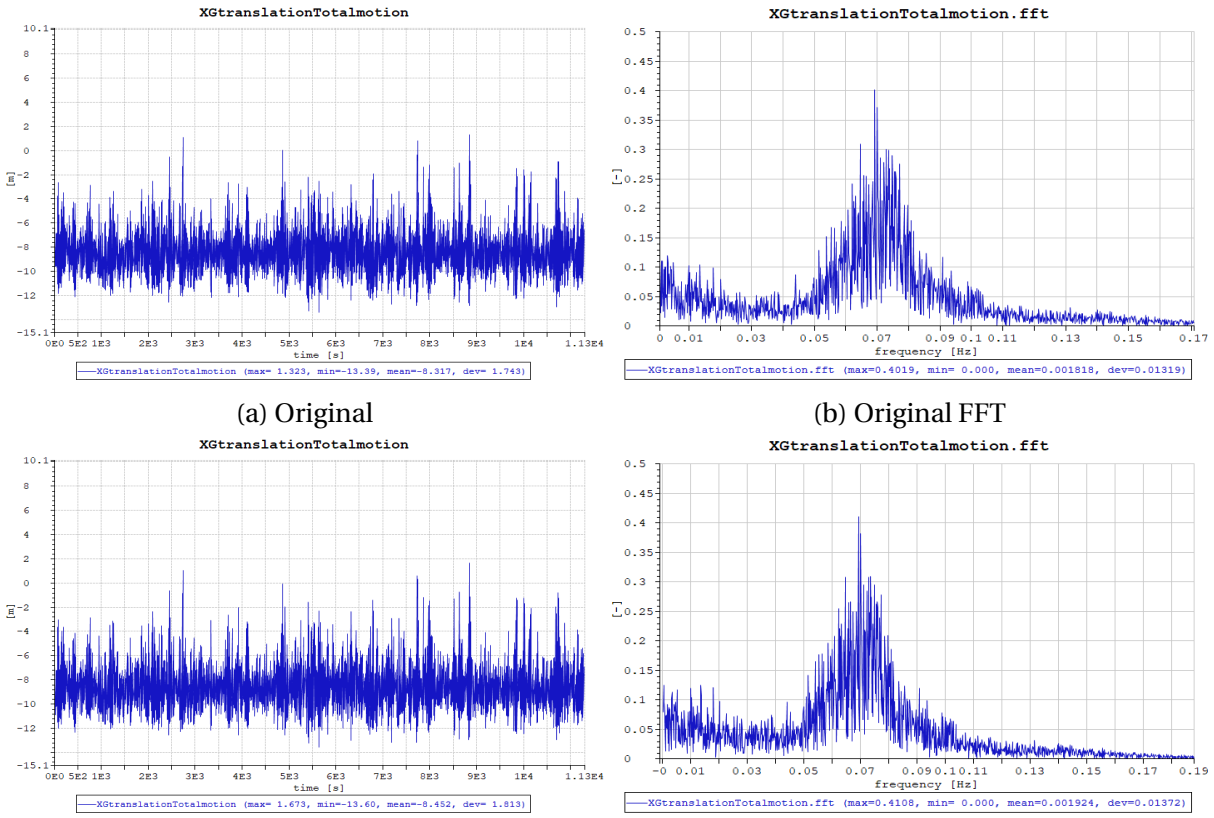

(a) Original

(b) Original FFT

(c) Simplified

(d) Simplified FFT

Figure A.3: Time series and FFT plot of the original and simplified model for surge motion, L=660m d=147mm $T_{pretension}$=1000kN

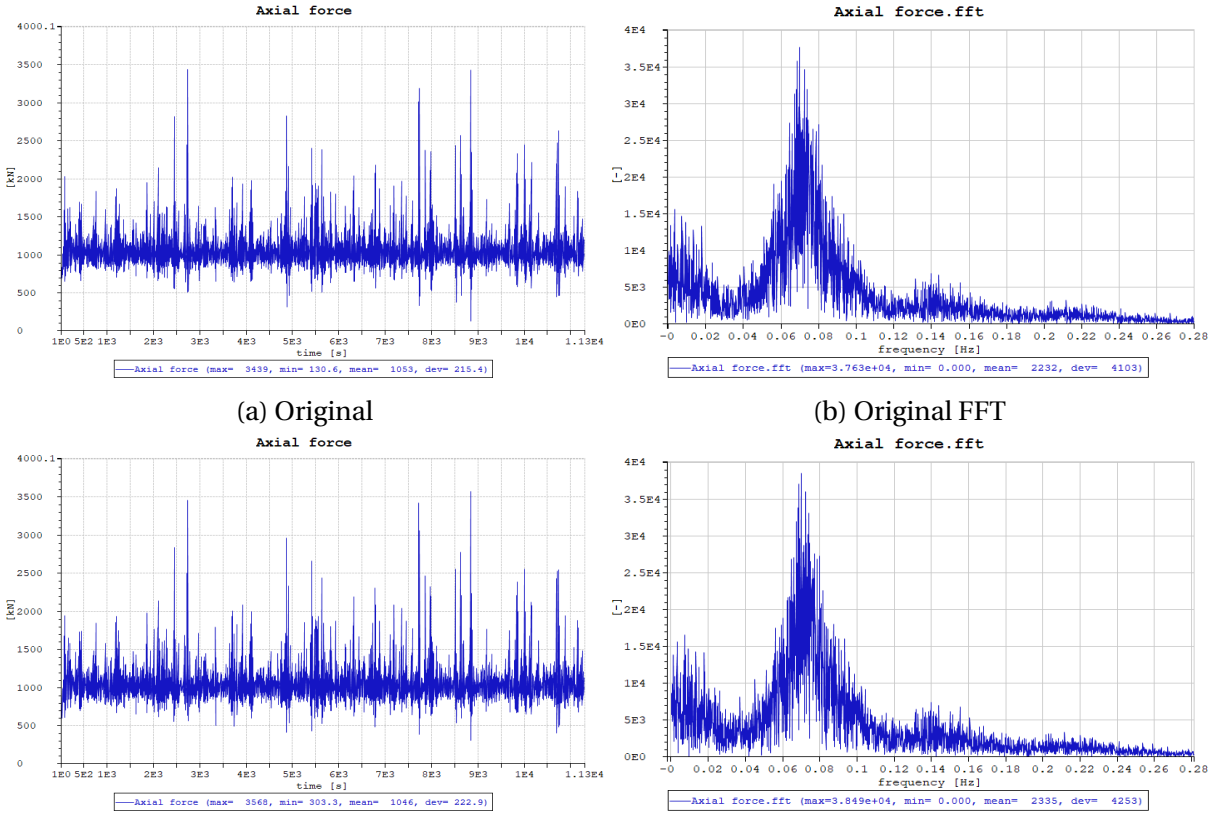

(a) Original

(b) Original FFT

(c) Simplified

(d) Simplified FFT

Figure A.4: Time series and FFT plot of the original and simplified model for tension in line 2, L=660m d=147mm $T_{pretension}$=1000kN

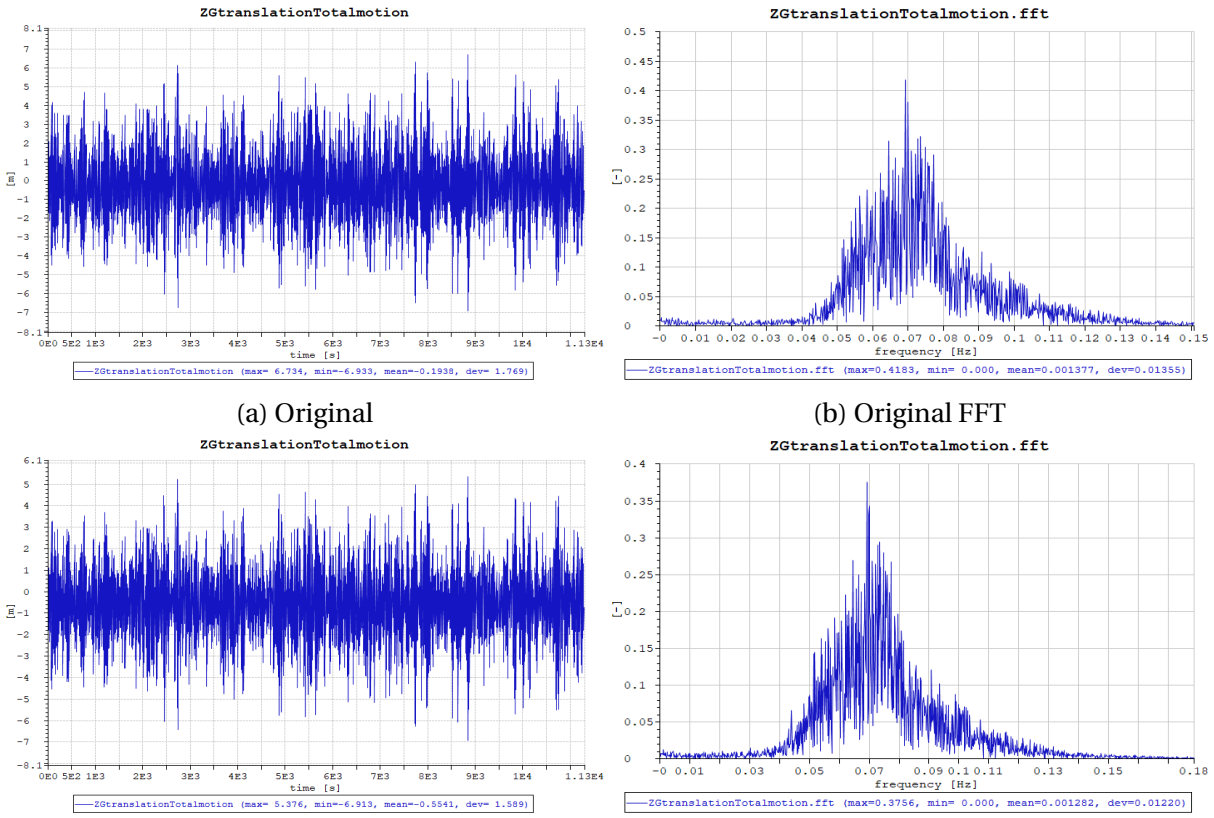

(a) Original

(b) Original FFT

(c) Simplified

(d) Simplified FFT

Figure A.5: Time series and FFT plot of the original and simplified model for heave motion, L=660m d=147mm $T_{pretension}$=1000kN

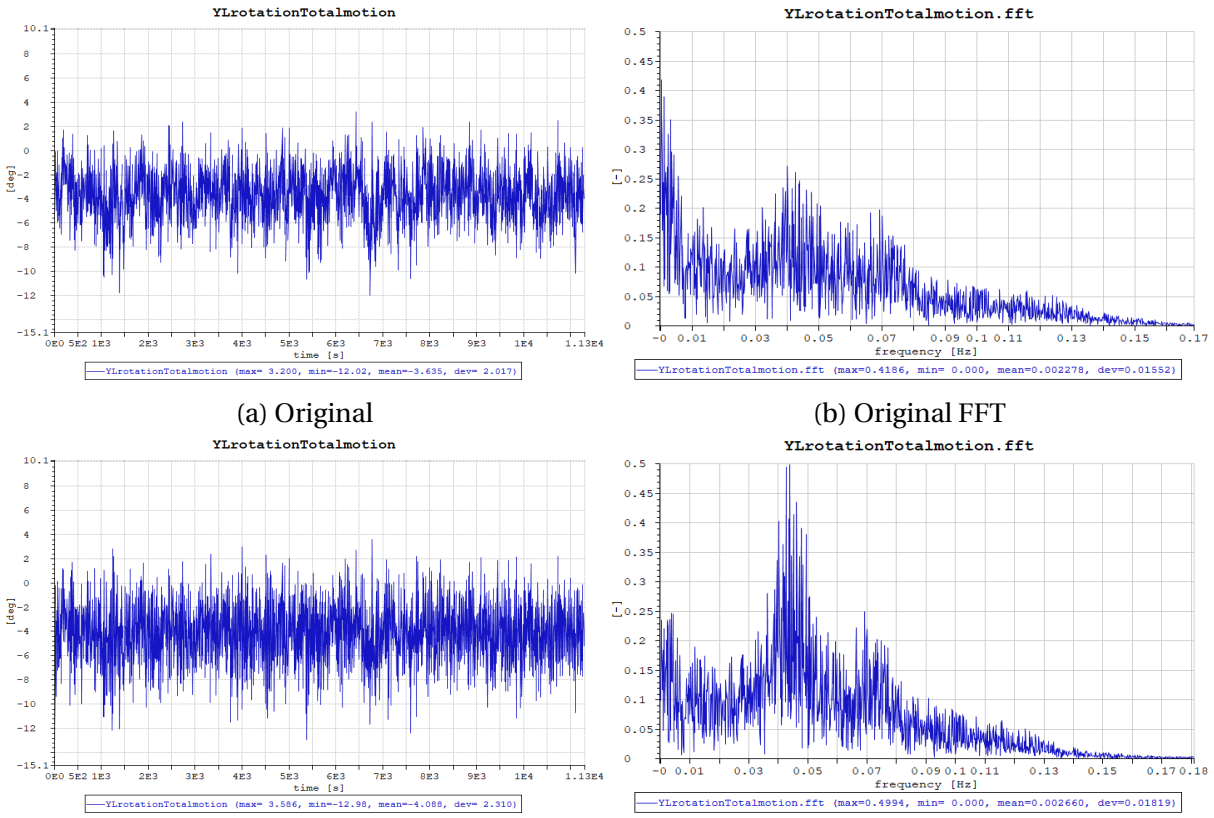

(a) Original (b) Original FFT

(c) Simplified (d) Simplified FFT

Figure A.6: Time series and FFT plot of the original and simplified model for pitch motion, L=660m d=147mm $T_{pretension}$=1000kN

A.2 Chain mooring system

A.2.1 Tension line 1

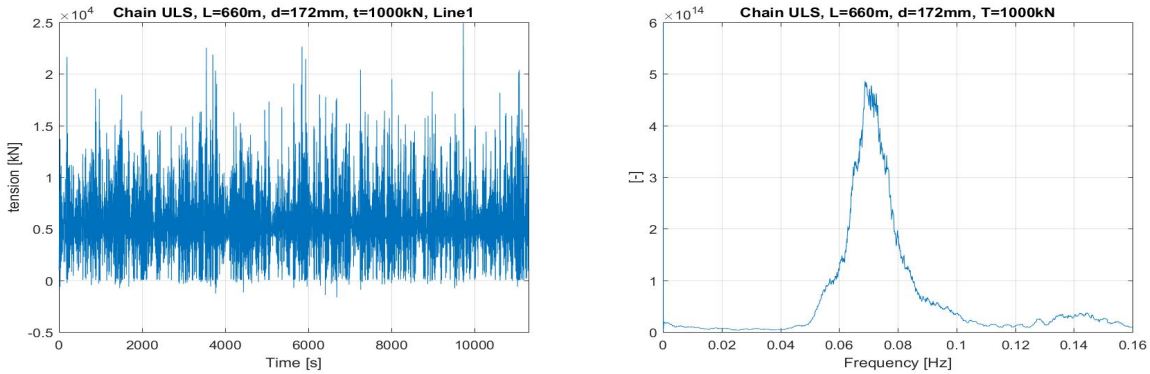

(a) Line tension (b) FFT

Figure A.7: Chain Line 1, L=660m d=172mm $T_{pretension}$=1000kN

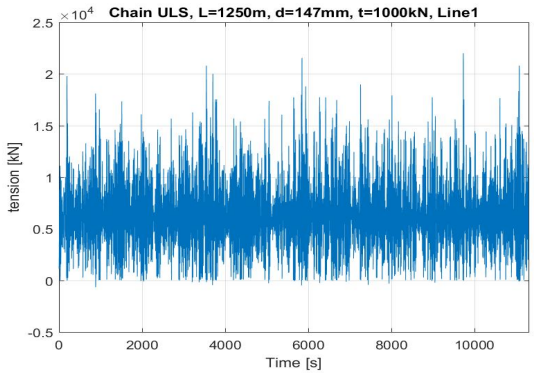

(a) Line tension

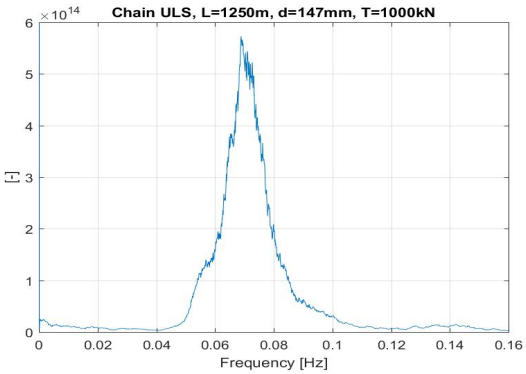

(b) FFT

Figure A.8: Chain Line 1, L=1250m d=147mm $T_{pretension}$=1500kN

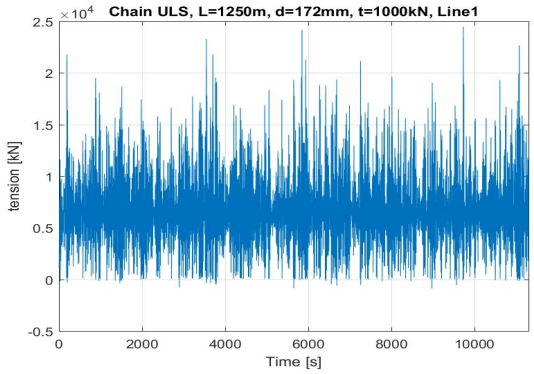

(a) Line tension

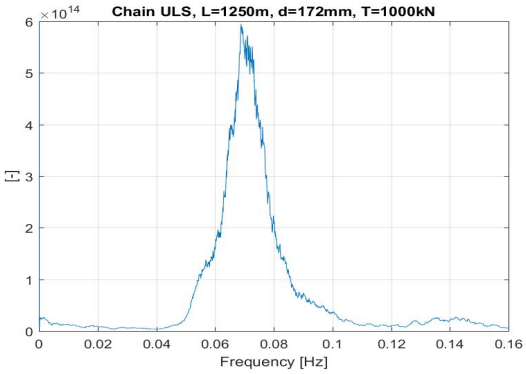

(b) FFT

Figure A.9: Chain Line 1, L=1250m d=172mm $T_{pretension}$=1000kN

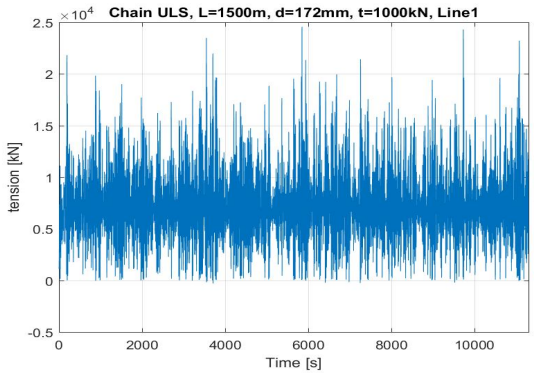

(a) Line tension

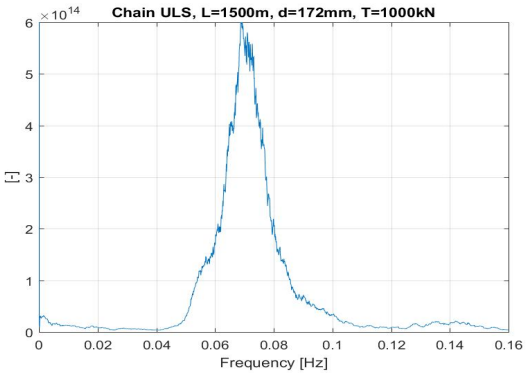

(b) FFT

Figure A.10: Chain Line 1, L=1500m d=172mm $T_{pretension}$=1000kN

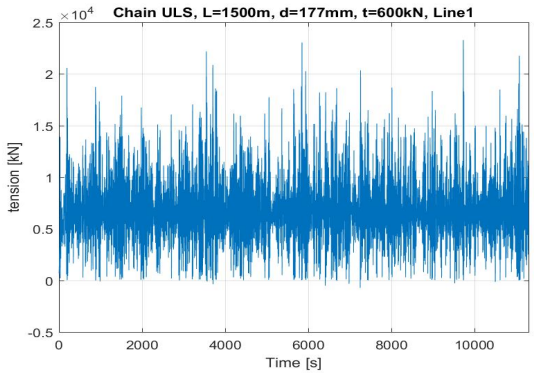

(a) Line tension

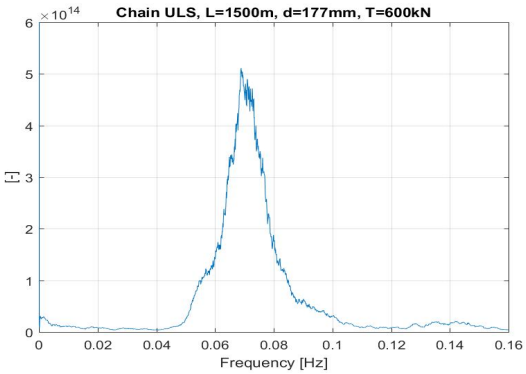

(b) FFT

Figure A.11: Chain Line 1, L=1500m d=172mm $T_{pretension}$=600kN

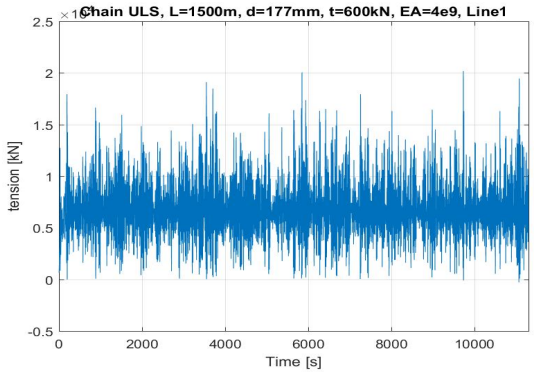

(a) Line tension

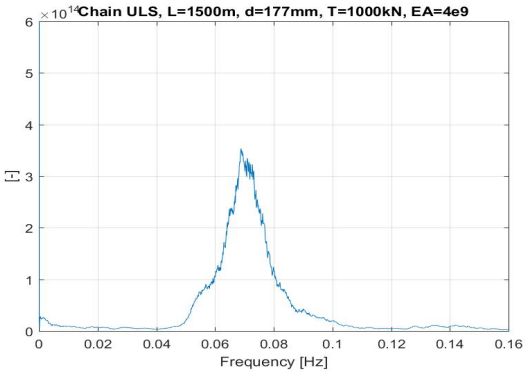

(b) FFT

Figure A.12: Chain Line 1, L=1500m d=172mm $T_{pretension}$=600kN EA=4.0E+09

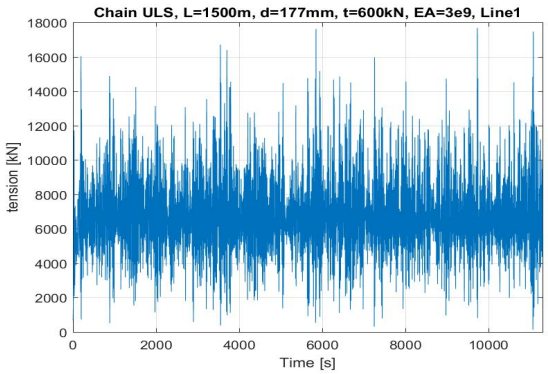

(a) Line tension

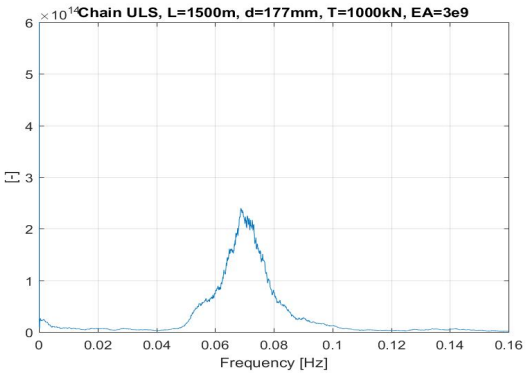

(b) FFT

Figure A.13: Chain Line 1, L=1500m d=172mm $T_{pretension}$=600kN EA=3.0E+09

A.2.2 Surge and pitch motion

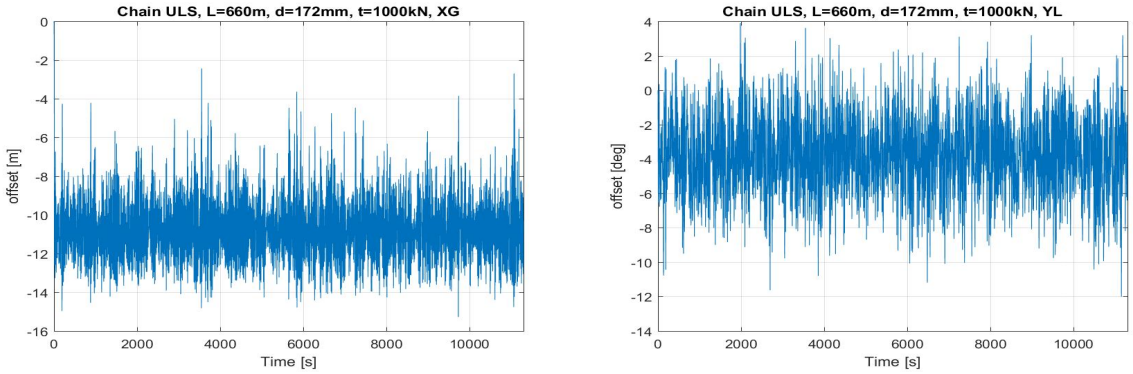

(a) Surge (b) Pitch

Figure A.14: Surgen and pitch motion, L=660m d=172mm $T_{pretension}$=1000kN

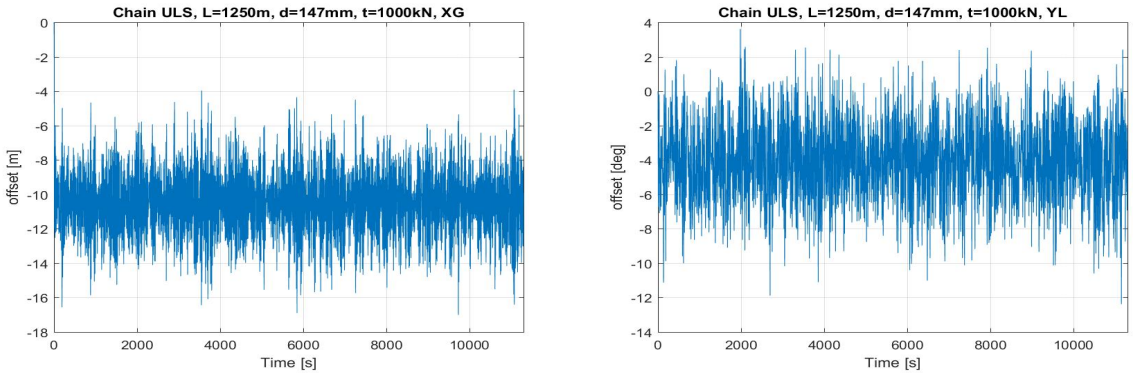

(a) Surge (b) Pitch

Figure A.15: Surge and pitch motion, L=1250m d=147mm $T_{pretension}$=1500kN

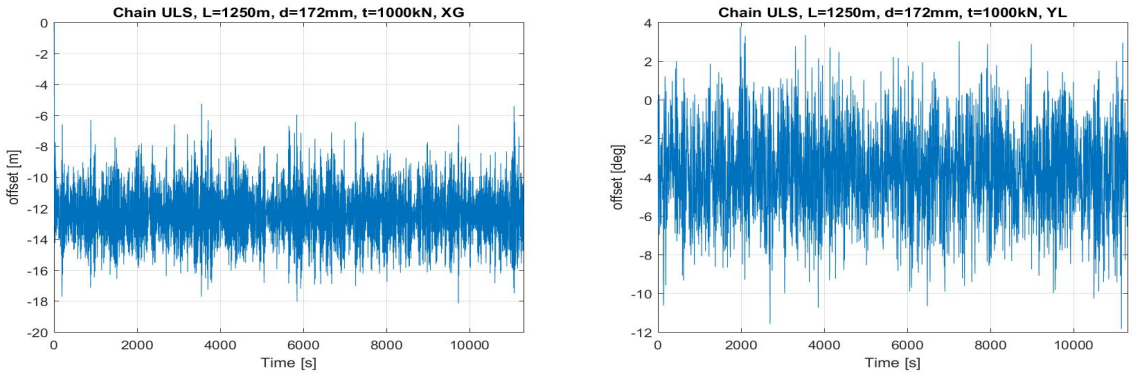

(a) Surge (b) Pitch

Figure A.16: Surge and pitch motion, L=1250m d=172mm $T_{pretension}$=1000kN

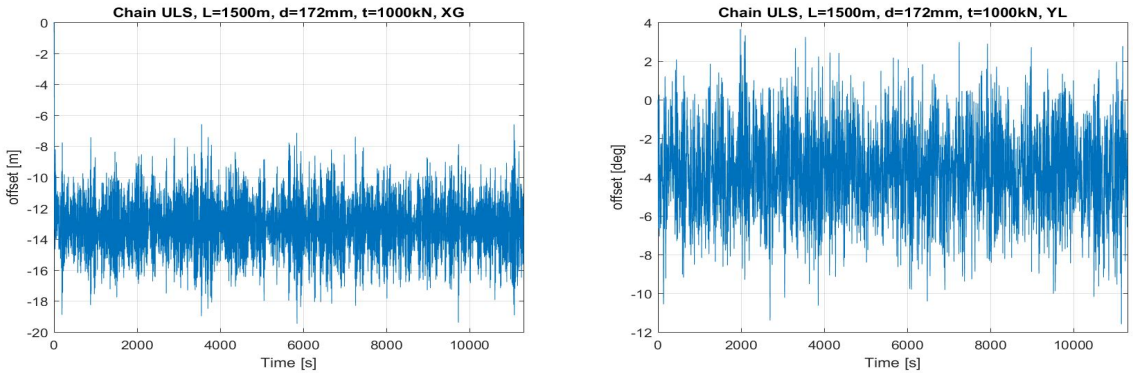

(a) Surge (b) Pitch

Figure A.17: Surge and pitch motion, L=1500m d=172mm $T_{pretension}$=1000kN

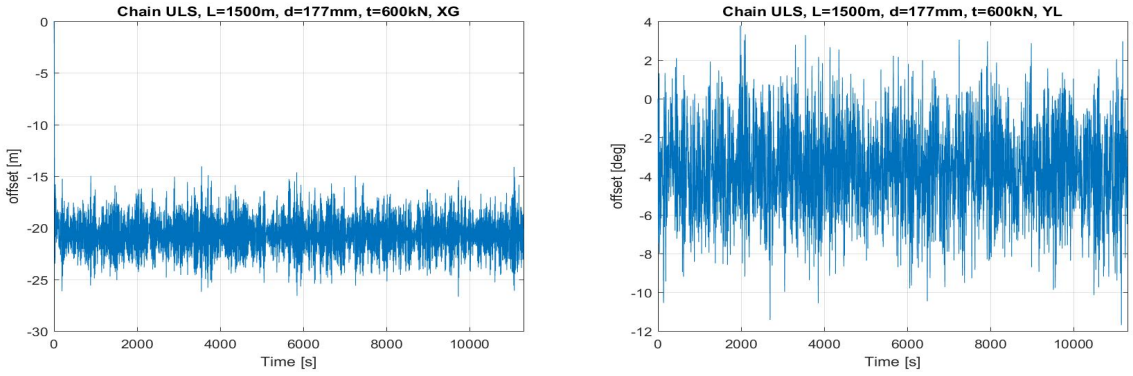

(a) Surge (b) Pitch

Figure A.18: Surge and pitch motion, L=1500m d=177mm $T_{pretension}$=600kN

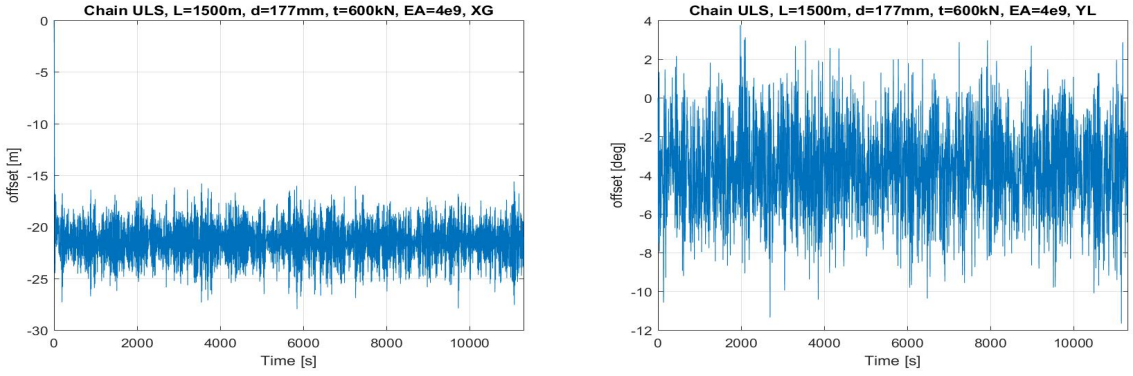

(a) Surge (b) Pitch

Figure A.19: Surge and pitch motion, L=1500m d=172mm $T_{pretension}$=600kN EA=4.0E+09

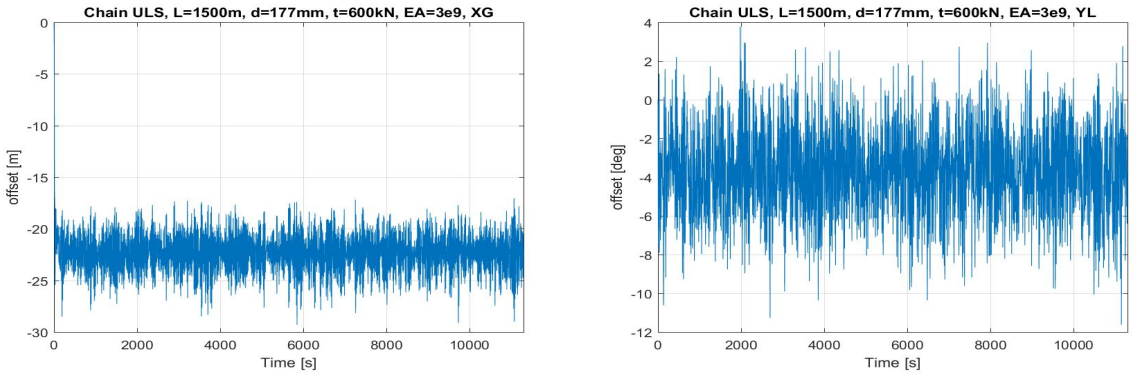

(a) Surge (b) Pitch

Figure A.20: Surge and pitch motion, L=1500m d=172mm $T_{pretension}$=600kN EA=3.0E+09

A.3 Polyester mooring system

A.3.1 Line 1

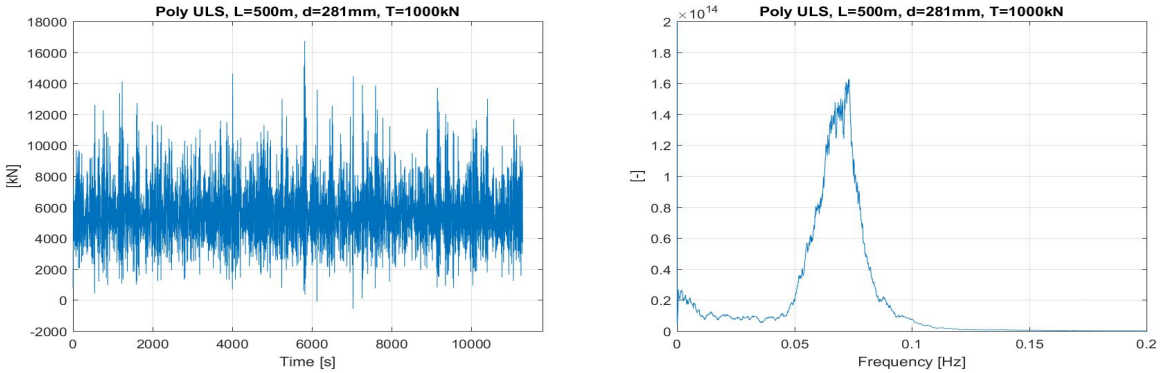

(a) Line tension (b) FFT

Figure A.21: Polyester Line 1, L=500m d=281mm $T_{pretension}$=1000kN

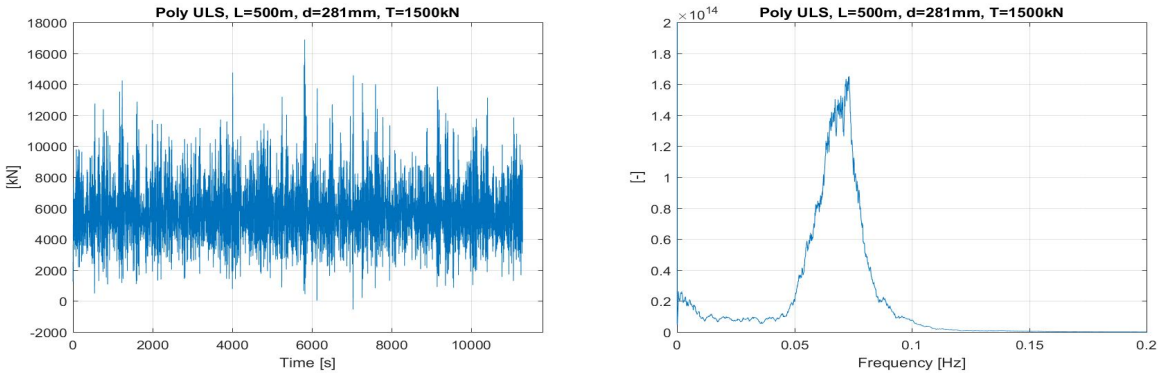

(a) Line tension (b) FFT

Figure A.22: Polyester Line 1, L=500m d=281mm $T_{pretension}$=1500kN

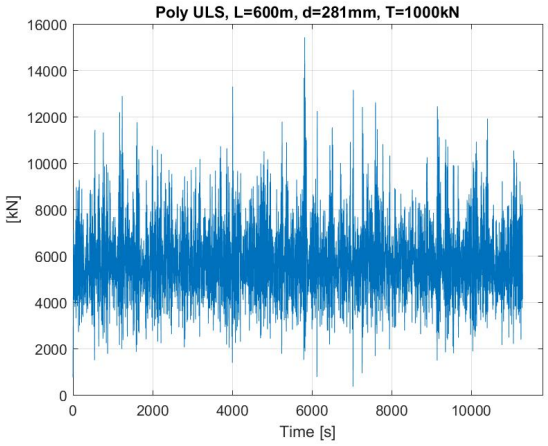

(a) Line tension

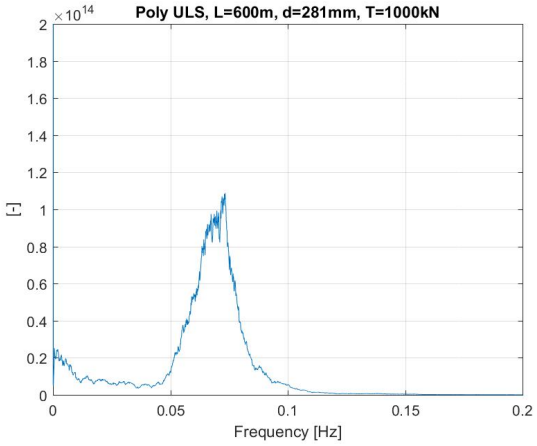

(b) FFT

Figure A.23: Polyester Line 1, L=600m d=281mm $T_{pretension}$=1000kN

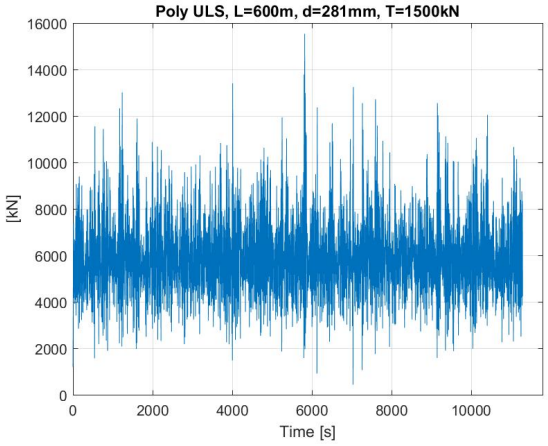

(a) Line tension

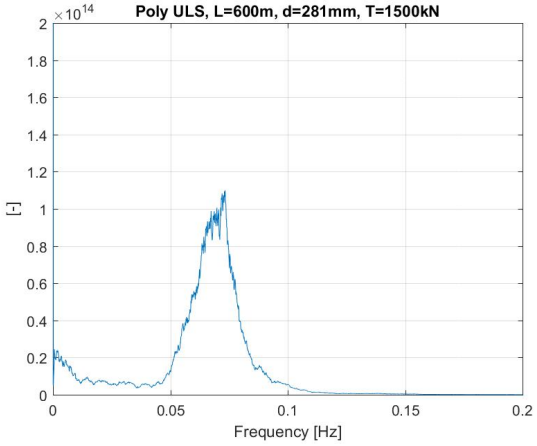

(b) FFT

Figure A.24: Polyester Line 1, L=600m d=281mm $T_{pretension}$=1500kN

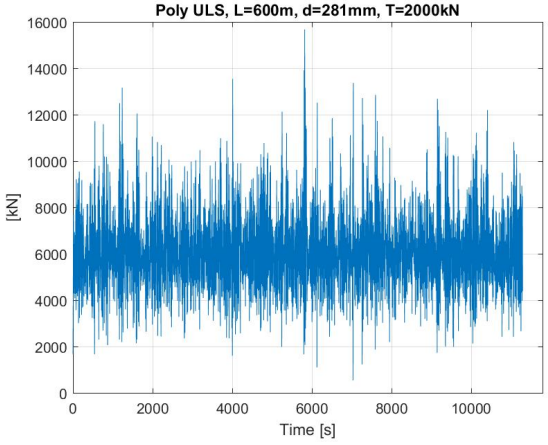

(a) Line tension

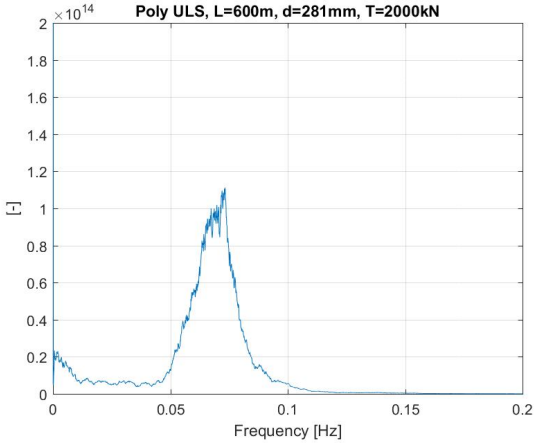

(b) FFT

Figure A.25: Polyester Line 1, L=600m d=281mm $T_{pretension}$=2000kN

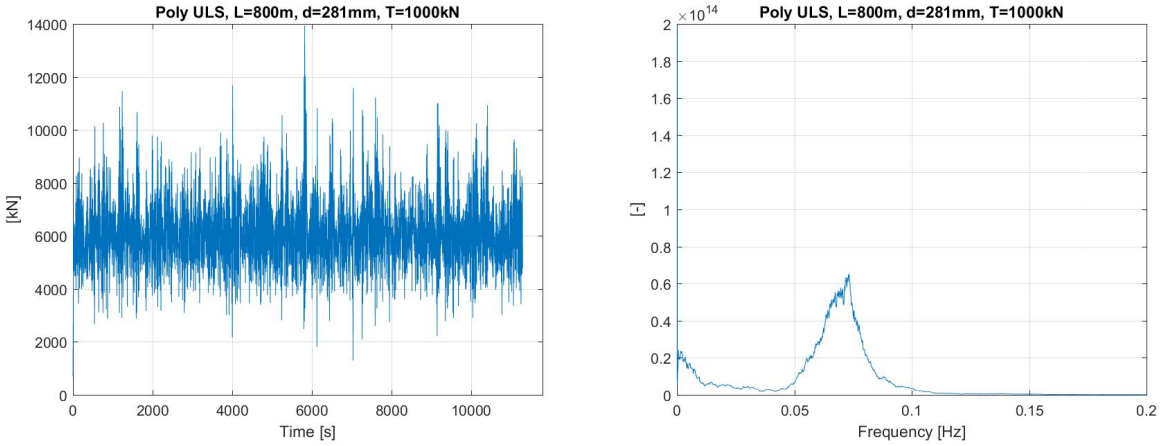

(a) Line tension (b) FFT

Figure A.26: Polyester Line 1, L=800m d=281mm $T_{pretension}$=1000kN

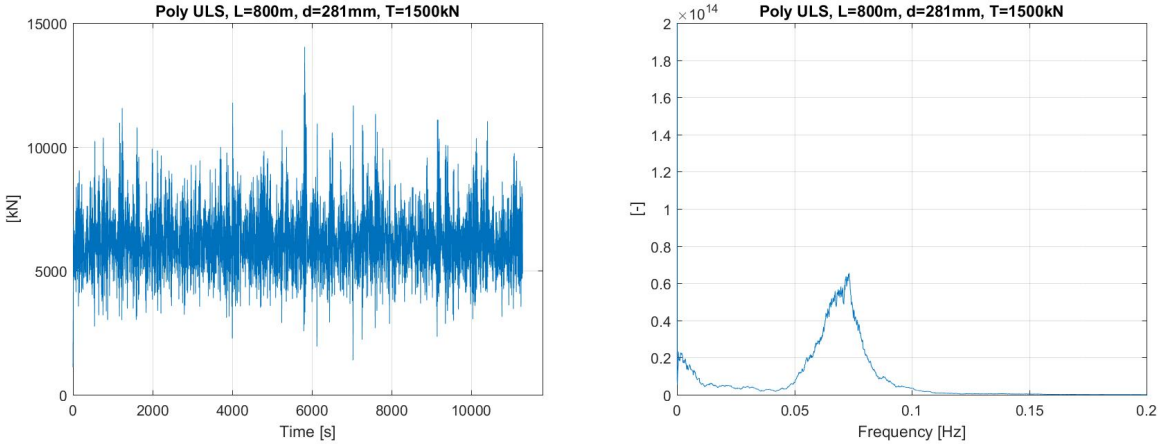

(a) Line tension (b) FFT

Figure A.27: Polyester Line 1, L=800m d=281mm $T_{pretension}$=1500kN

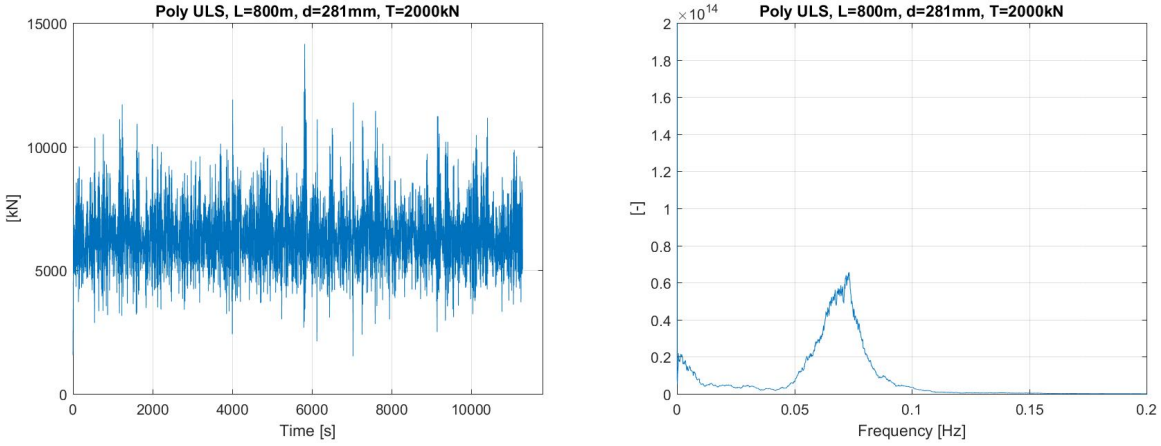

(a) Line tension (b) FFT

Figure A.28: Polyester Line 1, L=800m d=281mm $T_{pretension}$=2000kN

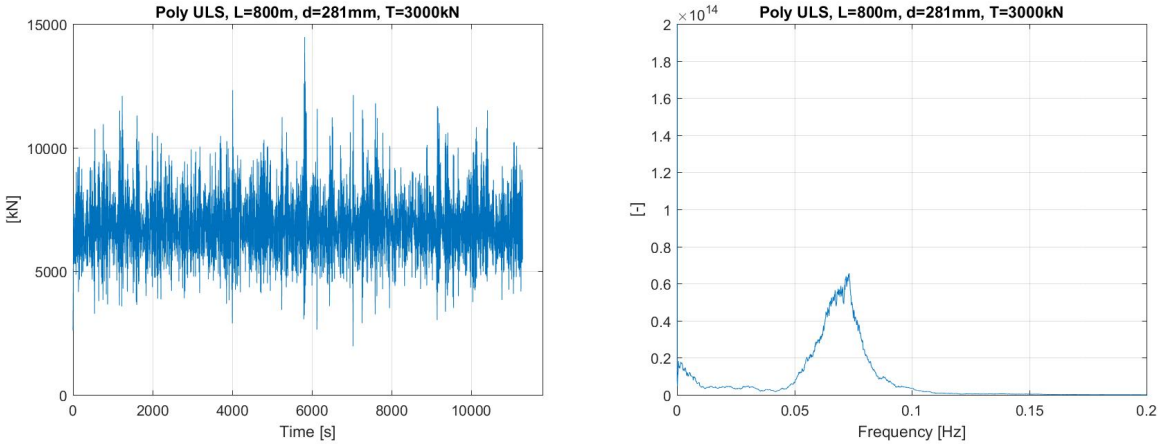

(a) Line tension (b) FFT

Figure A.29: Polyester Line 1, L=800m d=281mm $T_{pretension}$=3000kN

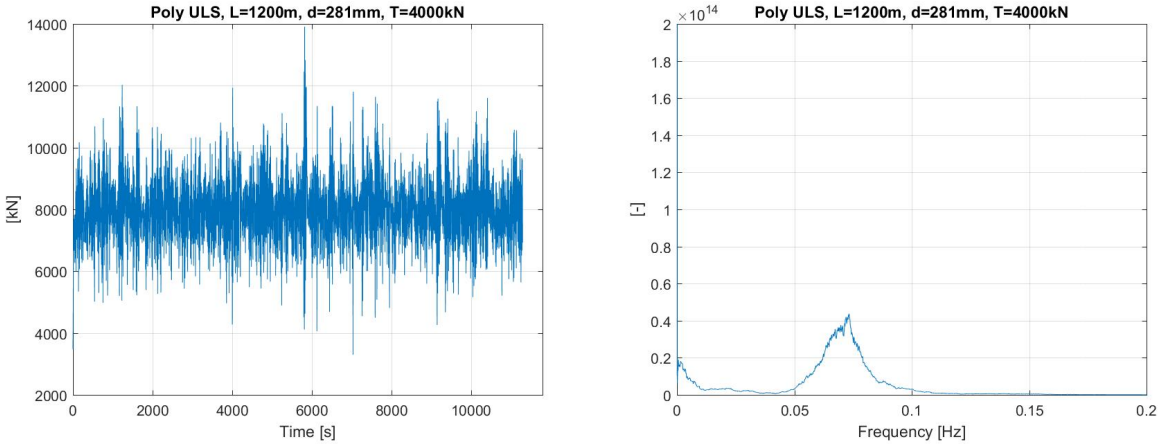

(a) Line tension (b) FFT

Figure A.30: Polyester Line 1, L=1200m d=281mm $T_{pretension}$=4000kN

A.3.2 Line 2

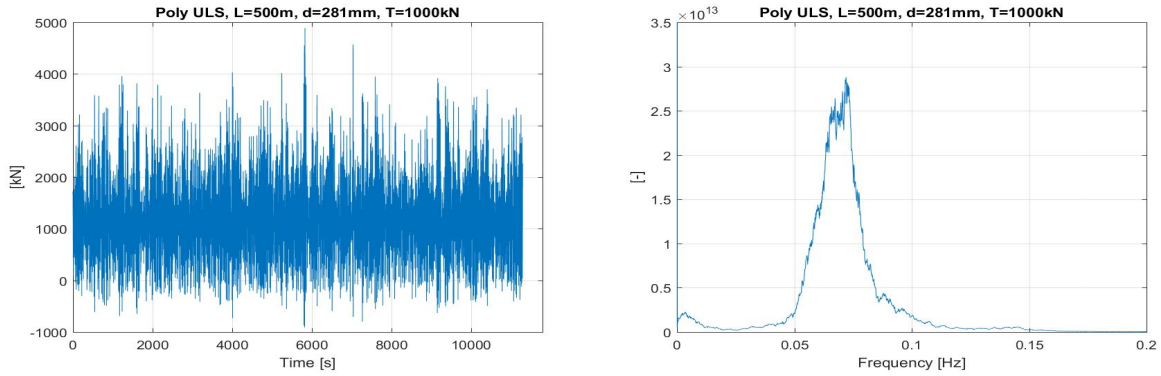

(a) Line tension (b) FFT

Figure A.31: Polyester Line 2, L=500m d=281mm $T_{pretension}$=1000kN

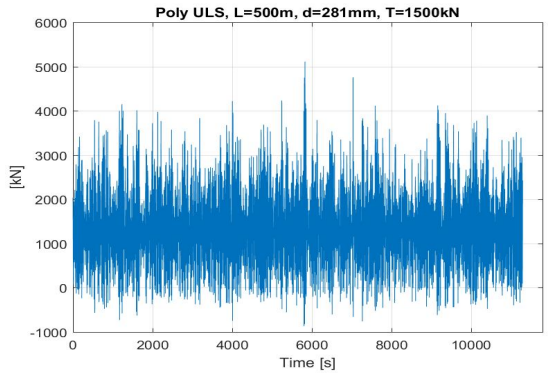

(a) Line tension

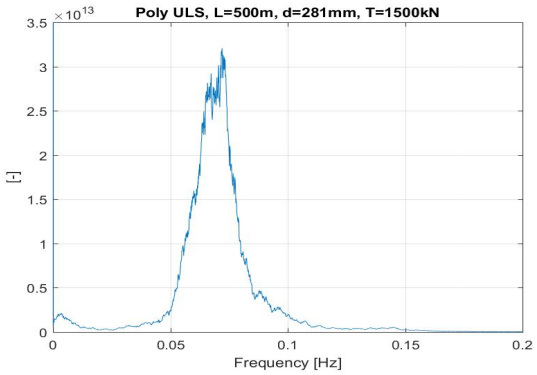

(b) FFT

Figure A.32: Polyester Line 2, L=500m d=281mm $T_{pretension}$=1500kN

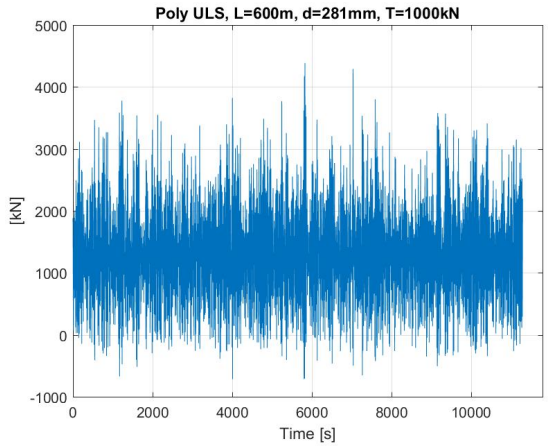

(a) Line tension

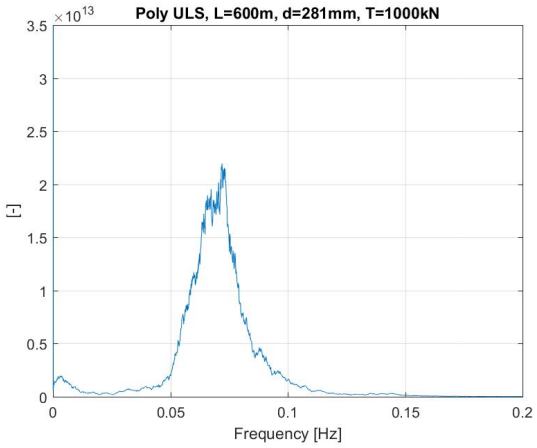

(b) FFT

Figure A.33: Polyester Line 2, L=600m d=281mm $T_{pretension}$=1000kN

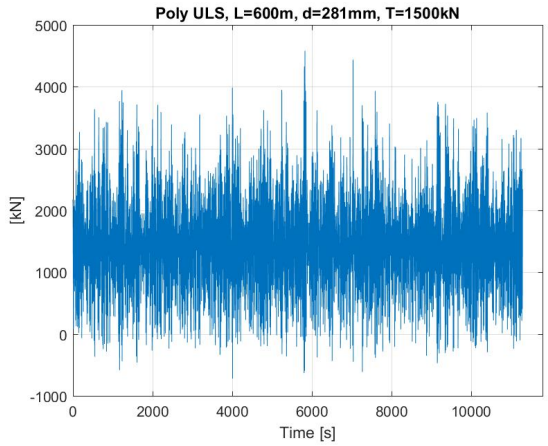

(a) Line tension

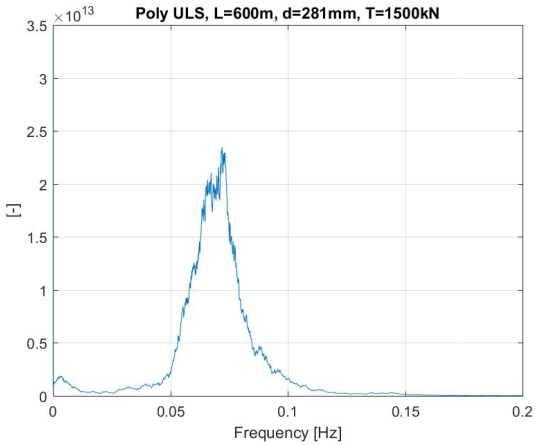

(b) FFT

Figure A.34: Polyester Line 2, L=600m d=281mm $T_{pretension}$=1500kN

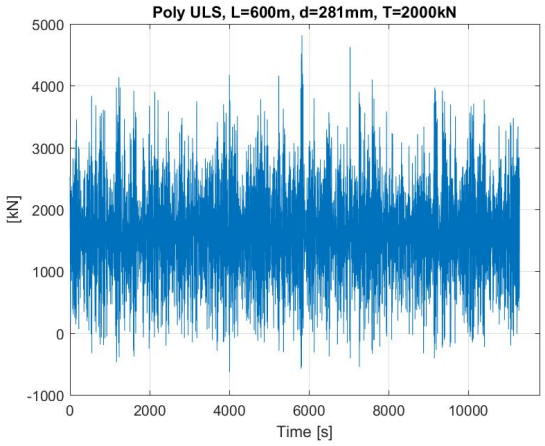

(a) Line tension

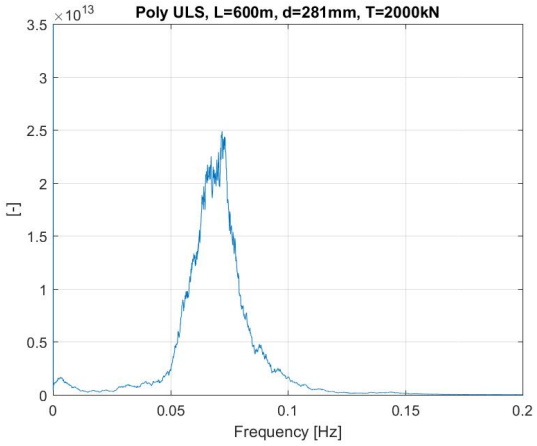

(b) FFT

Figure A.35: Polyester Line 2, L=600m d=281mm $T_{pretension}$=2000kN

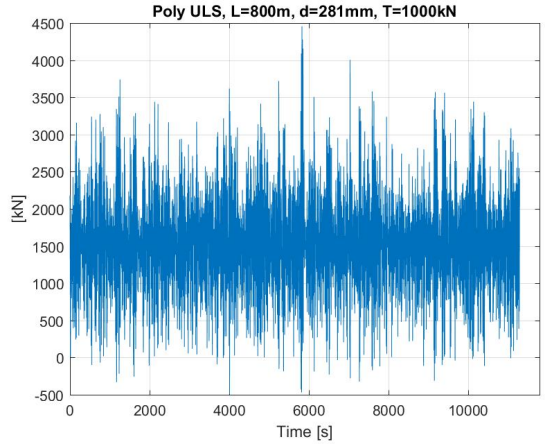

(a) Line tension

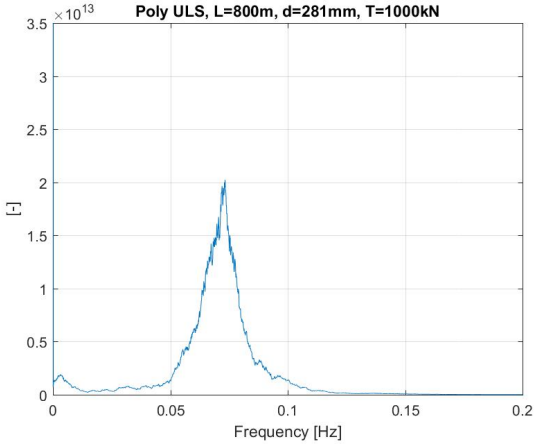

(b) FFT

Figure A.36: Polyester Line 2, L=800m d=281mm $T_{pretension}$=1000kN

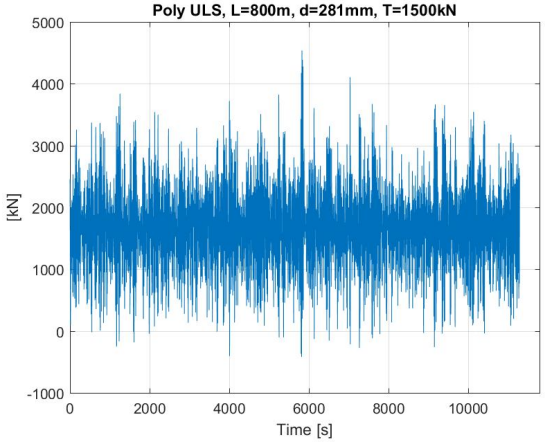

(a) Line tension

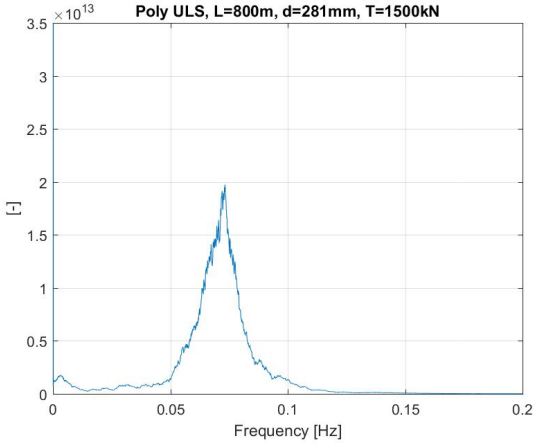

(b) FFT

Figure A.37: Polyester Line 2, L=800m d=281mm $T_{pretension}$=1500kN

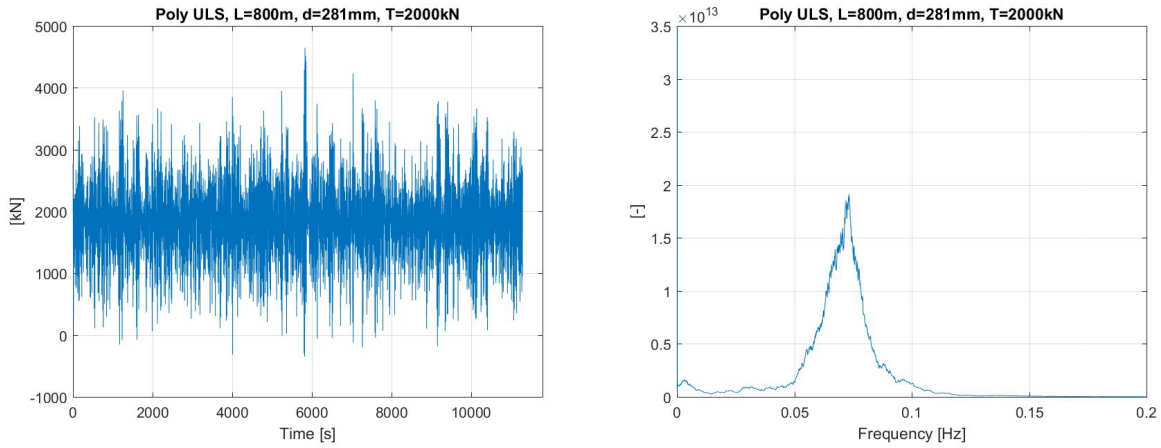

(a) Line tension (b) FFT

Figure A.38: Polyester Line 2, L=800m d=281mm $T_{pretension}$=2000kN

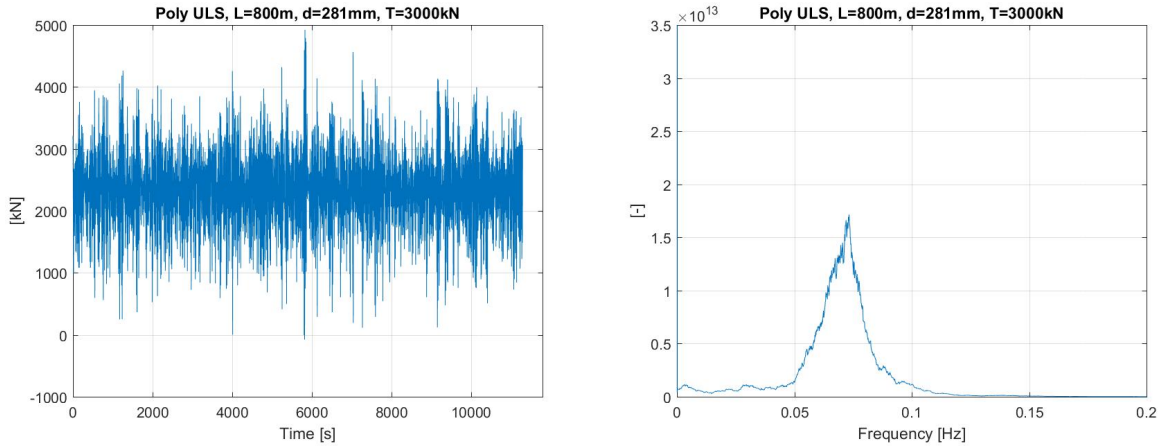

(a) Line tension (b) FFT

Figure A.39: Polyester Line 2, L=800m d=281mm $T_{pretension}$=3000kN

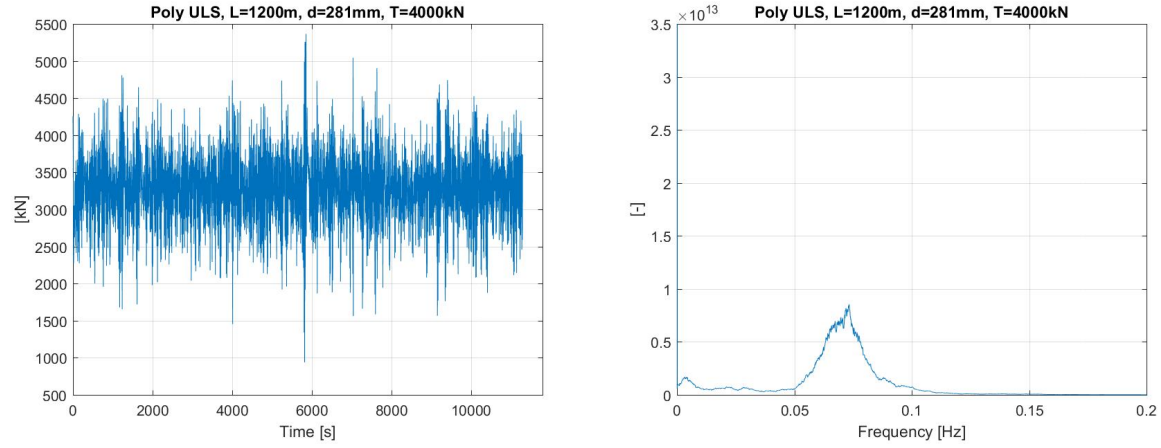

(a) Line tension (b) FFT

Figure A.40: Polyester Line 2, L=1200m d=281mm $T_{pretension}$=4000kN